2-24-2012 12:00 AM

Bacterial Cellulose Templates for Nano-Hydroxyapatite Fibre Synthesis

Jordan A. DeMello, *The University of Western Ontario*

Supervisor: Dr. Wankei Wan, *The University of Western Ontario*

A thesis submitted in partial fulfillment of the requirements for the Master of Engineering Science degree in Biomedical Engineering

BACTERIAL CELLULOSE TEMPLATES FOR NANO-HYDROXYAPATITE FIBRE SYNTHESIS

(Thesis format: Monograph)

by

Jordan A. DeMello

Graduate Program in Biomedical Engineering

A thesis submitted in partial fulfillment
of the requirements for the degree of
Master of Engineering Science

The School of Graduate and Postdoctoral Studies
The University of Western Ontario
London, Ontario, Canada

The UNIVERSITY of WESTERN ONTARIO
The School of Graduate and Postdoctoral Studies

CERTIFICATE OF EXAMINATION

Supervisor	**Examiners**
_____	_____
Dr. Wankei Wan	Dr. Argyrios Margaritis
	_____
	Dr. Dimitre Karamanev
	_____
	Dr. Don Hewson

The thesis by

Jordan A. DeMello

entitled:

Bacterial Cellulose Templates for Nano-Hydroxyapatite Fibre Synthesis

is accepted in partial fulfillment of the
requirements for the degree of
Master of Engineering Science

Date: _____ _____
Chair of the Thesis Examination Board

Abstract

Guided bone regeneration is a medical procedure which induces *in vivo* re-growth of bone using membranes and osteopromoting fillers. In this work, bacterial cellulose fibres were isolated and used as a basis for biomimetic hydroxyapatite growth, with the ultimate goal of producing GBR filler materials. *Acetobacter xylinum* generated BC using various carbon sources. Fibres were treated with phosphoric acid to phosphorylate functional groups and preconditioned with calcium to nucleate the HA. Simulated body fluid (SBF) furthered the growth. Over 14 days, the product was characterized via EDX, SEM, FTIR, and XRD. The effect of media composition, phosphorylation time, pre-treatment, and structure on the resultant composites was examined. Samples possessed a Ca-to-P ratio as high as 1.45±0.92, encompassing the HA standard of 1.67. Higher ratios were observed on the surface of pellicles, implying crystal deposition. Results indicate potential in three-dimensional samples and a basis for further BC-HA scaffold optimization for GBR.

Keywords: *guided bone regeneration, bacterial cellulose, hydroxyapatite, biomimetic synthesis, simulated body fluid, Acetobacter xylinum, phosphorylation.*

Acknowledgements

I would like to express my deepest gratitude to my parents, first and foremost. Everyone always says that their parents supported them throughout the course of their degree; I do not know of a time when my family has not supported me. Thank you for your love and support since time immemorial.

To my friends, for being yourselves. We`ve had our ups and downs, but you are the people that I aspire to be. To Adam Kirchhefer and Allison Hill. To Jeff Hujan. To Brian Chan. To the entire UWO Fencing Club and Executives. To Abe, Marco, Erik, Rizwan, Helen, and the entire multitude of international people who I have met in my time here at Western. Thank you for being the instrumental motivating factor in the existence of this document, as well as being an outlet when writing became too difficult.

To my professors, for providing me with the access and freedom to pursue my ideals, and the diligence to tell me when I was being unrealistic. To Dr. Wan, for being a fount of knowledge in the field and for supervising me over the last couple of years.

To my lab, for being an unbounded source of data and information, and for providing me with the scientific contacts needed when I started down this road. To the late Dr. Kenneth Wong, for his help in procuring all the SEM and EDX spectra. To Donna Padavan and Xinsheng Li for their advice, revisions, and constant assistance in characterization experiments.

To those I have TAed. Ironically, I think I have learned more about myself through you, than I have afforded you in return.

To The University of Western Ontario; for seeing something in me many years ago.

Table of Contents

Title Page ..... **i**
Certificate of Examination ..... **ii**
Abstract ..... **iii**
Acknowledgements ..... **iv**
List of Figures ..... **vii**
List of Tables ..... **ix**
List of Abbreviations ..... **x**
1.0 Introduction **1**
1.1 Overview 1
1.2 Thesis Objectives 4
2.0 Background and Literature Review **5**
2.1 Tissue Engineering of Bone 5
2.2 Bone Biology and Physiology 7
2.3 Guided Bone Regeneration 13
2.3.1 Brief Historical Background of Guided Bone Regeneration (GBR) 16
2.3.2 Principles of Guided Bone Regeneration 17
2.4 Material Selection 19
2.4.1 Cellulose 19
2.4.2 Hydroxyapatite 22
2.5 Biomimetically Synthesized Composites via Simulated Body Fluid 25
2.6 Bacterial Cellulose-Hydroxyapatite Composites 31
3.0 Materials and Methods **36**
3.1 General Procedure 36
3.2 Stages of Bacterial Cellulose Growth 38
3.2.1 Apparatus 38
3.2.2 Procedure 39
3.3 Phosphorylation 42
3.3.1 Apparatus 42
3.3.2 Procedure 42
3.4 Pre-treatment 43

3.5 Hydroxyapatite Growth 44
3.5.1 Preparation of SBF 45
3.6 Characterization 49
3.6.1 Fourier Transform Infrared Spectroscopy 49
3.6.2 Scanning Electron Microscopy 50
3.6.3 Energy Dispersive X-ray Spectroscopy 50
3.6.4 X-ray Diffraction 51
4.0 Results and Discussion 52
4.1 Overview 52
4.2 Production of BC using Maple Syrup as a Carbon Source 53
4.2.1 BC Characterization 56
4.3 Phosphorylation of BC 60
4.3.1 Characterization of Phosphorylated BC 61
4.3.2 Characterization of Phosphorylated BC After Treatment in SBF 70
4.4 Effectiveness of Pre-treatment of BC 78
4.4.1 SEM Characterization 79
4.4.2 EDX Characterization 83
4.4.3 Crystallite Dimensional Analysis 84
4.5 Characterization of HA 87
4.6 Variations in Choice of Pre-treatment Media, and Cellulose Morphology in HA Growth 98
4.6.1 HA-Biofill® Composites 99
4.6.2 Calcium Hydroxide Versus Calcium Chloride 100
4.6.3 Effect of Pre-treatment Methodologies Internally Within the Pellicle 104
5.0 Conclusions and Future Work 110
6.0 References 115
7.0 Curriculum Vitæ 121

List of Figures

Figure 2.2.1: Bone microstructure 9
Figure 2.2.2: Bone physiology 11
Figure 2.3.1: Guided bone regeneration summary 15
Figure 2.4.1.1: The repeating unit of pure cellulose 20
Figure 2.4.2.1: Crystal structure of pure hydroxyapatite 22
Figure 2.6.1: Proposed means of functional group replacement on bacterial cellulose backbone 32
Figure 3.1.1: Flowchart for the production of hollow hydroxyapatite fibres for guided bone regeneration 37
Figure 3.2.1.1: Continuous baffle flask growth of bacterial cellulose over the course of 14 days 38
Figure 3.3.1.1: Experimental set-up for the phosphorylation of bacterial cellulose. 42
Figure 4.2.1: Chemical structure of fructose 54
Figure 4.2.2: Chemical structure of sucrose 54
Figure 4.2.3: Weight analysis of dry cellulose per litre of prepared growth media 55
Figure 4.2.1.1: SEM of fibres formed from fructose media 57
Figure 4.2.1.2: Fibre diameters for fibres formed from fructose media 57
Figure 4.2.1.3: SEM of fibres formed from maple syrup based media 58
Figure 4.2.1.4: Fibre diameters for fibres formed from maple syrup 58
Figure 4.3.1.1: Scanning Electron Microscopy (SEM) outputs of a) untreated BC and b) 2 hour phosphorylated BC 62
Figure 4.3.1.2: Statistical distribution of fibre diameters in both a) bacterial cellulose (105.5 ± 26.0 nm) and b) 2-hour phosphorylated BC (56.7 ± 16.5 nm) 63
Figure 4.3.1.3: SEMs of BC fibres after 1, 2, and 4 hours of phosphorylation 64
Figure 4.3.1.4: Distribution of BC fibre diameters for samples exposed to 1, 2, and 4 hours of phosphorylation 64
Figure 4.3.1.5: Sample expansion (950 to 1200 cm^{-1}) of an FTIR taken of a bacterial cellulose sample (red), a BC sample after 2 hours of phosphorylation (green) and the same sample after 14 days in SBF (blue) 65
Figure 4.3.1.6: P-to-C ratio for BC samples after 1, 2, and 4 hours of phosphorylation .. 67
Figure 4.3.1.7: Titration curve for a two hour phosphorylated cellulose sample 69
Figure 4.3.2.2: The Ca-to-P and P-to-C ratios as functions of the number of hours of phosphorylation after week long reaction in SBF 73
Figure 4.3.2.3: Ca-to-P molar ratio for samples undergoing 1, 2, or 4 hours of phosphorylation time and subsequent SBF reaction 75

Figure 4.3.2.4: P-to-C ratio for samples undergoing 1, 2, or 4 hours of phosphorylation and subsequent SBF reaction 76
Figure 4.4.1.1: SEM of pre-treated BC fibres after 3 days in SBF 79
Figure 4.4.1.2: SEM of untreated BC fibres after 3 days in SBF 80
Figure 4.4.1.3: Comparison of pre-treated and non-pre-treated samples of BC (3-day immersion in $CaCl_2$) before (left) and after (right) 14-day term in SBF 82
Figure 4.4.2.1: Observed Ca-to-P molar ratio of the bacterial cellulose/hydroxyapatite fibre sample over the course of 14 days 83
Figure 4.4.3.1: Major HA crystallite dimension (length) as a function of the length of time in SBF 84
Figure 4.4.3.2: Minor HA crystallite dimension (diameter) as a function of the length of time in SBF 86
Figure 4.5.1.1: FTIR for hydroxyapatite prepared via biomimetic conditions 88
Figure 4.5.1.2: FTIRs for, from bottom to top; BC-PO_4H_2, 1 hr long phosphorylated BC-HA, 2 hr long phosphorylated BC-HA, 4 hr long phosphorylated BC-HA, 2 hr long phosphorylated HA-Biofill®, and "pure" hydroxyapatite procured via a chemical precipitation method in conjunction with SBF 90
Figure 4.5.1.3: Expansion (900 – 1900 cm^{-1}) of the characteristic region of HA-BC composites shown in figure 4.5.1.2 92
Figure 4.5.1.4: A sample EDX pattern for the BC-HA pellicle samples 94
Figure 4.5.1.5: Sample XRD of the produced HA crystallites 96
Figure 4.6.1.1: SEMs of the HA-Biofill® composites 99
Figure 4.6.2.1: Cross section of a BC pellicle pre-treated with calcium chloride 102
Figure 4.6.2.2: Cross section of a BC pellicle pre-treated with calcium hydroxide 103
Figure 4.6.3.1: Molar ratio (Calcium to Phosphorus) of the pellicle immersed in $CaCl_2$ pre-treatment as a function of the interstitial thickness 104
Figure 4.6.3.2: Molar ratio (Calcium to Phosphorus) of the pellicle immersed in $Ca(OH)_2$ pre-treatment as a function of the interstitial thickness 105
Figure 4.6.3.3: Phosphorus content as a function of distance into the sample 106

List of Tables

Table 3.2.2.1: Reagents for *Acetobacter xylinum* growth medium 39
Table 3.5.1: Ionic concentrations in regular (1.0x) SBF and human blood plasma 44
Table 3.5.1.1: Reagents for Kokubo's simulated body fluid (1.5x) 46
Table 4.2.1.1: Summary of EDX results for BC 59
Table 4.3.1.1: Wavelength assignment of most significant PO_4^{3-}/HA peaks (950-1200 cm^{-1}) 66
Table 4.3.1.2: DS_P as a function of length of phosphorylation time 68
Table 4.5.1.1: EDX results for biomimetically produced HA ($Ca_{10}(PO_4)_6OH_2$) 95
Table 4.5.1.2: Assignment of peaks from XRD shown in figure 4.5.1.5 and corresponding diffraction planes 97

List of Abbreviations

AFM	Atomic Force Microscopy
ATCC	American Type Culture Collection
ATR	Attenuated Total Reflectance
BC	Bacterial Cellulose
BC-HA	Bacterial Cellulose/Hydroxyapatite composite
BC-PO_4Ca	Calcium Pre-treated Phosphorylated Bacterial Cellulose
BC-PO_4H_2	Phosphorylated Bacterial Cellulose
BMP	Bone Morphogenetic Protein
DMF	Dimethylformamide
DSP	Degree of Substitution (by Phosphate)
EDX	Energy Dispersive X-ray Spectroscopy
FTIR	Fourier Transform Infrared Spectroscopy
GBR/GTR	Guided Bone Regeneration/Guided Tissue Regeneration
HA	Hydroxyapatite
hBMSC	human Bone Marrow Stromal Cells
ICP-AES	Inductively Coupled Plasma Atomic Emission Spectroscopy
IGF	Insulin-like Growth Factor
OCP	Octacalcium Phosphate
PAA	Polyacrylamide
PDGF	Platelet-Derived Growth Factor
PE	Polyethylene
PMMA	Polymethylmethacrylate
PTFE	Polytetrafluoroethylene
SBF	Simulated Body Fluid
SEM	Scanning Electron Microscopy
TCP	Tricalcium Phosphate
TEM	Transmission Electron Microscopy
TGF-β	Transforming Growth Factor β
TRIS	Tris(hydroxymethyl)aminomethane
XRD	X-ray Diffraction Spectroscopy
α-MEM	α-Minimal Essential Medium

Chapter One

1.0 Introduction

1.1 Overview

Hard tissues, such as that of bone, are exquisite structures in both composition and function. They form naturally through a biomineralization process, by which an inorganic phase is sequentially and meticulously overlaid upon an organic template. In attempting to replicate the physiological capabilities of vertebrates, scientists, over the last several decades, have made strides in bone tissue engineering and implantable devices, the most promising of which are biomimetic in nature. That is to say, the natural process of bone growth is partially mimicked *in vitro*, before being implanted into a patient. Nevertheless, the ideal combination of organic substrate and inorganic adjunct has managed to elude the scientific community, mainly due to failings in structural integrity, adaptability and cellular response.

Cellulose, as a long-chain saccharide polymer, has been used extensively in the biomedical field for its high degree of biocompatibility and significant tensile strength. This glucosidic biomaterial is usually obtained through the harvesting of fibrous plant tissue, although, recently, cellulotic growth via bacteria has come to the forefront due to higher crystallinity, larger degree of polymerization, nano-scaled diameter and simplified purification[1]. In addition, the high hydrophilicity and surface-area-to-volume ratios of the product fibres lend themselves well to industrial applications in the form of composites, thickeners, as well as membranes and coatings in a variety of fields[1, 2].

Comparatively, hydroxyapatite (HA), a crystalline, calcium phosphate-based mineral found in bone tissue, has been used, to a large extent, as a major component in the development of osteal tissue regeneration, implants and bone grafts, though it lacks a directed crystal structure and the ability to be moulded. Instead, the millimetre-scale powder must be adsorbed onto surfaces, or poured in open cavities in bone and covered with a semi-permeable membrane in a process known as Guided Bone Regeneration (GBR). Unfortunately, this has the added side effect of poorly maintained scaffolding (due to the large size discrepancy between the 20 micrometer bone cells and the macromolecular particles), and the instability of the implant site.

To overcome this problem, the addition of nanometre-sized hydroxyapatite coatings onto natural polysaccharide polymers such as chitin[3], chitosan[4], and cotton[5] has been reported, in recent years, with varying degrees of success. The use of bacterial cellulose (BC) fibres for such applications, however, has long been unexplored. Recent articles[6, 7] have dabbled in BC pellicles (or 'sheets') for the seeding of hydroxyapatite, but the existing processes to adhere HA to the three-dimensional nature of the pellicle limits the success of the resultant composite, and potential permeation of both cells and crystallites throughout the biomass. In this work, individual bacterial cellulose fibres were suspended in solution and used as a basis for HA crystal ($Ca_{10}(PO_4)_6(OH)_2$) growth, with the ultimate goal of producing growth factor-seeded *hollow* bone fibres for GBR.

The BC was produced via *Acetobacter xylinum* (currently obtainable as *Glucoacetobacter xylinus* via ATCC), in 250 mL baffled flask increments, using a fructose- or maple syrup-based media. The samples were left to grow in combination static/agitated culture, for 14 days, before being homogenized and purified. The individual fibres were then treated

with orthophosphoric acid, in the presence of an aprotic solvent (dimethylformamide, DMF) and high temperature (136 °C), to phosphorylate the –OH functional groups in cellulose. Samples were then preconditioned with ionic calcium salt solution for 3 days. Simulated body fluid (SBF) containing several salts found in natural bone was then used to promote growth of the HA crystallites for two more weeks.

In 14-day experiments, the resultant product was characterized on a semi-daily basis via Energy Dispersive X-ray Spectroscopy (EDX), Scanning Electron Microscopy (SEM), and Fourier Transform Infrared Spectroscopy (FTIR). EDX confirmed the presence of several mineral elements naturally occurring in bone, whilst FTIR confirmed the presence of phosphate groups. SEMs were used for qualitative and dimensional analysis. As a final characterization, X-ray Diffraction (XRD) was employed to quantitatively assess the crystallinity of the hydroxyapatite powders. The final molar Ca/P ratio of the pure hydroxyapatite was found to be as high as 1.51±0.22, which encompasses the standard ratio for hydroxyapatite of 1.67, although the fibre composites could only ascertain a 1.45±0.92 ratio.

The current study ultimately intends to further research into specific materials for the space-forming component of most guided bone regeneration solutions. To accomplish this, the nanometre-scaled bacterial cellulose fibre was utilized as a backbone for crystalline hydroxyapatite growth. The composite was characterized in its variety of pre-treatment methods, and by means of its capability to nucleate the crystalline HA material. Similarly, the procedure was scrutinized in both the quality of the resultant composite, and the distribution of crystallites within the surrounding organic matrix.

1.2 Thesis Objectives

1. To explore the functionality of bacterial cellulose, obtained via static and agitated cultures in the presence of different sugars (fructose, glucose/sucrose from maple syrup, etc.).

2. To both produce and develop phosphorylated bacterial cellulose for the ultimate goal of application in guided bone regeneration therapies, using phosphorylation techniques.

3. To grow significant amounts of calcium phosphates, ideally pure hydroxyapatite ($Ca_{10}(PO_4)_6(OH)_2$), on the surface of nanometre-scaled bacterial cellulose fibres, via pre-treatment and subsequent immersion in SBF.

4. To characterize said composite fibres via Fourier Transform Infrared Spectroscopy (FTIR), Scanning Electron Microscopy (SEM), Energy Dispersive X-ray Spectroscopy (EDX) and X-ray Diffraction (XRD) techniques.

5. To evaluate differences in the samples formed as pellicles versus those formed and dispersed as individual fibres. In addition, to evaluate the differences in calcium pre-treatments as theorized by Kokubo [8].

Chapter Two

2.0 Background and Literature Review

2.1 Tissue Engineering of Bone

The reconstruction of skeletal deficiencies has presented a significant challenge to the medical community for decades. The repairable defects in question often occur specifically in the facial maxima as a result of trauma, surgery, tumour excision, infection or a variety of arthritic complications[9]. The major encumbrance to the widely-accepted procedures of rebuilding bone is the pervasion of the wound site via the rapid expansion of soft tissue material. In the oral cavity, this in-growth is particularly worrisome as the fibroblasts have experimentally been found to both inhibit the osteogenic properties and structure of the native material and the differentiation of the bone cells, leading to a substantially weak jaw line. Similarly, the atrophy that often surrounds the wound sites prevents the anchoring of prostheses or similar techniques of reconstruction[10].

To this end, numerous technologies have evolved to help in localized bone tissue growth. The most common method of this reconstruction is the harvesting and implementation of autogenous bone from another site on the patient for grafting purposes. This procedure, whilst ensuring the compatibility of the surgery for each individual case, results in higher operative costs and intensive surgical recovery, as well as potential for the donor site to become morbid or otherwise infected[11, 12].

Alternatively, an allogeneic or xenogeneic implant may be chosen, although these options are similarly fallible. First, considerations must be made as to whether or not to demineralise the implant. In the case of non-demineralised grafts, research has shown that an extremely low quantity of immediate osteoinduction occurs, largely attributable to a lack of adequate permeation of the requisite bone morphogenetic proteins (BMPs) and cells[12, 13]. Demineralised matrices find themselves to have similar problems. Although they have the potential to stimulate relatively significant amounts of initial osteoinduction, harsh treatments are necessary in order to both minimize the non-organic, crystalline component and subsequently sterilize the implant. These techniques result in a large variability in success rates, owing to partial hindrance of compression strength and structure of the scaffold, and leading ultimately to a significant (~10%) reduction in requisite bone salts[14, 15]. In addition, depending on the means used for sterilization purposes (glutaraldehyde, formaldehyde, ethylene oxide, irradiation), long-term osteoinduction may be compromised by potential cytotoxicity[16].

During the past two decades, however, industrially-produced hydroxyapatite has received the gross majority of attention as a substitute for techniques involving bone reconstruction. In this way, the open wound could be supplemented with a quasi-amorphous, osteoconductive coating material that can be marginally adjusted to fit its surroundings. Similarly, within this time frame, the discovery of a new technique known as Guided Tissue (or Bone) Regeneration capitulated to the demand for a means of repairing tissue damaged by inflammatory periodontal disease. In a series of animal studies, several aspects of this technique were examined, resulting in wide acceptance of its legitimacy[17]. The addition of the membrane to the open wound site provided a

physical barrier to the effect of excluding non-desirable tissue cells (fibroblasts) from populating the area whilst simultaneously favouring the proliferation of requisite bone cells (osteoblasts and osteocytes). The membrane also had the added effect of necessitating space between the inner surface of the implant and the cavity, enabling room for further tissue growth. The above aspects – the hydroxyapatite powders and semi-permeable membranes – were mutually beneficial; the adjustability of the powders and the segregating properties of the membranes were found to be quite complimentary.

2.2 Bone Biology and Physiology

Bone is a composite material made up of two major components; an organic phase, predominated by collagen (Types I and II) and an inorganic phase made up of calcium phosphates, carbonates, and fluorides with a smattering of magnesium salts. Collagen, in the case of bone tissue, is a protein with good durability and a compounded structure, leading to a significantly high tensile strength (in excess of 140 MPa, for a single fibre, in the longitudinal direction)[18], and providing a secure place for the nucleation of the inorganic bone phase. In addition, collagen fibrils are osteoconductive to cell attachment.

The materials comprising the inorganic phase are often collectively combined into a homogeneous mineral form known as apatite. The most abundant form of said apatite is hydroxyapatite; a compound with a strict stoichiometric formula of $Ca_{10}(PO_4)_6(OH)_2$. Apatites, in general, are found to be highly-crystalline minerals with a ceramic-like molecular structure, leading to higher compression strength and, due to the stoichiometry, play an important role in regulation of the body's natural pH levels. It is the combination

of these above biomaterials, in an alternating structure of nano-scaled crystallites and coiled proteins, which provides the hardness and rigidity of bone. In terms of weight percentage, on average, the inorganic content is about 65%; the organic component and water makes up the remaining 35% of non-cellular bone weight[9].

On a nano-scale basis, bone is visually defined by the typical banding and fibril patterns of collagen. The collagen fibril, itself, a combination of three or more individual strands of collagen woven together in a gamma-helical pattern, lies in a collinear arrangement, with the hydroxyapatitic crystals capping the terminal ends (See Figure 2.2.1). These fibrils lie overlapping each other and are approximately 300 nm long with an end spacing of approximately 67 nm. The hydroxyapatite crystals, in turn, are even smaller (50 nm along its longest axis[19]), filling the 67 nm interim spaces between ends of fibrils, and forming a composite 'cement', which effectively binds the structure together. It is this ideal alternating spacing that produces the categorical banding pattern observable in transmission electron microscope (TEM) and atomic force microscope (AFM) images of bone. Fibrils group themselves together in bundles (collectively referred to as the collagen fibre) of 40-50 nm in diameter[20].

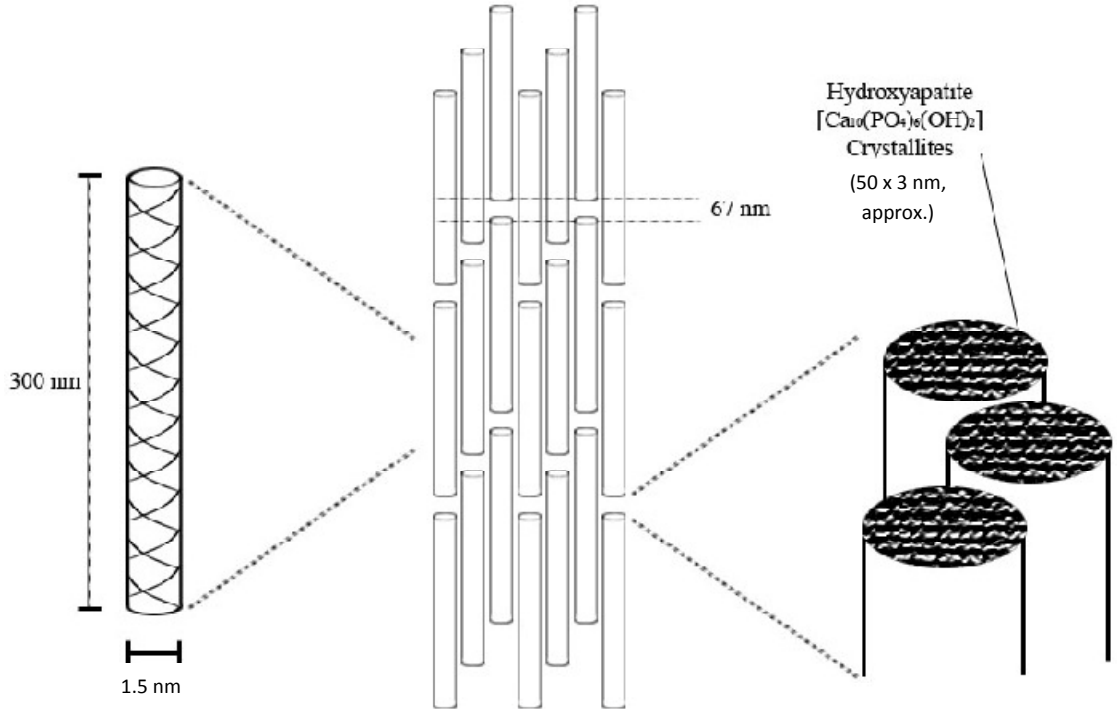

Figure 2.2.1: Bone microstructure, showing individual collagen fibril (left), a collagen fibre (centre), and the terminal end spacing of collagen, with hydroxyapatite crystals (right).

The skeleton of a typical adult is perpetually in a dynamic state of being broken down and reformed by the coordinated actions of bone cells. These cells are responsible for the maintenance and repair of the tissue, which is central to the structural support, health and metabolism of the human body.

The microstructure of bone contains a wide array of vascular networks and nerves, connected via horizontal spaces known as Volkmann canals. Larger bones in the body are made up of two distinct types of osteal tissue; a dense, cortical bone and a spongy, cancellous (or trabecular) bone. In figure 2.2.2, this distinction is emphasized with cortical tissues, in a solid colour, surrounding the trabecular tissue, with its distinctive

honeycombed structure. The cortical bone (a) exists mostly on the external ‘surfaces’ of the osteal tissue; in contrast, the cancellous bone is present internally, in the cuboidal/flat bones or in the terminal ends of long bones, as a space-saving device, ultimately existing to minimize the bone weight. In both cases, bone is vascularised by blood vessels (b) extending from a membranous, supporting tissue known as the periosteum (c) or through the Volkmann canals/Haversian system. In addition, the interior of most long bones contain an area of completely non-mineralized space known as the medullary cavity (shown as a darker area in the left figure). This space is filled with marrow; a tissue consisting of blood vessels, adipose tissue, nerves and other varied cell types/progenitors whose principal purpose is to generate the necessary cells present in blood and bone, as well as furthering existing vascularisation. The combination of osteal tissue and supporting tissue allows for a material in which maximal strength is achieved with minimal mass, and hence, all material substitutes must cater to both the structural and biological necessities.

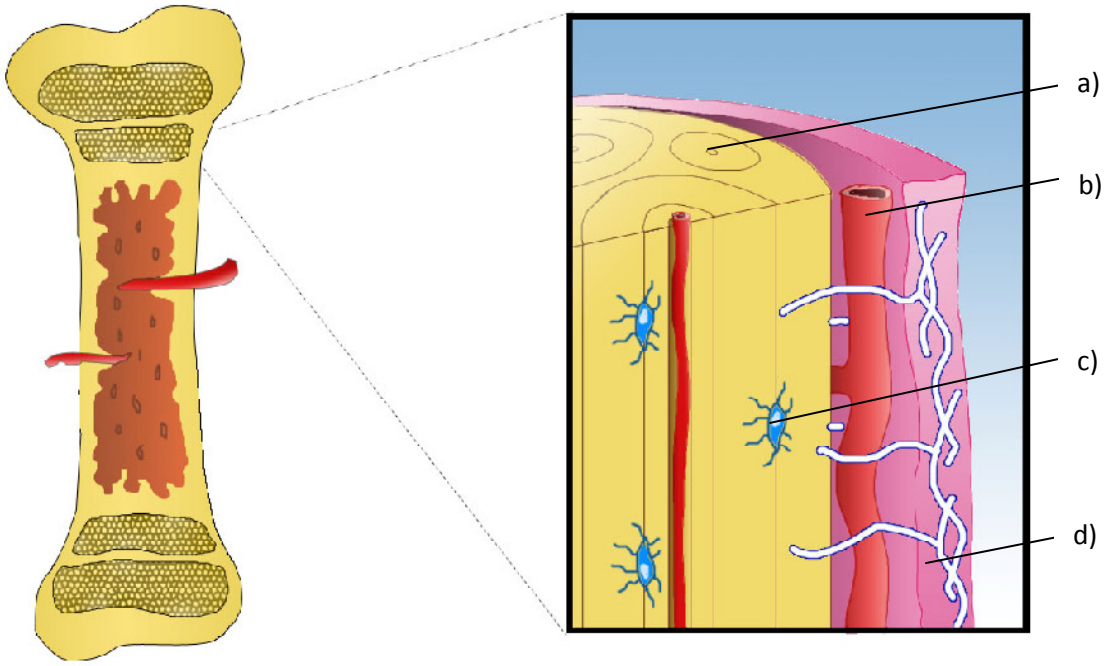

Figure 2.2.2: Bone physiology. On a microscopic scale, the bone is further comprised of an interwoven network of osteal tissue surrounding Haversian canals (osteons) (a), blood vessels/capillaries (b), and bone cells (osteocytes) (c), as well as the aforementioned periosteum (d).

The main types of cells associated with the metabolism and physiology of bone are osteoblasts, osteocytes and osteoclasts.

Osteoblasts are the primary builders of bone. Their purpose is to produce proteins of the bone matrix; collagen and other non-structural proteins (such as differentiation markers) necessary to the tissue. Osteoblasts actively lay down successive concentric circles of bone within the inner walls of a cavity, creating osteons – the fundamental, cylindrical, structural unit of compact bone. This action continues until new bone encroaches on the blood vessels or nerves running down the length of the bone, ultimately resulting in what is referred to as the Haversian system. In addition to providing the matrix for the

mineralization of bone tissue, during osteogenesis, osteoblasts take on the role of secreting growth factors (including, but not limited to, Transforming Growth Factor (TGF-β), Insulin-like Growth Factor (IGF), Platelet Derived Growth Factor (PDGF), and Bone Morphogenetic Proteins (BMPs)[21, 22] to promote the influx of new bone cells. For a material to be deemed adequate for bone tissue engineering, these cells are of the utmost importance; the osteoblasts must be able to interact with, and adhere to, the surrounding scaffold matrix.

Once osteoblasts become embedded in the bone matrix, they develop more dendritic structures and become osteocytes. These are the most abundant bone cells, communicating to one another via the existing canal system. The change in cell morphology results in cytoplasmic extensions of their cell membrane, which now create a direct continuity between the bloodstream and the remaining bone cells. This allows for the exchange of metabolic and biochemical transmissions, and to direct the further growth of underdeveloped woven bone[23].

Osteoclasts, on the other hand, are exclusively responsible for bone resorption; they appear as large, multi-nucleated, giant cells with several villi along one side. This side, referred to as the ruffled border, secretes the proteolytic enzymes and acids necessary to break down bone tissue - resorbing it - and releasing requisite ionic calcium, carbonates and phosphates back into the bloodstream. This continues for up to 3 weeks, during which the osteoclast can bore a hole several millimetres long, and after which the cell itself is degraded back into resorbable products[24]. This cavity is then seeded with new osteoblasts, and the cycle begins again.

It is this constant state of flux, bone growth, and resorption, provided by the bone cells, that allows the human body to maintain the structural integrity of bone. In addition, as the calcium and phosphate present in bone is also necessary to the regulation of the body's natural pH balance, conduction of musculature, electrical impulses and metabolic state, the continuous breakdown and rebuilding of bony tissue is a necessary procedure in preventing disease and general health. As such, maintenance of diseased or otherwise compromised bone (via implants or tissue engineering techniques) is a necessary process to keep existing tissue from degrading uncontrollably, or otherwise becoming infected. Furthermore, for techniques of bone regeneration to be considered effective, the resultant process must kowtow to the above aspects of the bone physiology, cells and microstructure.

2.3 Guided Bone Regeneration

Guided Bone Regeneration (also known as GBR or Guided Tissue Regeneration) is a technique by which a surgeon artificially encourages re-growth of a lost portion of osteal tissue via a filler substrate and a membrane. The composition of this substrate is important as the material must be biocompatible and should preferably allow for proliferation of 'bone-matrix producing' osteoblasts. In the case of the filler, the required biomaterial must be requisitely fine enough and porous so that the aforementioned cells can affect their environment allowing the expansion of the extracellular matrix into the cavity. As such, the filler material is often composed of a porous hydroxyapatite powder, with grains ranging from 250-1000 μm[9]. As a corollary to this, the material is more

often than not covered by a barrier of sorts; this is done in order to simultaneously prevent unwanted migration of the filler into the surrounding tissue, the soft tissue into the cavity, and the collapse of the attempted remodel. The currently employed barrier membrane is usually composed of a non-resorbable compound such as expanded polytetrafluoroethylene (e-PTFE) or titanium foils. Reasoning behind the use of these particular materials is that their known biocompatibility will simultaneously eliminate the contamination of the wound by migrating soft tissue cells (the pericutaneous flap is sutured over top of the membrane) and, similarly, prevent unexpected osteoinduction of bone cells into the surrounding tissue. Non-resorbable membranes, in particular, are often used, as they are more likely to hold up under the biological stresses of the wound reconstruction site. Unfortunately, this also results in two unwanted consequences; the same membrane that must be occlusive to cells must also be simultaneously permeable to oxygen and gases, nutrients, etc. In addition, the membrane must, after a given time of regeneration, be removed from the wound site, causing excess discomfort and further anguish to the patient.

As is shown in figure 2.3.1, the site of the technique must be (a) cut open in order to expose the cavity. A barrier (b) is inserted, providing cell occlusion, whilst also containing the filler material (textured). The barrier also allows for the proliferating bone cells to enter and reform the matrix, as indicated by the arrow (c).

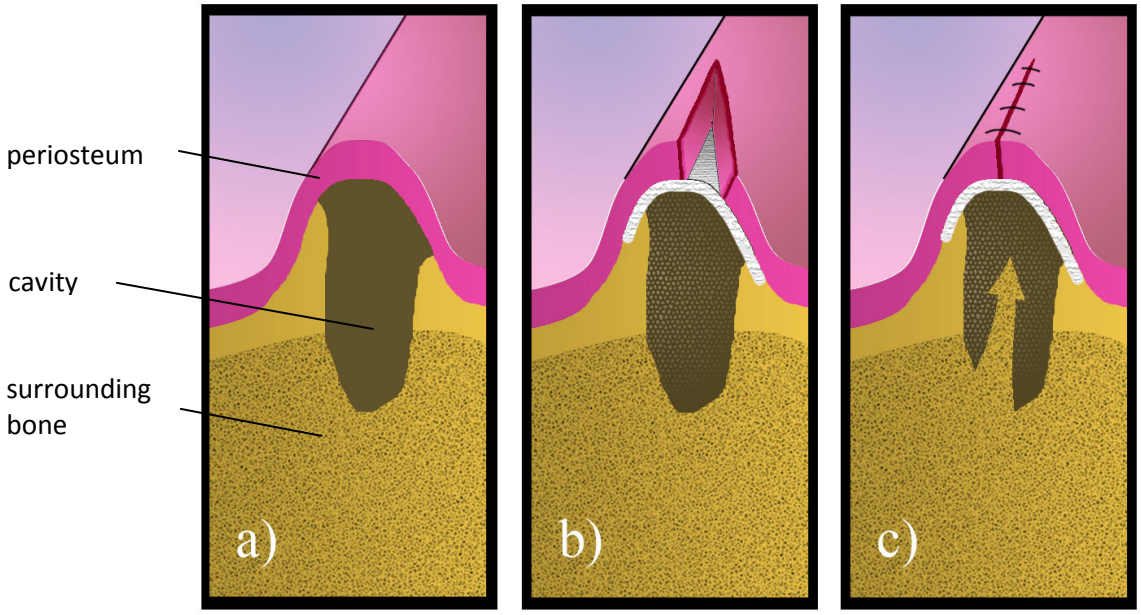

Figure 2.3.1: Guided bone regeneration summary, showing the eroded bone site (a), the surgery and implantation of matrix/membrane (b), and the migration of cells to the wound site post-surgery (c).

Whilst this technique is certainly applicable to all types of bone, the particular nature of the wound cavity and the prerequisites of the site environment lend themselves well to applications in dentistry. Quite often, in the case of root canals, the jaw bone must be excavated in order to set the metal supports in place[25]. At the time of this writing, guided tissue regeneration has been shown to further promote the growth of the dental bone into the space and threading between the implant screws and the existing mandible[26], more so than typical osteointegration. That said however, guided bone regeneration is not without its fallacies, largely inherent to the nature of the procedure. It fails to work successfully on vertical surfaces (little to no basis for filler attachment), large or single-walled defects (coverage of the wound site is difficult), or regeneration

sites where the bone is not close to the surface (advanced trauma of subsequent procedures)[9].

As such, there are several requirements that have to be made of the materials and the technique itself. The membrane barriers and 'filler HA material' must be used in tandem to simultaneously close the cavity, allow for vascularisation (have pores of adequate size and morphology), prevent dissolution of existing bone and stabilize the wound site[17]. Quite often, as discussed, membranes are also non-resorbable, requiring additional surgery. These principles are discussed in much further detail in section 2.3.2.

This technique, in practice, can be atypically costly and ineffective in promoting cell migration and growth, despite attempts to increase induction of bone cells into the area. Nevertheless, several commercially available products have been introduced to the market, attempting to secure a niche. Some examples of these products include Bio-Oss®, OsteoGraf®, and PepGen®, the latter of which substitutes amino acid residues (RGD sequences) in an attempt to draw more significant osteoblast attachment[9].

2.3.1 Brief Historical Background of Guided Bone Regeneration (GBR)

The first indication of physically sealing off an anatomic site for improved healing and tissue regeneration stems from the mid-1950s. Campbell and Bassett in 1956[27], and Hurley et al. in 1959[28] actually used cellulotic material for nerve and tendon regeneration, respectively. It wasn't long before this technology extended into the realm of bone regeneration. Brånemark and his colleagues[29, 30], in 1969, first proposed the idea of implant dentistry via the use of pure titanium implants in dental surgery.

Ironically, this came from an unforeseen incident in which the proposed titanium became largely integrated into natural canine bone tissue, and existing bone began anchoring itself to the interim spaces between implant and tissue.

In the subsequent years, several authors continued the landmark work, culminating with the discovery of Page et al. in 1976[31], whereby a direct bone-to-implant contact of a non-submerged titanium implant promoted what the authors termed osteointegration. Whilst this actually proved the ability of non-native materials to stimulate the subsistence of bone and the capability to manipulate surrounding tissues, it in no way actually suggested the induction of bone growth or osteogenesis of the material. As such, two seemingly occlusive branches of the research were integrated with an experimental evaluation of the healing process of mandibular defects in rabbits. This work, pioneered by Kahnberg in 1980[11], used Teflon leafs to prevent in-growth of scar tissue, whilst maintaining a titanium implant surface. From there, the leap to expanded polytetrafluoroethylene (e-PTFE), and the addition of osteopromoting filler materials (such as autogenous bone chips) is easy to see. By the time of Dahlin et al. in 1989[32], the fundamental theories of GBR as a legitimate means of bone growth were well established. Although this employed titanium structures in the tibiae of rats and rabbits, the work nonetheless pioneered what was to be a large and widely recognized field.

2.3.2 Principles of Guided Bone Regeneration

Guided bone regeneration is used fairly often in implant and reparative dentistry. The requirements of the wound site, stipulated by Dahlin[17], for the successful predilection of bone growth via GBR are as follows:

- **Source of Osteogenic Cells**. Viable bone must be present in the surrounding tissues.
- **Existing Vascularity**. More often than not, this comes from existing bone marrow, Volkmann canals, and intermediate lacunae of existing bone.
- **Mechanical Stability**. The repair site should not collapse upon itself.
- **Adequate Spacing**. This is usually generated by a temporary filler material of sufficient porosity.
- **Occlusion of Soft Connective Tissue,** such as periosteum, from the site of bone growth (assisted via the use of membranes).

In addition, the materials of the filler and membrane themselves must have further additional requirements[33]:

- Biocompatibility – All immunological reactions must be accounted for and, in the course of preparation of the filler/membrane, must be adequately tested. This may or may not include the lyophilisation and complete sterilization of the material.
- Functionality – Diffusion of nutrients and oxygen into the tissue must be maintained.
- Tissue adhesion and integration – Often, the tissue must grow into the thickness of the filler, and even partially into the membrane, but not through it. Should periosteal tissue grow through the porous exterior surface of the membrane, this

has the potential to result in an aptly named "flap-membrane complex", which would seal the membrane in place and prevent apical re-growth of epithelial soft tissue cells, allowing exposure to bacterial infection.

- Structural stability – The filler and membrane, as a composite treatment, must be able to hold up under the pressure of the soft tissue, and often, due to the implantation procedure itself, the weight of the suture pressing down upon it.

- Adaptability – This is more of a commercial requirement, and more applicable to the membrane, however, the chosen material must be able to encompass the wound site without resulting in folds, protrusions or edges. This is done to ensure complete site occlusion, and is usually accomplished by cutting membranes to fit precisely and adding a saline solution (or the patient's blood/plasma) to stretch and soften both the membrane and filler first.

2.4 Material Selection

2.4.1 Cellulose

Over 160 years ago, Anselme Payen isolated and purified cellulose from green plants[34]. Since then, cellulose has held an important place in the biomedical and industrial fields, being one of the most abundant polysaccharides on Earth. For years, the material was lauded for its high degrees of biocompatibility, high tensile strength, and a Young's modulus for individual fibres (35-90 nm thick) of 78 ± 17 GPa[35], although later papers have placed the value for the fibrils as high as 138 GPa[36, 37]. Coupled

with a tensile strength of at least 2 GPa, this effectively makes the strength of the fibres themselves comparable to that of aramid fibres. In addition, the substance has the added benefits of widespread availability and significant crystallinity. These benefits have oft been tempered by the complications derived in purification; the cellulose found in plant matter is contaminated with proteins, lignin and uncontrolled branching of the main chain, resulting in what is referred to as hemi-cellulose. Cellulose is nevertheless traditionally produced in industry from fibrous plant matter, as availability and access outweighs the costs of purification via acid hydrolysis and separation.

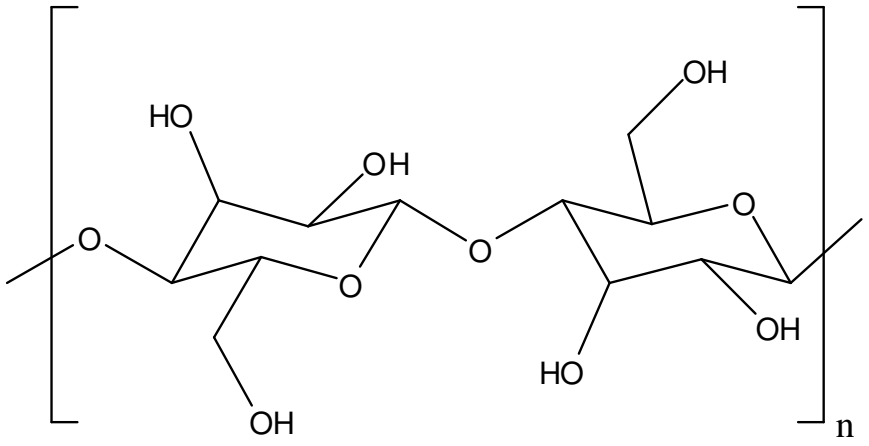

Figure 2.4.1.1: The repeating unit of pure cellulose, showing glucose monomer units and the β (1→4) linkages.

Bacterial cellulose, on the other hand, provides an advantage over the conventional material, as the bacterial culture can be directed into the production of cellulose chains exclusively, yielding the purest form of the polymer (containing no lignin or hemicelluloses). Experimentally, it was found that BC also provided the benefit of finer

fibrils of the material, suitable for use in composites. In literature, BC is reported as being produced with high crystallinity, fine microstructure (25-50 nm in diameter) and long fibre length (~5 μm)[1]. Bacterial cellulose has also been found to have a larger degree of polymerization in comparison to that of wood pulp cellulose. The average residue monomers of glucose per molecule of bacterial cellulose is around 6000 in acidic shaken culture (see Figure 2.4.1.1). Note that plant cellulose glucose residues can occasionally approach 15000[38] for a single molecule although, these values fail to take into account the presence of the hemi-cellulose branching.

BC was first discovered and isolated by A.J. Brown in 1886[1], from the acetic fermentation of fruits and vegetables in various states of decay. Although he was the first to identify the culture of *Acetobacter xylinum* (also known as *Acetobacter xylinus* or *Glucoacetobacter xylinus*), his work proved premonitory as people in the Philippines have often used the material (and its bacterial progenitor) in the manufacturing of 'nata-de-coco', a coconut-flavoured snack with the consistency of gelatine. Based upon this groundbreaking work, the field soon exploded, including, at the time of this printing, applications in fields of separation membranes, speakers, paper-making, burn recovery and wound dressings[6, 39, 40]. Concurrently with this research, the use of the bacterial cellulose as an additive in the field of heart valve or vein replacement has come to fruition[2].

2.4.2 Hydroxyapatite

In a similar manner, the major inorganic constituent of bone, hydroxyapatite, has often been greatly acknowledged as an applicable and popular material for research. Formed in the body, and known to be a commonly-occurring synthesis product of calcium and phosphates, non-stoichiometric hydroxyapatites (or occasionally "hydroxyl-apatites") are largely responsible for the characteristic sturdiness of bone. Whereas the collagenous component of the bone largely defines the structural tensile strength, the hexagonal crystal structure of hydroxyapatite, coupled with the bonding between ionic groups leads to a material that, similar to many ceramics, boasts extremely high compression strength.

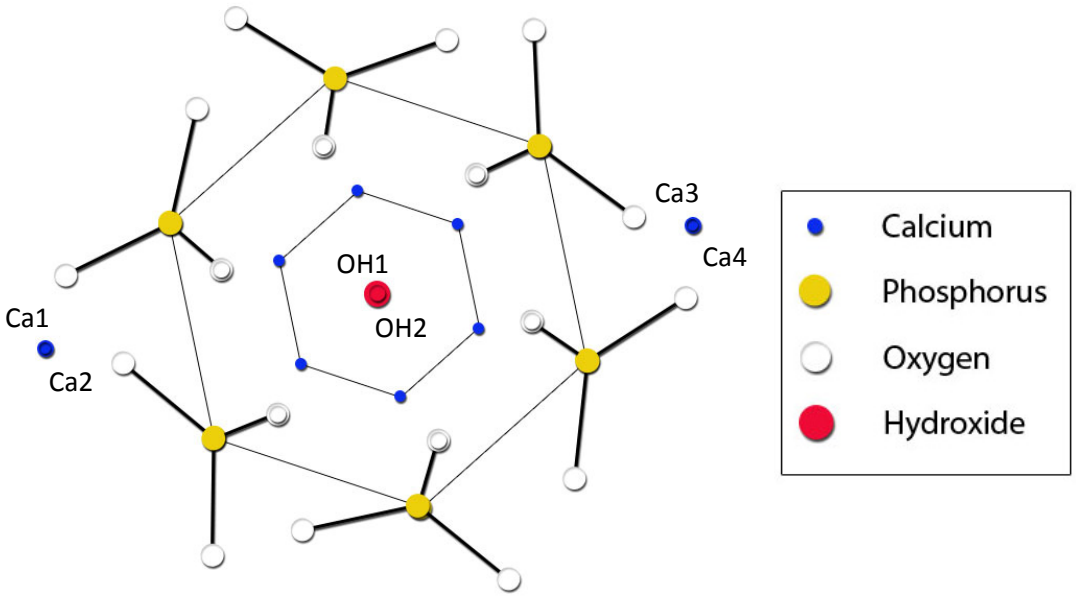

Figure 2.4.2.1: Crystal structure of pure hydroxyapatite [$Ca_{10}(PO_4)_6(OH)_2$] as projected down the c-axis. Note the overlap of two pairs of columnar calcium (Ca1, Ca2, Ca3 and Ca4) on the far left and right, and the paired hydroxide groups (OH1 and OH2) in the centre.

Hydroxyapatite falls into a categorization scheme largely based upon its essential chemical elements. This places it under an umbrella group of materials known as apatites. As an apatite, comparisons can be drawn between HA and a wide array of substances with similar mechanical properties, such as tourmaline, beryl, limestone, chlorapatite, bromapatite, and fluoroapatite. In fact, the similarities are so great that, often, other members of this categorization scheme are found in smaller amounts within each natural HA deposit, collectively making up the bone salts. To this end, the generic form of all apatites is defined as being "a crystalline material with a composition of $M_{10}(XO_4)_6Y_2$" , in which M is a metal from Group II, X is either phosphorus or sulphur, and Y is a halogen, or similarly valent chemical compound[41].

Within the limitations of this composition, hydroxyapatite, specifically, is characterized by its chemical formula, $Ca_{10}(PO_4)_6(OH)_2$, and its distinctive 'Ca-to-P' molar ratio of 1.67. This precise ratio also identifies the substance as differing from most other calcium phosphates such as tricalcium phosphate (TCP) and octacalcium phosphate (OCP), both of which, however, are known precursors. In terms of chemical structure, HA consists of a ring of six phosphate ions, bounding a similar ring of six calcium ions (see figure 2.4.2.1). The entire structure surrounds the overlapping hydroxide ions in the center of both these rings. A quartet of calcium ions, in two separate overlapping sites (occasionally referred to in literature as being 'columnar calcium'), completes the crystal structure. The morphology of the HA is therefore hexagonal in nature, and takes on the appearance of spiny to platy crystals (or 'squama') with a Mohs hardness of about five. The crystals themselves have six (100) faces, therefore explaining the interfacial properties and potential derivation from a similar structure found in precursors such as

octacalcium phosphate[42]. It is qualitatively described as having a waxy, slightly off-white appearance, with a space group of $P6_3/M$ and lattice parameters of a = 9.424 Å, b = 9.424 Å and c = 6.879 Å ($\gamma = 120°$, so as to maintain the hexagonal pattern)[43].

Biological apatite is found in its highest concentrations in nature in cortical bone, or in that of the teeth (dentine, enamel, etc.), of most species of bird, animal and fish. This inorganic material accounts for approximately 55%, 70% and 96% of the weight of average human bone, dentine and enamel, respectively[41], with the remaining constituents being cell mass, collagen and other components of the extracellular matrix, not to mention a significant proportion of water.

Non-biological hydroxyapatite, in turn, is often produced *ex vivo* as a high temperature (>900°C) precipitation reaction between orthophosphoric acid and calcium salts. Nevertheless, in a quest to obtain a more economically sound means of producing the apatite, several methodologies have recently come to the forefront, such as pyrolysis[44], sol-gel synthesis[44] and biomimetic synthesis via Simulated Body Fluid (SBF)[43]. Kokubo first proposed the latter method in which he foresaw applications to the biomedical industry. As it stands presently, the biomaterial itself, obtained via this biomimetic route, has found niches in dental implantations, pericutaneous and periodontal devices/treatments, and spinal surgery, but to name but a few[32].

It has long been discussed that the integration of both calcium and phosphate ions into a matrix of hydroxyapatite takes place over several determinate intermediates. The discovery of the mineral itself and the role it played in bone tissues has been known since the late 1920's[42], however, it took several more decades before the process by which

this component materializes was even considered, let alone quantified. In several landmark papers published by W.E. Brown around 1962[45, 46], the necessary evolution of "lower quality" calcium phosphates such as TCP ($Ca_3(PO_4)_2$) and OCP ($Ca_8(HPO_4)_2(PO_4)_4$) into HA became evident, and the nature of the long, spindly, needle-shaped, amorphous hydroxyapatites observed in SEMs and the like became more and more well-known. As the bone requires small amounts of disorganization in its crystals (through the presence of carbonates, other apatites, and the aforementioned calcium phosphate precursors), it is clear to see that, although the term 'HA' is used interchangeably here in this document, variability of things such as Ca/P ratios and crystallinity is quite common in nature. The goal to ascertain idealistic stoichiometry, in this respect, is therefore merely for posterity's sake.

2.5 Biomimetically Synthesized Composites via Simulated Body Fluid

By virtue of its definition, the success of a biomimetic process largely depends on the quality of the pre-existing materials as well as the success of the natural process it is imitating. In the case of hydroxyapatite, this effects itself in the form of a solution known as SBF or simulated body fluid. As discussed previously, Kokubo et al.[8] first identified the usefulness of such a biological process to introduce hydroxyapatite crystals to surfaces and fibres, from metals to ceramics. The necessity behind an adequate biomimetic system in this particular case was driven by existing methods of apatite coating requiring a heat treatment step, creating layers of HA that were different in structure to their bone counterparts, not to mention the possibility of compromising the

foundation material. On the basis of a previous experiment, which included silicate glass and excess Ca ions, the authors proposed that the same apatite coating could be formed on the surface of non-bioactive materials placed in the vicinity of a SiO_2 glass ceramic plate. The glass was formed using CaO, MgO, P_2O_5 and CaF_2, in addition to silicon dioxide, in order to promote the precipitation of HA. The glass was then milled and polished. These glass discs, together with the samples for HA growth, were placed into a carefully prepared solution of bone salts. This fluid became the true champion of this experiment. It contained ratios of salts and a buffer – tris(hydroxymethyl)aminomethane – otherwise known as TRIS, formulated in order to mimic the characteristic ion concentrations of human blood plasma. Substrates used included commercially-fused silica glass, sintered alumina ceramics, slide glass, sintered yttria-stabilized zirconia ceramic, stainless steel (316), various titanium alloys, and several polymers (including poly(methylmethacrylate) and polyethylene). All samples were cut to the appropriate size and then left in 36.5°C solution with the aforementioned nucleating glass for 7 days.

XRD and SEM characterization experiments showed significant apatite crystal growth on the sample surface. The FTIR experiments also confirmed this hypothesis, adding that the bands around 1400 cm^{-1} indicate not only HA, but HA with an appropriate amount of carbonate ions, similar to that found in bone. All the samples appeared to have a significant coverage of the apatite as well; the biomimetic growth was not limited to substrate type or morphology. The experimenters also quantified the mechanism of hydroxyapatite growth; first, the silicate ions in the prepared glass were adsorbed onto the surface of the scaffold. Second, the calcium and phosphate nucleation occurs on the adsorbed silicate ions; and third, the apatite nuclei grow from a reaction with SBF, which

is supersaturated with respect to apatite (HA is only weakly soluble). This concluded that the stability of a substrate in SBF will solely determine its ability to grow HA adequately. As long as the scaffold materials do not dissolve into apatite inhibitors, and the solution maintains its supersaturation, the bone-like material was theorized to continue to grow.

Lickorish et al.[47] proposed a typical collagen-based scaffold for bone graft substitutes using a similar biomimetic process. The scaffold, of significantly high porosity, required a glutaraldehyde vapour to stabilize and cross-link, which, as it is cytotoxic in high enough concentrations, significantly calls into question the viability of a biocompatible product. The collagen was derived from bovine dermal tissue and moulded before being freeze-dried. The resultant discs were then cross-linked using glutaraldehyde vapour. The scaffolds were allowed to grow in a nucleation solution of NaCl, $NaHCO_3$, KCl, K_2HPO_4, $MgCl_2$ $6H_2O$, $CaCl_2$, and Na_2SO_4, buffered with TRIS, for an excess of four days before being removed from solution, washed, and placed in SBF for an additional 14 days, with daily replenishment of solution. The resultant samples were then characterized via SEM, XRD and EDX, concurrently with cell culture experiments to assess cytotoxicity and cell attachment.

The resulting analysis of these samples shows a scaffold with a variety of thermal stabilities based on degree of cross-linking. The samples were also characterized as having a honeycomb surface, comprised of collagen, along with spherical beads/clusters of nano-crystalline HA. The samples also, depending on the degree of exposure to the nucleation solution and SBF, led to some thicker coats of HA, which might, as the author admits, obscure the natural porosity. The Ca/P molar ratios of scaffolds were found to be well within the expected limits for HA (approximately 1.61 ± 0.23).

Cell culture work using L-929 fibroblasts and rabbit periosteal cells on the scaffolds showed a relatively cytocompatible product, with decent proliferation up until the 48th hour. At this point the proliferation rate seemed to trail off in the HA-seeded samples (in comparison to the pure collagenous controls). Nevertheless, the cell morphology was qualitatively considered to have developed as normal.

Oliveira et al.[48] suggested the application of Kokubo's solution to a then uncommonly utilized polymer in the form of starch. The main difference in the proposed procedure was to add a sodium silicate step into the process to effectively augment the necessary nucleation. The backbone for HA growth was obtained as a pre-existing composite blend of starch and ethylene vinyl alcohol, and the samples required microwave baking to sinter and form the necessary architectures.

Once the samples were obtained, they still needed to have the above sodium silicate pre-treatment. This was performed using a commercially available silica gel ($Na_2SiO_3 \bullet H_2O$). Viscosity had to be proportionally adjusted so as to assure permeation of the gel into the fibres as well as maintain the homogeneous and thin layer of sodium silicate gel thought necessary for impregnation. The authors predicted that, with the –OH groups already on the surface, and the natural hydrophilicity of starch, the apatite layer would be nucleated effectively.

Resultant composites had a very rough appearance, showing a cohesive layer of apatite formation, but with fragmentation due to polymer swelling. This was compounded with the presence of several alkali metals (Na, Mg and K) that displaced the Ca in the apatite formation, leading to a lower Ca/P molar ratio than that described elsewhere (1.4 to 1.5,

versus 1.67 expected). This still falls within the range of bone calcium phosphates, lending itself more towards tricalcium phosphate or octacalcium phosphate than HA. XRD confirms this by showing a poorly crystalline HA formation.

Fricain et al.[49] showed promise in their use of cellulose phosphates (otherwise known as phosphorylated cellulose) as biomaterials as well. The premise of their work was not to quantify or justify yields of the material, but rather to ascertain the *in vivo* biocompatibility of the resultant composites. The motivation behind this experimentation was the sudden prevalence of non-phosphorylated cellulose as a biomaterial due to its promotion of cell attachment and proliferation, yet waning mineralization in terms of simulated bone conditions. The authors predicted that the presence of phosphorylated cellulose might beget a better chance of nucleating calcium phosphate growth, in controlled conditions, so as not to cause the decrease of the inherent biocompatibility of the cellulose scaffold.

To produce these results, the scaffold of choice was reconstituted cellulose machined into a disc shape, and phosphorylated in n-hexanol ($C_6H_{13}OH$). The modified material was then dried at room temperature before being pre-treated in $CaCl_2$ solution and inserted into the femoral condyles of four month-old white rabbits. The pre-treatment step also allowed for the samples to be moist enough to prevent excess swelling in vivo. The samples were retrieved after two and six months, fixed in formalin (for histological purposes), and characterized. The extracted cellulose phosphates showed promise in that they were coated by significant amounts of periosteum-like tissue and seemed to be well integrated into the bone structure. Multinucleated ‘giant’ cells were also observed, similar to those found in natural bone as osteoclasts. The phosphorylated cellulose samples had

an added advantage of adherence to the implant site and partial/total incorporation into the surrounding bone tissues. The SEM and concurrent EDX results confirmed the presence of HA with significantly low Ca/P molar ratio (1.06), although the needle-like protrusions that are indicative of calcium phosphate growth were present.

Svensson et al.[50] proposed the use of bacterial cellulose in the growth of cartilage, a tissue known to be closely related to that of bone. As the native mechanical properties of cartilage are very specific and hard to replicate, the existence of legitimate tissue engineered constructs are few and far between. Bacterial cellulose was used, in both a native and chemically-modified form, as a scaffold for the growth of chondrocytes, or cartilage cells. The material properties of the cellulose lend themselves particularly well to the natural collagen-based extracellular matrix, as does the porosity of the nano-scaled fibres. The bacterial cellulose was grown in the form of pellicle disks and purified before being phosphorylated in DMF and phosphoric acid. Samples were then rinsed and lyophilized before being seeded with primary bovine chondrocytes and incubated for up to 8 days. A concurrent cell study also used human articular cartilage cell lines.

Resultant samples were characterized using SEM and confocal microscopy, as well as a mechanical analysis of the unseeded samples. The mechanical testing confirmed that the phosphorylation did not change the Young's modulus or the ultimate tensile strength of the fibrous network to any significant degree. In addition, in testing, the Young's modulus of the phosphorylated bacterial cellulose composite was found to be similar to that of the native articular cartilage.

Cell cultures on the various samples showed that, in the case of non-phosphorylated fibres, chondrocytes took on a relatively more spherical appearance, whereas, in the presence of phosphorylated BC (BC-PO_4H_2), the cells spread out, took on an extended morphology, and adhered more strongly to the surface. The viability and proliferation of cells in the phosphorylated samples occurred more readily and to a greater extent. Collagen (types I, IIA and IIB) expression was also noted in the secondary cell culture experiments with human articular cartilage cells. In addition, TEM analysis showed that the cells migrated partially into the pellicle scaffold.

2.6 Bacterial Cellulose-Hydroxyapatite Composites

Wan, et al.[6] first provided pioneering work in the field of hydroxyapatite-bacterial cellulose composites. In their paper, a basic procedure to procure these fibre composites was outlined, beginning with pellicles formed by *Acetobacter xylinum*, after seven days of growth. The pH was carefully monitored throughout, as it was during the NaOH purification of the resultant cellulose. The pellicle was then phosphorylated to initiate calcium phosphate precipitation. This was performed using 200 mL of dimethylformamide and 15 g of urea. As the solution was heated, a source of phosphate groups – 19 mL of 98% orthophosphoric acid – was added to the flask, along with excess DMF. The solution was allowed to remain this way for about one hour under a blanket of nitrogen gas. This served to add PO_4^{3-} groups to the cellulose backbone and allowed for sites of HA growth. As evidenced in figure 2.6.1, the group proposed a replacement of

the –OH groups on the cellulose with the phosphate groups via their phosphorylation reaction.

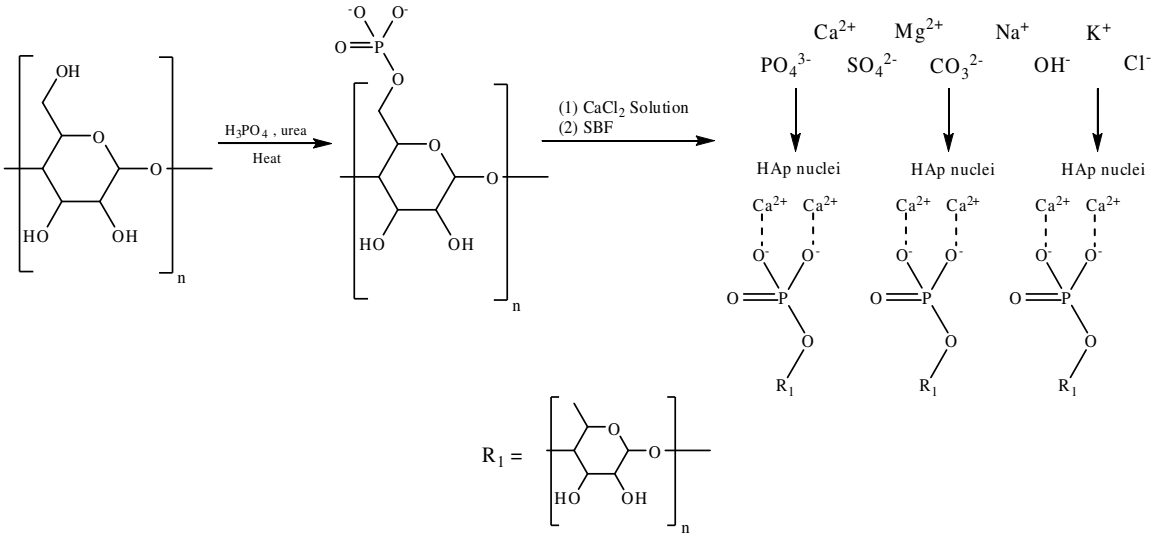

Figure 2.6.1: Proposed means of functional group replacement on bacterial cellulose backbone, as it pertains to the current experiment.

Once phosphorylated, the cellulose pellicles were pre-treated with $CaCl_2$ solution at 37°C, before being mixed with Kokubo's 1.5x SBF solution[8]. The pellicles were then allowed to grow HA crystals in incubation at 37 °C for 7 to 14 days. After this treatment in SBF, the calcium and phosphate groups were found to be further supplemented with those of magnesium, carbonate, sodium, hydroxide, potassium and chloride, all of which can be indicative of an apatitic coating. The results of this experiment show a surface that is rife with HA nano-crystallites. The characterization of the pellicles, using scanning electron microscopy (SEM), X-ray diffraction (XRD) and inductively coupled plasma atomic emission spectroscopy (ICP-AES) indicate a homogenous precipitation of the HA, as well as an abundance of carbonate-containing crystals, mimicking that of natural bone

apatites. The XRD analysis indicated that the HA was of significantly low crystallinity, however, the crystal sizes were on a nanometre scale.

Wan et al., in a subsequent paper published in 2007[7], further extolled the virtues of using bacterial cellulose as a means for growth of hydroxyapatite crystals. The samples were prepared much as before, using bacterial cellulose pellicles grown for a period of 7 days, a NaOH pre-treatment, and a surface modification via $CaCl_2$. The viability of the phosphorylation step was questioned this time, however, as the experimenters used a non-phosphorylated pellicle for a control. The samples were then left in SBF solution for 7 and 14 days, to quantitatively compare the two degrees of growth. Resultant scaffolds were compared via scanning electron microscopy (SEM), transmission electron microscopy (TEM), X-ray diffraction (XRD), Fourier-transform infrared spectroscopy (FTIR) and energy dispersive X-ray spectroscopy (EDX).

As before, the samples were found to have significant amounts of hydroxyapatite growth, with crystallite sizes growing proportional to whether or not the sample was phosphorylated and the length of time grown in SBF. The interesting thing to note, however, was that the use of non-phosphorylated samples appeared to grow crystals as well; however, the clusters of crystals grouped together to form large spheres instead of even coatings on the fibres. In addition, the crystallites themselves had more amorphous regions. Also, the researchers questioned the legitimacy of the procedure when it came to growth of HA within the samples. The pellicles appeared to have a significant decrease in crystallite growth interior to the pellicle when it came to non-phosphorylated samples, implying that the growth of crystals was more of a physical deposition than in samples that were phosphorylated.

These same nano-composite scaffolds were used in subsequent papers in the investigation of proliferation/differentiation experiments with stromal cells [51]. In a series of experiments, the researchers replicated the procedures discussed above for producing BC-HA nano-composites, and then exposed said disks to a cell suspension of stromal cells obtained from human bone marrow (hBMSC). Cells were incubated in alpha minimal essential medium (α-MEM) for up to 132 hours (5.5 days) to ascertain cell viability and proliferation.

SEMs revealed the morphology of the cells attached to the surface of the scaffolds. Although cross-sectional data was not provided, the cells on the surface appeared to tightly anchor themselves to the matrix using their pseudopodia. Proliferation was found to be similarly committal, although statistically significant growth was observed on plain bacterial cellulose controls as well, owing to its known biocompatibility. Alkaline phosphatase, osteopontin, osteocalcin, and bone sialoprotein expressions, all of which are key osteoblastic differentiation markers, were found in the scaffolds of both the control and the nano-composite. Activity was notably higher in the latter and on the topographic surfaces of the samples, as the pore sizes were found to be much smaller than the stromal cells. To this end, it was concluded that there exists a niche for substantial hydroxyapatite-bacterial cellulose nano-composites, especially in the fields of dentistry and orthopaedic oncology.

Despite the apparent success of aforementioned works, there is yet a significant amount of research to be done. Even with arguable evidence to the contrary, there is means to suggest that the resultant hydroxyapatite is merely adhered to the surface of the cellulotic pellicle, and not consistent throughout. In addition, complete coverage of individual

fibres has not been extensively examined, merely composites of compressed or reconstituted fibres tested mainly for strength and viability.

Similarly, the idyllic, albeit extensive, coating of the fibres necessitates a belief that the final product of this experimentation would be a hollow hydroxyapatite fibre which, after extensive pre-treatment, could be filled with growth factors and bone morphogenetic proteins of its own. This could ultimately result in the growth of the natural bone tissue on a substrate that was nano-scaled, three-dimensional (from the perspective of the cells), and easily malleable, with the added benefits of osteoinductive properties.

Chapter Three

3.0 Materials and Methods

3.1 General Procedure

The impetus behind this study was to ultimately procure HA fibres for guided bone regeneration therapy, through a process illustrated in figure 3.1.1, below. The procedure by which this would theoretically be accomplished followed several succinct and determinable steps. First, the bacterial cellulose was to be obtained, using the bacteria *Acetobacter xylinum* (BPR 2001), utilizing a maple syrup-based media. The bacteria would be grown in a shaker incubator for a period of two weeks, at which point it would be washed and purified.

Resultant cellulose was to be treated to replace the hydroxyl groups on the chain with phosphate groups using phosphoric acid. The phosphorylated cellulose would be subsequently pre-treated with calcium ions, displacing the acidic protons. After several days in an environment mimicking the temperature of the human body, the pre-treated cellulose would then be doused in simulated body fluid for two weeks, hopefully resulting in an even and uniform coating of hydroxyapatite on bacterial cellulose fibres. The composite material could then be treated with a cellulase enzyme, which would ultimately break down the cellulose fibres, and leave behind the shell of HA, now in a nanometre-scaled, fibre form. These fibres could consequently be seeded with several growth factors necessary to bone growth, such as bone morphogenetic proteins (BMPs), platelet-derived growth factors (PDGFs), insulin-like growth factors (IGFs) and/or their

analogues. At this point, the fibres would theoretically be sufficient for employment in bone regeneration techniques, as they would fulfill the necessary requirements of structural integrity, mouldability, and biocompatibility.

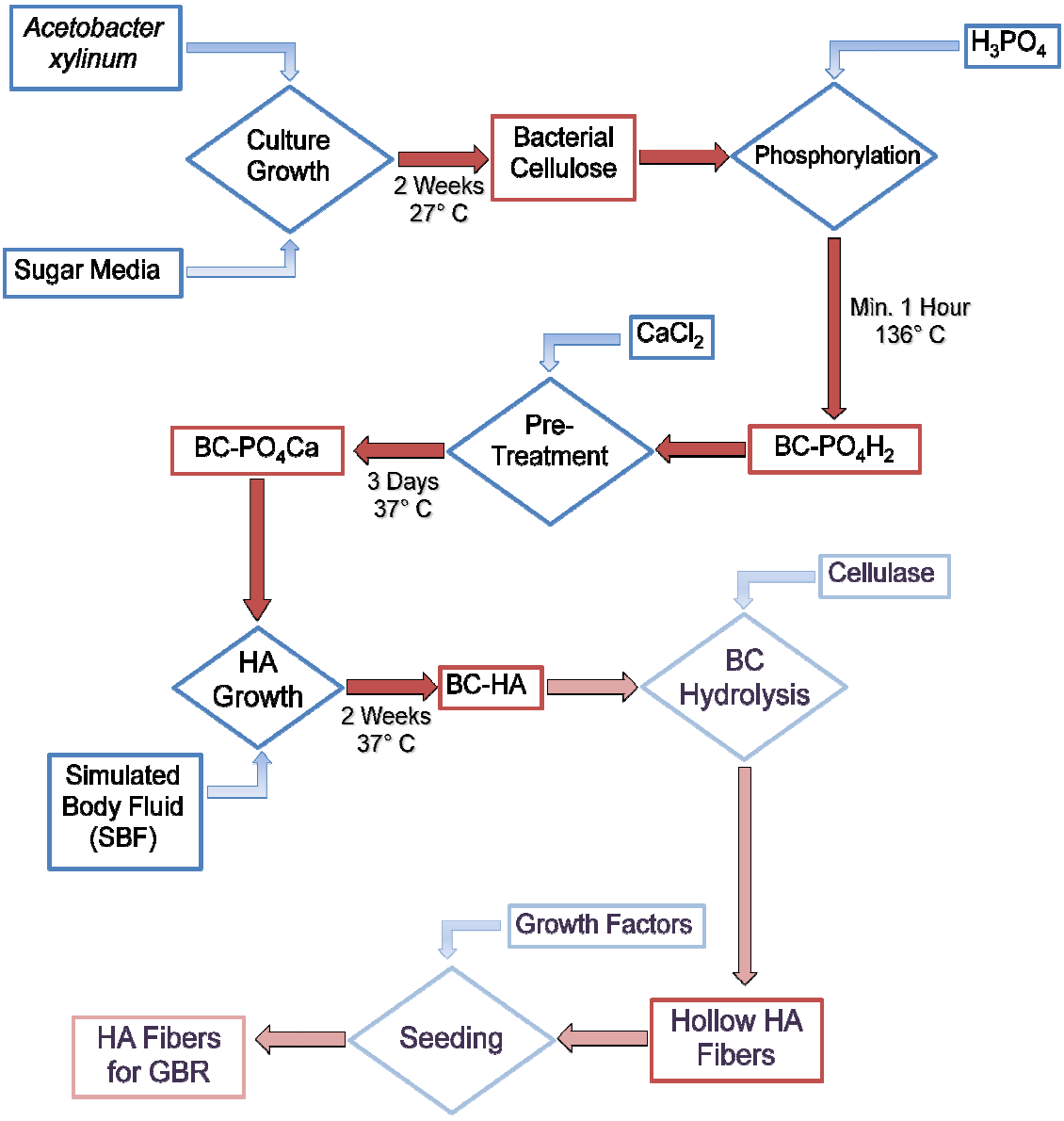

Figure 3.1.1: Flowchart for the production of hollow hydroxyapatite fibres for guided bone regeneration.

In practice, however, not all these steps could be completed for a variety of reasons to be discussed later. Only the BC-HA fibres were actually reproducible *in vitro*. Nevertheless, the biocompatible BC-HA fibres are also applicable as a filler material, with a significant degree of potential for further development.

3.2 Stages of Bacterial Cellulose Growth

3.2.1 Apparatus

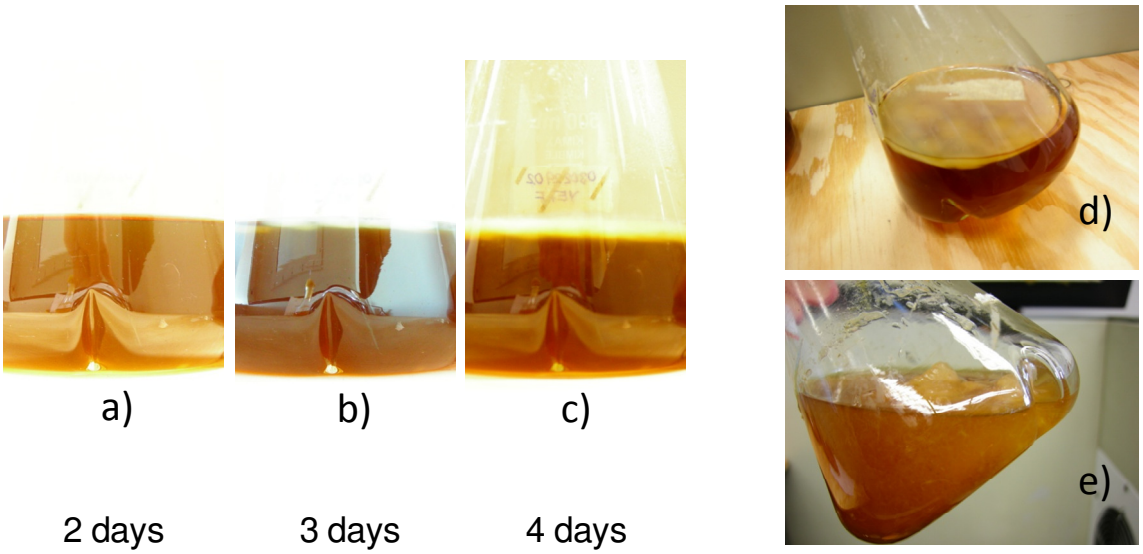

Figure 3.2.1.1: Continuous baffle flask growth of bacterial cellulose over the course of 14 days. Figure shows the development after 2 days (a), 3 days (b), 4 days (c), 7 days (d) and 14 days (e).

Above (Figure 3.2.1.1) is an image of the required apparatus for producing bacterial cellulose (a simple baffle flask and sample of the bacteria). In the first three images (a-c), the pellicle growth is observed pressing downward in the baffle flask. Subsequent images

highlight the pellicle after 7 days of incubation (d), and the BC growth, as a large mass, once the shaker was employed for an additional 7 days (e).

3.2.2 Procedure

The procedure for obtaining bacterial cellulose is derived from that of Joseph[1] and adapted by Guhados[35] and Zeng[52]. These sources were instrumental in proposing the specialized aqueous media for the re-growth of *Acetobacter xylinum* under static/shaken conditions as follows:

Table 3.2.2.1: Reagents for *Acetobacter xylinum* growth medium

Order of Addition	Reagent	Quantity		
		Fructose-based media (250 mL)	Fructose-based media (per litre)	Maple syrup-based media (250 mL)
1	Deionised H_2O	250 mL	1 L	243.5 mL
2	Maple Syrup	-	-	6.5 mL
3	Fructose	5 g	20 g	-
4	$(NH_4)_2SO_4$	0.825 g	3.32 g	0.825 g
5	KH_2PO_4	0.25 g	1 g	0.25 g
6	$MgSO_4 \bullet 7H_2O$	0.0625 g	0.25 g	0.0625 g
7	Trisodium Citrate	0.105 g	0.42 g	0.105 g
8	Citric Acid	1.1 g	4.4 g	1.1 g
9	Yeast Extract	10 g	40 g	10 g

For a 250 mL sample, components 2 through 8 in the above table were dissolved, in order, in a 500 mL baffled shaker flask filled with 150 mL of the deionised water.

Assurances were made, each occasion, to dissolve the entirety of the previous component before the addition of the next.

In a smaller flask (~125 mL), the yeast extract alone was dissipated in the remaining 100 mL of DI water for several minutes, using a magnetic stirrer. Both flasks were then autoclaved at 121 °C and 20 psig for 15 minutes. After sterilization, the two flasks were mixed aseptically in a laminar hood. It was determined to be necessary to isolate these two flasks in order to prevent the degradation of the media via side reactions from autoclaving nitrogen with other components (such as the Maillard reaction).

The flasks were then allowed to cool back down to room temperature overnight before seeding with sample of liquid culture. The optimum amount of sample was ascertained to be 6% v/v of liquid from a pre-cultured sample flask[52] – approximately 15 mL. In the case of re-growth from plates, first 5 mL of media was poured off into a sterile test tube and seeded with a colony from the agar plate before scaling up to the 250 mL flask. This was done in order to prevent shocking the bacterial culture. Samples were then kept in the shaker incubator at 27 °C for a minimum of 12 days, and as much as three weeks. If employing shaken cultures, 2-3 drops of Antifoam 289 were added to the flask before incubating. Growth of cellulose was found to work best if samples were allowed to sit in static culture for a period of 7 days before shaking was started (140 RPM), as it is thought to be conducive to the growth kinetics[1].

In order to produce pellicles, samples were left undisturbed in static culture. A 1 cm thick pellicle was achievable after approximately one week. In both shaken and unshaken

conditions, growth of cellulose was visible after 2-3 days (4-5 days if re-growing from plate culture).

Once obtained, the pellicles were sent through a rigorous treatment and purification step. The flasks were autoclaved once again to arrest the growth of the bacteria. The flasks were allowed to cool, before being homogenized via a laboratory blender for a period of no longer than 40 seconds. This was done to break up the cellulose pellicle and free the fibres; it has been determined in literature that this has little to no effect on the fibre length or crystallinity[53, 54]. After homogenization, 100 mL of 1 M NaOH solution (for a 250 mL sample) was added. The resultant mixture was then boiled, at a temperature of 90 °C, for 90 minutes, during which the cell mass was ruptured and removed from solution.

Once treated in the alkaline solution, the cellulose fibres were isolated by centrifugation in a DuPont Sorvali® RC-5B refrigerated centrifuge for 20 minutes at 5000 RPM. The supernatant was then poured off, more deionised water was added and the process repeated 5 times, until the liquid ran clear. Once the last centrifugation was complete, the cellulose fibres were then retrieved, bottled and stored in a refrigerator. Weight analysis of the concentrated fibrous mass showed a dry cellulose weight of approximately 0.013 g/mL of sample; although this value varies slightly from batch to batch, this was the ascertained average, and was used exclusively in calculations.

3.3 Phosphorylation

3.3.1 Apparatus

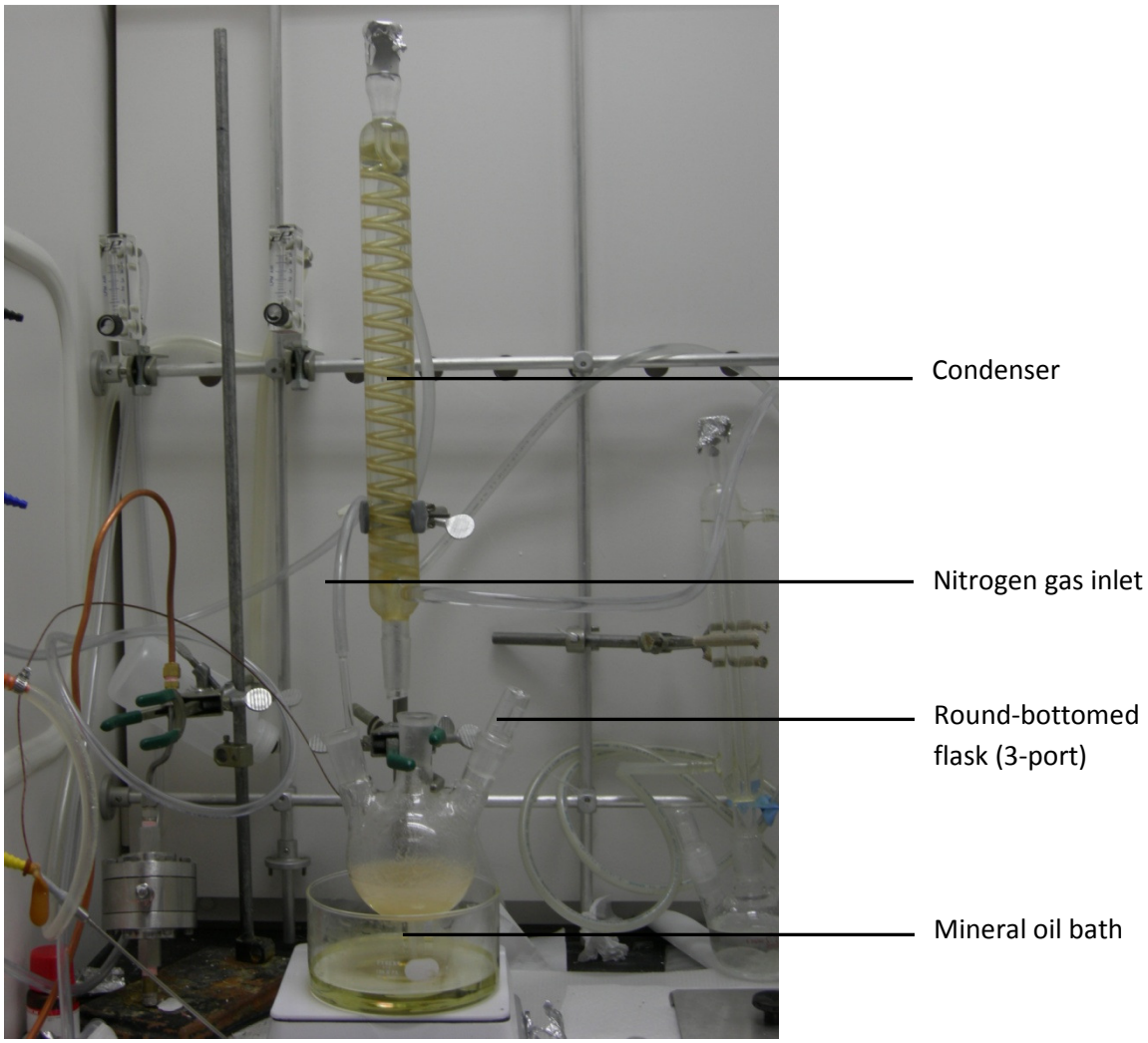

Figure 3.3.1.1: Experimental set-up for the phosphorylation of bacterial cellulose.

3.3.2 Procedure

In order to phosphorylate the resultant fibres, the water remaining in the cellulose first had to be solvent exchanged with dimethylformamide, an aprotic solvent. This was done in order to facilitate the addition of phosphate groups without side reactions from residual

water. The DMF (~50 mL) was added to small quantities of cellulose and shaken to distribute the fibres evenly; the solution was centrifuged, the supernatant poured off, and more DMF was added. This was done 5 times in order to assure complete solvent exchange.

50 mL of resulting cellulose mixture was then added to a three-port round bottomed flask in addition to 15 g of urea and 150 mL of DMF. The flask was placed in a bath of mineral oil, and equipped with a condenser and a nitrogen inlet in order to prevent airborne contamination. The cellulose was then raised to a temperature of 110 °C, at which point a solution comprised of 32 g of orthophosphoric acid dissolved in 50 mL of DMF was added to the flask. The mixture was raised to 136 °C, and left to react for up to 8 hours. The entire apparatus was allowed to cool to room temperature – maintaining a nitrogen blanket – before being removed from the fume hood. The now-phosphorylated cellulose was rinsed with deionised water, centrifuged, and stored at 5 °C until required.

3.4 Pre-treatment

Pre-treatment of the phosphorylated fibres took place with the addition of excess 0.1 M solution of $CaCl_2$ (or $Ca(OH)_2$ – see section 4.6.2). 100 mL of this pre-treatment solution was added to a sample of cellulose, and left to incubate for three days at 37 °C. Additional solution was added every day, in an attempt to maintain saturation, and pH was tested daily to ensure it was approximately 9. After pre-treatment, fibres were once again centrifuged and immediately placed in SBF.

3.5 Hydroxyapatite Growth

Kokubo et al. outlined the growth of hydroxyapatite crystals on substrates in several papers[8, 55, 56]. The most notable of these is the development of an acellular simulated body fluid containing inorganic ion concentrations comparable to that of human blood plasma. The idea behind this innovation is to reproduce formation of apatite on bioactive materials *in vitro*, by using a solution of several major ionic constituents of bone. This solution is supersaturated in relation to apatite, which alone is relatively insoluble.

The aforementioned fluid was similarly applied to the production of apatite coatings on various materials under biomimetic conditions. Ion concentrations of the simulated body fluid (as in comparison with that of human blood plasma) are listed in table 3.5.1 below.

Table 3.5.1: Ionic concentrations in regular (1.0x) SBF and human blood plasma

Ion	**Concentration (mmol/L)**	
	Simulated body fluid (SBF)	**Human blood plasma**
Na^+	142.0	142.0
K^+	5.0	5.0
Mg^{2+}	1.5	1.5
Ca^{2+}	2.5	2.5
Cl^-	147.8	103.0
HCO_3^-	4.2	27.0
HPO_4^{2-}	1.0	1.0
SO_4^{2-}	0.5	0.5

(adapted from Kokubo et al., 1990[8])

In order to obtain these specific quantities of ionic components, a precise amount of each reagent must be added to the solution, and care was taken to assure the accuracy of these factors. Variables such as buffering capacity and pH can greatly affect the usefulness of the SBF. To this end, the pH of SBF must be adjusted to 7.25 (or 7.40, in certain conditions) at 37 °C, and maintained by using 50 mM tris(hydroxymethyl)aminomethane ($(CH_2OH)_3CNH_2$) buffer and HCl, as needed.

3.5.1 Preparation of SBF

The following reagents were procured from their described sources and used to produce all batches of 1.5x SBF (in the volumetric increments of 1 L). Solutions of SBF other than 1.5 times the concentration in human blood plasma could also be generated (2x, 5x, etc.), however, crystallite formation would be significantly harder to control, and crystals could possibly be too large to be applicable[57].

Table 3.5.1.1: Reagents for Kokubo's simulated body fluid (1.5x)

Order of addition	Reagent	Description	Amount
1	H_2O	Deionised and Reverse Osmosis filtered	750 mL
2	NaCl	99.5%, Sigma-Aldrich	11.994 g
3	$NaHCO_3$	99.5-100.3%, Sigma-Aldrich	0.525 g
4	KCl	99.5%, Sigma-Aldrich	0.336 g
5	$K_2HPO_4 \cdot 3H_2O$	99.0%, Sigma-Aldrich	0.342 g
6	$MgCl_2 \cdot 6H_2O$	98.0%, Sigma-Aldrich	0.458 g
7	1 M HCl	87.28 mL of 35.4% HCl (Sigma-Aldrich) is diluted to 1000 mL with volumetric flask	60 mL
8	$CaCl_2$	95.0%, Sigma-Aldrich Used after drying at 120 °C for more than 12 hours	0.417 g
9	Na_2SO_4	99.0%, Sigma-Aldrich	0.107 g
10	$(CH_2OH)_3CNH_2$	99.9%, Sigma-Aldrich	9.086 g
11	1 M HCl	As above (Reagent 7)	To adjust pH
12	H_2O	As above (Reagent 1)	To adjust volume

(adapted from Ohtsuki, 2006[57])

Kokubo's simulated body fluid is a meta-stable solution containing both calcium and phosphate ions concentrated with respect to the stoichiometric formula of human blood plasma hydroxyapatite. In addition, it is supersaturated with respect to apatite solubility. Therefore, several meticulous steps in *preparing* the SBF solution were also deemed necessary in order to prevent premature precipitation.

3.5.1.1 Cleaning of glassware

All of the storage bottles, flasks, pipettes, beakers etc. first needed to be washed extensively with dilute hydrochloric acid solution and purified water. Contamination would potentially disrupt the delicate balance of the solution and cause improper formation of HA crystals.

3.5.1.2 Creation of SBF

The first reagent, 750 mL of reverse osmosis-filtered, deionised water, was poured into a 1 L glass Erlenmeyer flask. This was continuously stirred and the temperature maintained at 36.5 °C via a hotplate and digital thermometer. The remaining chemicals (up to the sodium sulphate in the above table) were added slowly to the flask in the order that they appear, with constant stirring after each addition to ensure complete dissolution. Remnants were washed off of weighing dishes with excess reverse osmosis-filtered, deionised water to ensure accuracy of concentration. The addition of the seventh reagent (the hydrochloric acid) was performed slowly so as to ensure that no pH 'hotspots' were created, which might inadvertently cause the premature precipitation of the solution.

3.5.1.3 Adjustment of pH

The pH meter was first calibrated with fresh buffer solution to maintain sterility. The TRIS-buffer (reagent 10) was added to solution. After addition, the temperature was once again checked to ensure that it had not fluctuated too wildly. When it was steady at 36.5 °C, the electrode of the pH meter was placed into solution and the pH was measured. Depending on the resultant value, additional HCl was titrated into the solution via pipette

until the pH reached 7.25, or 7.4 if the material was not conducive to HA crystallite attachment. After adjusting the pH, the entire flask contents were transferred into a clean, 1000 mL, volumetric flask. The insides of the Erlenmeyer flask were rinsed repeatedly with more purified water in order to maintain concentration. Purified water was then added to the solution, adjusting the total final volume up to 1 L. The flask was then stoppered, shaken vigorously to mix the contents, and left under the fume hood to cool down to room temperature before being bottled. If the volume of solution changed dramatically whilst cooling, additional water was added to maintain the volumetric level.

3.5.1.4 Storage of SBF

The solution was then transferred a 1 L polyethylene bottle and stored in a refrigerator for several days, at a temperature of 5 °C, before being used. The stability of the solution obtained was examined (see section 3.5.1.5) once every couple of days.

3.5.1.5 Testing for Stability

Before use, 50 mL of the solution was placed into a well-cleaned glass vial with a stopper and left in a Revco® Ultima II incubator, set at 36.5 °C. After 3 days, the solution was checked for flecks of precipitated HA. If precipitation was present, the batch was determined to be unstable and therefore completely unusable. As the solution was supersaturated, any bottles in which early precipitation occurred were immediately disposed of and could not be used in further experiments. This was done in order to prevent the further precipitation of HA in subsequent experiments, as the presence of microscopic crystals on the surface of the bottles would immediately nucleate more.

For the production of the hydroxyapatite nano-fibres, the cellulotic materials (pellicles or fibres) were phosphorylated, pre-treated with Ca ions, and then exposed to 50 mL of 1.5x SBF. The mixture was stored in a glass container in an incubator set at 37 °C for two weeks. As the cellulose fibres could not be adequately removed from solution without potentially disrupting HA growth, the solution needed to be topped up every day to maintain concentration. Measurements were made in an attempt to assure constant pH throughout the experiment.

After a period of 14 days, the cellulose was removed and the BC-HA composites were characterized via SEM, EDX, FTIR and XRD.

3.6 Characterization

3.6.1 Fourier Transform Infrared Spectroscopy

FTIR utilizes principles of infrared energy absorption (or transmission) in certain chemical bonds to ascertain the nature of those bonds. In addition, as the elements have a significant effect on the bond structure, FTIR can often help classify additional parameters of the substance, such as entire functional groups, crystallinity and concentration.

In this experiment, samples were characterized using a Bruker® Vector 22 FTIR with Attenuated Total Reflectance (ATR) using a Diamond/ZnSe crystal and 64 scans, minimum. The samples were either in solid (pellicle or powder) or liquid (loose fibre, suspended in water) forms, depending on the nature of the comparison.

3.6.2 Scanning Electron Microscopy

SEM uses a high energy electron beam, in a particular pattern known as a raster scan, in order to produce high quality images of the surface of a given substance. Using an adequate scanning electron microscope, characteristics such as material fibre diameter and extent of deposition, in addition to a multitude of qualitative observations, can be found.

This experiment employed the use of a Leo (Zeiss®) 1530 scanning electron microscope, using an accelerating voltage of 2 kV. This voltage was necessary to achieve the highest resolution possible without affecting the integrity and condition of the fibre samples.

3.6.3 Energy Dispersive X-ray Spectroscopy

EDX employs electromagnetic radiation in the form of emitted X-rays to analytically characterize matter. By bombarding a sample with a charged beam (usually electrons, although, some proton and incident X-ray variations are in existence) and detecting the resultant radiation, the electrons in energy shells around a given atom are forced to 'jump' to lower energy adjacent shells, resulting in a characteristic emission that is specific to a given element. Using relative concentrations and intensity of these peaks, the quantity of each element may also be obtained, in relation to its associated chemical components.

EDX was performed in the lab via the Leo (Zeiss®) 1530 EDX attachment, employing Oxford Instruments INCAEnergy™ X-ray Microanalysis software.

3.6.4 X-ray Diffraction

XRD utilizes X-ray beams, which, when striking incident to a sample surface diffracts (breaks up) into a variety of reflected points. These points, when taken over a wide range of incident angles, provide insight into the chemical bond structure of the sample in question, and similarly, can provide insight into the crystallinity of a sample; a characteristic which is largely specific only to certain isomers of a compound.

XRD was performed with the utilization of a Rigaku® MiniFlex™ X-ray diffractometer with CuKα radiation, generated at 30 kV and 15 mA. This analysis was run over an incident angle range of 5 to 80°.

Chapter Four

4.0 Results and Discussion

4.1 Overview

The successful creation and development of a novel biomaterial for bone tissue repair rests largely upon the extensive investigation into each of its necessary components. Although cellulotic biocomposites consisting of hydroxyapatite have been at the forefront of technology for several years[49, 58, 59], studies on the combination of said material with individual fibres of bacterial cellulose were not conducted. To this end, the major factors of the current experimentation are the bacterial cellulose substrate itself, the calcium pre-treatment media, the phosphorylation process specific to BC, and the SBF/calcium phosphate formulations that will nucleate and cultivate newly formed HA crystallites. Significant development and characterization can occur at each level, and would ideally contribute to a thicker coating of hydroxyapatite, a finer and more crystallized substrate, a higher purity of the complex, and a more malleable and apt scaffold material, all of which ultimately result in a higher biocompatibility. The innate biomimetic nature of the SBF, in addition to the potential usefulness of increasing the salt concentrations from one to five times that of the normal composition, has already been examined in numerous perspectives. As such, factors such as the use of varying formulations of bacterial cellulose growth media, the effect of bacterial cellulose pellicles versus individual fibres and the employ of alternative sources of calcium ions (as opposed to the typical calcium chloride solution) for the pre-treatment experiments will

instead be evaluated. In addition, the effect of diverse phosphorylation times, and the applicability of pre-treatment steps in the general process will be explored.

4.2 Production of BC using Maple Syrup as a Carbon Source

Prior to the investigation into the production of a bacterial cellulotic composite biomaterial, the initial aim of this research was to explore the production of its key components. Notably, a major goal was to investigate the media composition suitable for producing bacterial cellulose via fermentation, utilizing a six-carbon 'simple' sugar; this traditionally implies fructose (or sometimes glucose) as a carbon source (see figure 4.2.1). It was therefore postulated that the production of cellulose could be increased or otherwise affected by varying the choice of specific sugar.

In order to facilitate definitive experimentation, distinctly different media formulations were incorporated. These media, although employing identical trace element compositions and nitrogen sources, significantly differed in their carbon source. The rationale behind this change was derived from work by Yezza et al, who, in 2007[60], proposed an innovative fermentation media. The research utilized sap from maple trees as a novel carbon source, providing the media with carbohydrates in the form of sucrose (89%), glucose (5.5%) and fructose (5.5%)[52]. With this research in mind, both a formulation using maple syrup (sucrose, amongst other simple sugars), and one employing a traditional fructose-based media, were investigated.

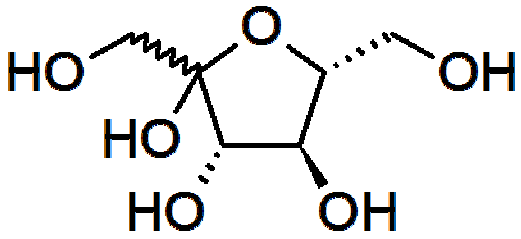

Figure 4.2.1: Chemical structure of fructose

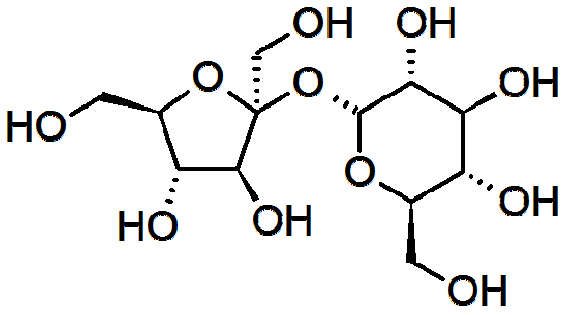

Figure 4.2.2: Chemical structure of sucrose

As discussed in a paper by Zeng et al. in 2011[52], the presence of alternative simple sugars in the media does not affect the production of the cellulose to any significant degree. In fact, the combination of the three sugars discussed above was found to produce more bacterial product than sucrose or glucose alone. In the case of sucrose, the two rings were broken down into fructose and glucose, before being reformed into a cellulose chain[60]. This effectively means that the bacteria can metabolize just about any simple six-carbon sugar to produce cellulose as a metabolic by-product. Literature reports that this is done via the Krebs cycle or the pentose phosphate pathway in conjunction with gluconeogenesis. It is similarly reported by Ross et al., in 1991 that this formation does not affect the anabolic processes associated with the bacterial growth, including, but not limited to protein synthesis[61], implying that resultant cellulose or its predecessors do not affect the growth or survival of the bacteria to any significant degree.

Based on the aforementioned work, and employing a ratio of 1.25 mL of maple syrup to each gram of required fructose-equivalent, the following results were obtained. The average yield of cellulose in the case of the fructose-based media was found to be

3.50±0.12 g per litre of media, compared to that of the maple syrup media which was found to be 3.14±1.07 g per litre, as seen below in figure 4.2.3.

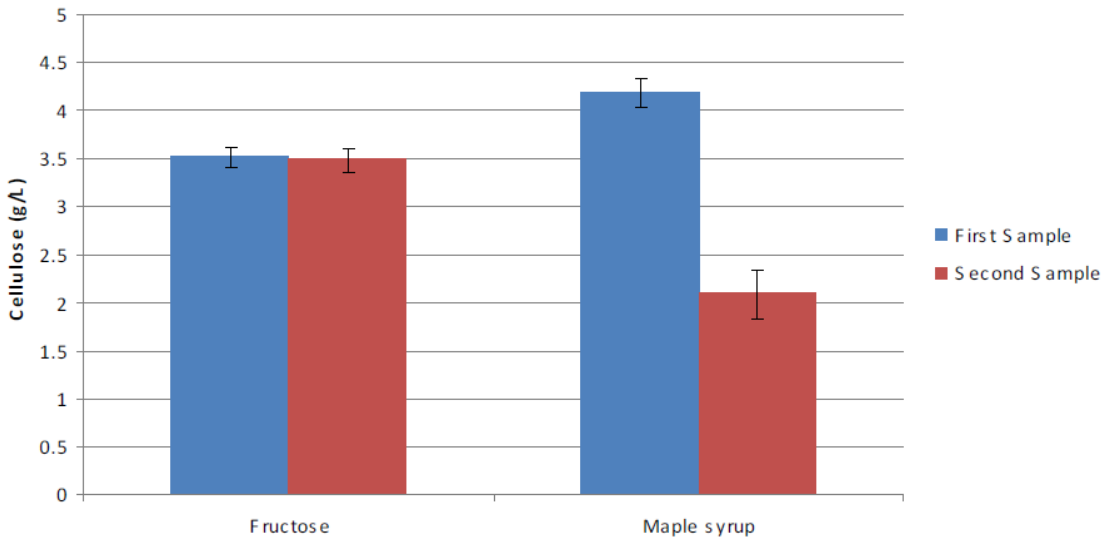

Figure 4.2.3: Weight analysis of dry cellulose per litre of prepared growth media

These results were obtained over the course of two completely independent batches of media – formulated from independent sources of maple syrup - with six flask samples cultivated from each batch. This indicates that the fructose media is much more consistent and reliable, despite the fact that the potential yields for maple syrup media appear to be much higher. Understandably, this conclusion is not hard to believe if one considers that the maple syrup is, in itself, an inconsistent fluid with a large degree of variability in its composition. This assertion is further supported by the fact that the syrup had to be pipetted into the flask based on the average concentration of sugars present, as calculated based on predicted percentage compositions, provided by the manufacturer.

Each source of maple syrup, being treated independently, was likely obtained from different trees and/or during different time periods, lending an element of uncontrollability to the procurement of any maple syrup standard. As a result, the high variation in the amount of product can be credited to the inherent inconsistency of the syrup, as well as the relative uncertainty in the sugar concentration as reported by the maple syrup farmer.

One major effect that the maple syrup-based media could have, however, is the possible increase of supplementary ions and cursory carboxylic acids, which, in the case of long-term agitated culture conditions (such as those found in bioreactors or shake flasks), may ultimately add to the cellulose yield. The immediate effects may appear to be marginal, but previous research[1, 52] has indicated that the addition of miniscule amounts (i.e. less than 0.003 g/mL of media) of polyacrylamide, green tea powder, acetic acid, or ethanol could have a significant effect on the growth kinetics of the bacterium over longer reaction times. Ultimately, this would have the added effect of increasing long term bacterial cellulose growth in agitated production conditions.

4.2.1 BC Characterization

4.2.1.1 SEM Characterization

SEM characterization of the resultant cellulose, as seen below in figures 4.2.1.1 and 4.2.1.3, shows similar morphologies and average fibre diameters between samples produced in maple syrup and those produced in fructose.

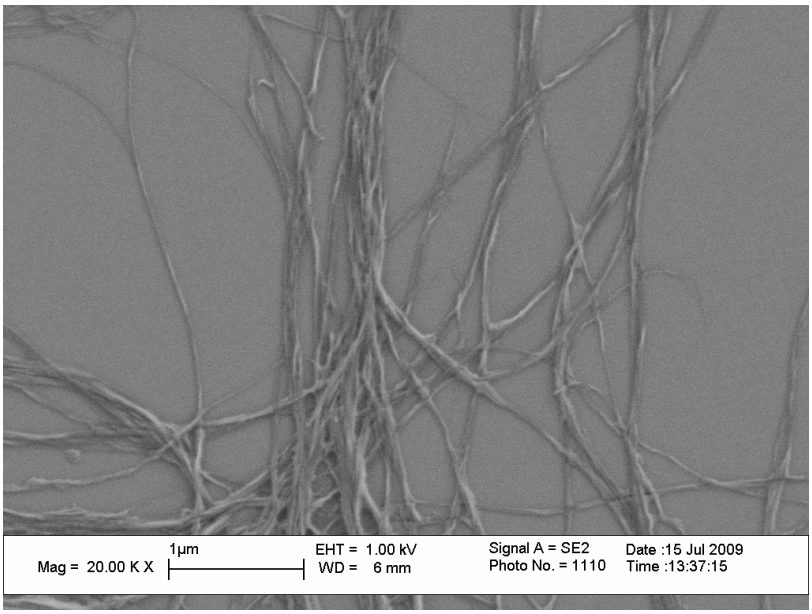

Figure 4.2.1.1: SEM of fibres formed from fructose media

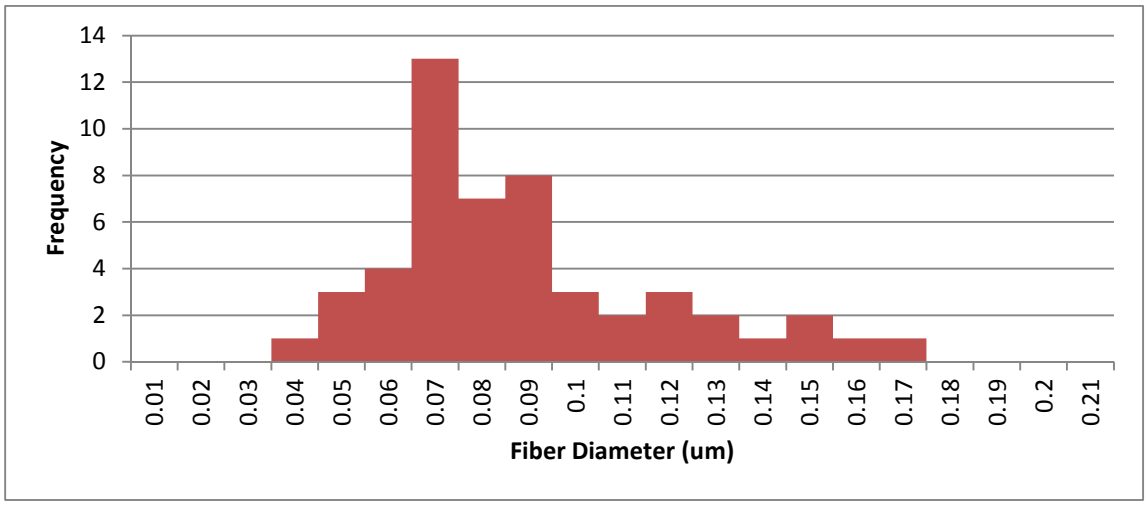

Figure 4.2.1.2: Fibre diameters for fibres formed from fructose media

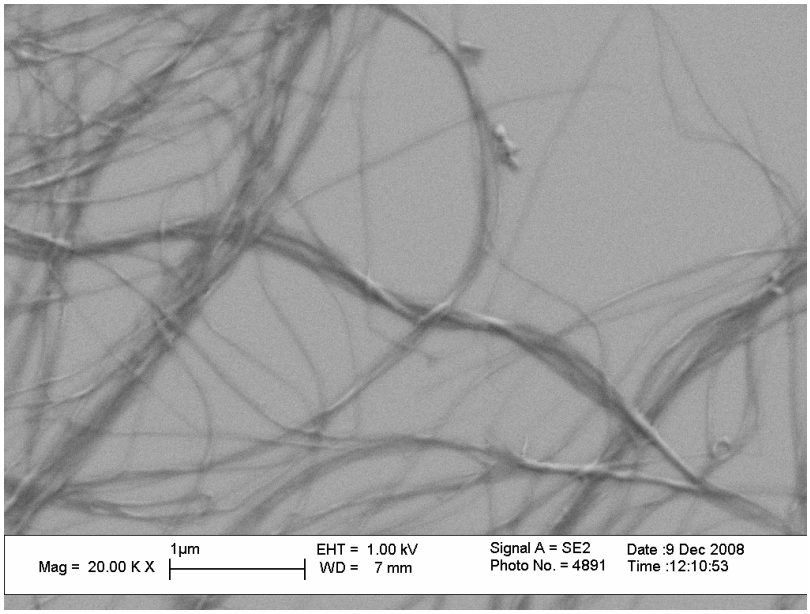

Figure 4.2.1.3: SEM of fibres formed from maple syrup based media

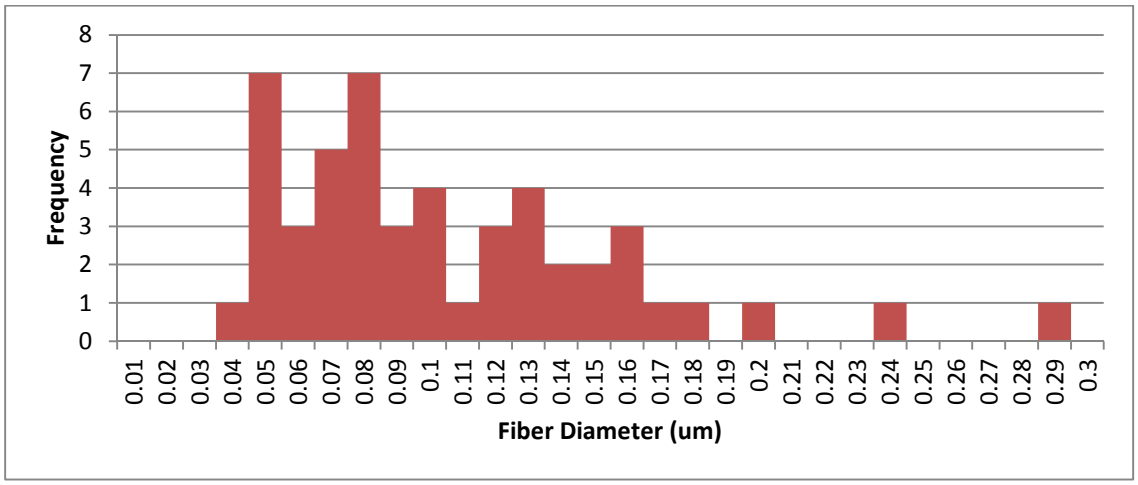

Figure 4.2.1.4: Fibre diameters for fibres formed from maple syrup

According to the fibre diameter distributions shown above (figures 4.2.1.2 and 4.2.1.4), the fibre morphology and dimensions are comparable, irrespective of the media composition. In fact, whilst the fibre diameters in the fructose sample are 83.9 ± 3.0 nm,

those in the maple syrup sample are 100.1 ± 51.7 nm, values that have no statistically significant difference.

4.2.1.2 EDX Characterization

Elemental composition of the BC produced was determined via EDX, confirming the presence of carbon and oxygen from hydrocarbons, and is summarized in Table 4.2.1.1 below. In both the maple syrup and fructose cases of bacterial cellulose, the carbon content was found to be around 55% of the atomic weight – excluding hydrogen – of the sample (52.89 ± 2.70% and 54.64 ± 0.40%, respectively), with the remainder of the sample predominantly comprised of oxygen and negligible concentrations of sodium from the purification. As the molecular formula for cellulose is $(C_6H_{10}O_5)_n$, this is legitimate based on idealized stoichiometry. The atomic ratio of carbon-to-oxygen of the fructose- and maple syrup-based samples was hence determined to be 1.53 ± 0.13 and 1.56 ± 0.68, respectively. Although the C/O ratio in cellulose should be 1.2 (based on the above stoichiometry of six carbon atoms to every five oxygen atoms), similarities between these results at least indicate a parallel in chemical composition. Discrepancies are likely due to unavoidable contamination from carbon in the EDX chamber.

Table 4.2.1.1: Summary of EDX results for BC

	Fructose-based		**Maple Syrup-based**	
	Average (%)	**SD (+/-)**	**Average (%)**	**SD (+/-)**
Carbon	54.64	0.40	52.89	2.70
Oxygen	35.84	3.29	37.10	8.57
C/O ratio	1.53	0.13	1.56	0.68

These results altogether serve to indicate that there is little to no significant difference in the stoichiometry, quality and amount of cellulose produced with regards to variable media compositions. Nevertheless, for simplicity and repeatability purposes, fructose-based samples of cellulose were employed for the remainder of this experiment, although it is strongly encouraged that maple syrup-based cellulose samples be pursued as a venue for research in the future, due to the potentially high yield of product demonstrated above.

4.3 Phosphorylation of BC

In order to phosphorylate the fibres, a mixture of orthophosphoric acid and urea was employed, using dimethylformamide as a solvent, held under nitrogen blanketing (see Materials and Methods). As the concentrations of the subsequent reactants in SBF were fixed by the required ratios of the phosphate involved in HA crystallites ($Ca_{10}(PO_4)_6(OH)_2$), and by the desired amount of HA crystal, the phosphorylation step was seen as a means of improving the odds of hydroxyapatite attachment and a full cohesive coverage of the fibres. Therefore, the effect of various phosphorylation reaction times was studied to determine the conditions for an optimally coated fibre. Traditionally, by adopting a procedure from an aforementioned work reported by Wan et al.[6], a phosphorylation time of two hours was used, largely based on the principles outlined by Fricain et al.[49] and Suflet et al.[62]. The aim of this work was to maximize the degree of phosphorylation, in comparable textiles, whilst simultaneously minimizing reaction time. The resultant phosphorylated cellulose fibres were subsequently treated with a Ca

pre-treatment step (calcium chloride solution) and SBF formulations (1.5x and 5x) to varying degrees of success.

To investigate the effect of reaction time on the phosphorylation reaction, a series of four data points, corresponding to 1, 2, 4 and 8 hours of phosphorylation, was proposed. It was unpredictably observed that longer phosphorylation reaction times corresponded to more cellulose appearing to "precipitate" at the bottom of the container, preventing the full removal of the sample. In fact, samples left reacting for 8 hours or more could not be removed from the flask at all, and had to be discarded through significant washings. This could be associated with a larger degree of substitution of hydroxide groups on the cellulose chain, leading to increased solubility of the phosphorylated products, and/or degradation of the sample into lower molecular weight fragments (nano-crystalline cellulose), which then fused to the glass, rendering them unusable. Nevertheless, samples with reaction times of 1, 2 and 4 hours were further scrutinized for data.

4.3.1 Characterization of Phosphorylated BC

To characterize the products of reactions at 1, 2 and 4 hours after initial exposure, the samples were examined via SEM, FTIR and EDX.

4.3.1.1 SEM Characterization

SEM images of the phosphorylated BC samples in question were used for diameter measurements employing image analysis software (ImageJ), and compared to that of untreated bacterial cellulose fibres. This was done to ascertain relative fibre diameter and

morphology, and to qualitatively interpret the fibre structure. Results are shown, as follows, in figures 4.3.1.1 and 4.3.1.2.

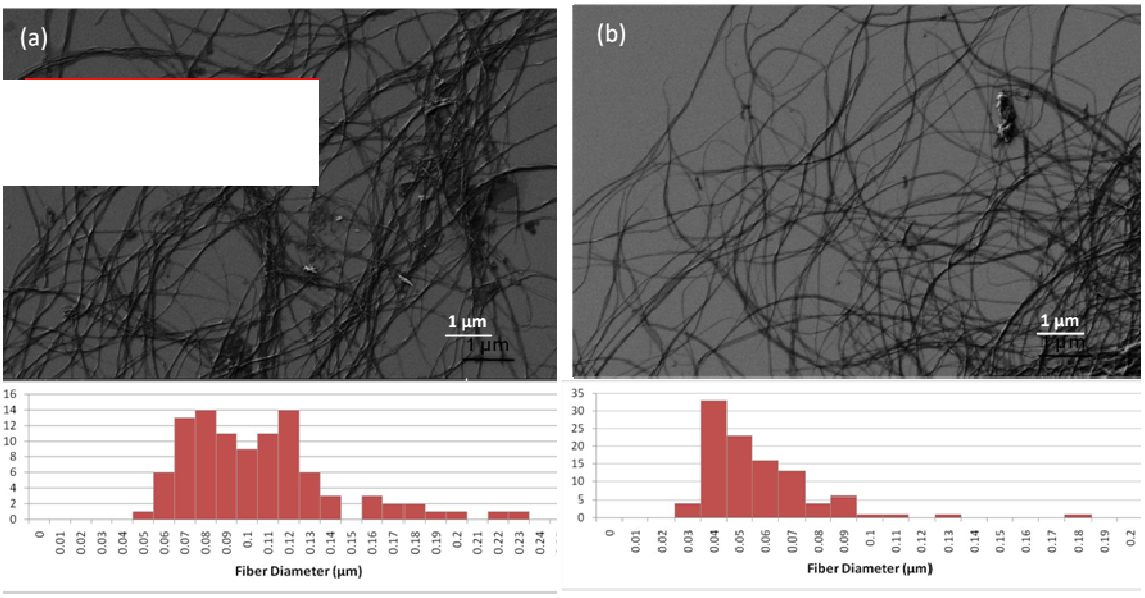

Figure 4.3.1.1: Scanning Electron Microscopy (SEM) outputs of a) untreated BC and b) 2 hour phosphorylated BC. Inset; histograms of fibre diameter (more detailed graphs shown below).

From the above figure, it can be seen that there is a decrease in the average fibre diameters, and a potential shift of the fibre size distribution, accompanying the phosphorylation reaction. Samples that had undergone any amount of phosphorylation possessed a mean fibre diameter of 56.7 ± 16.5 nm; those that had not, maintained a much larger, 105.5 ± 26.0 nm fibre diameter, seen above. This occurrence is likely due to the presence of the added phosphate groups effectively forcing the fibres apart (charge repulsion on the fibrils) from their intertwined quaternary structure, resulting in the appearance of much finer fibres. Known as ‘debundling’, the phenomenon implies that phosphorylation not only provides adequate reaction sites for the addition of calcium

ions, but also provides the previously unanticipated added benefit of increased smaller fibre diameter, higher surface area-to-volume ratios, and a better "three-dimensional" structure for micron-sized cell attachment and proliferation.

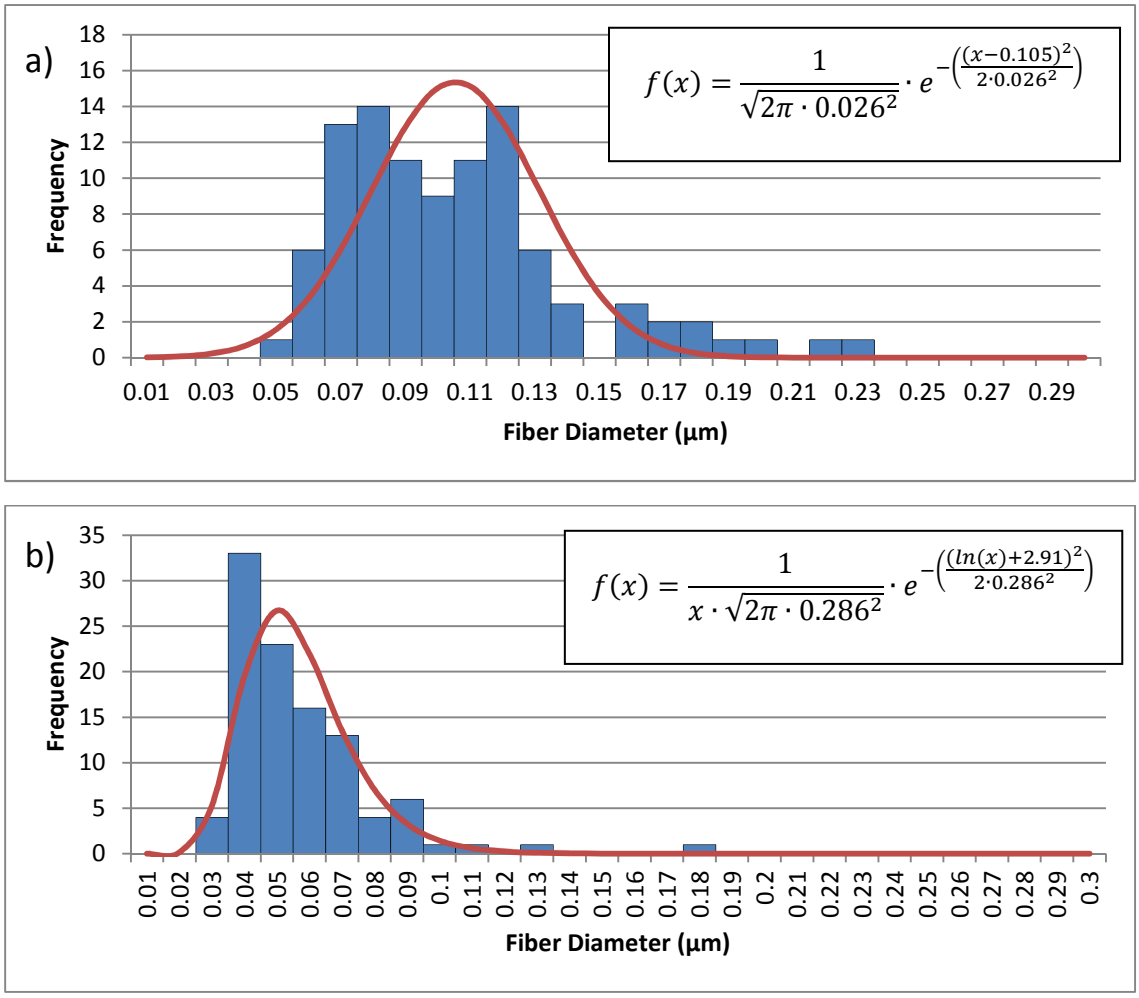

Figure 4.3.1.2: Statistical distribution of fibre diameters in both a) bacterial cellulose (105.5 ± 26.0 nm) and b) 2-hour phosphorylated BC (56.7 ± 16.5 nm)

Similarly, after examining the histograms from a statistical perspective, it is postulated that the fibres after phosphorylation are more likely to be distributed log-normally in comparison to that of the ordinary bacterial cellulose, which has a Gaussian distribution

(see figure 4.3.1.2). This is of particular importance, as, historically, the distribution of fibre diameters in natural tissue is found to be primarily log-normal[63, 64].

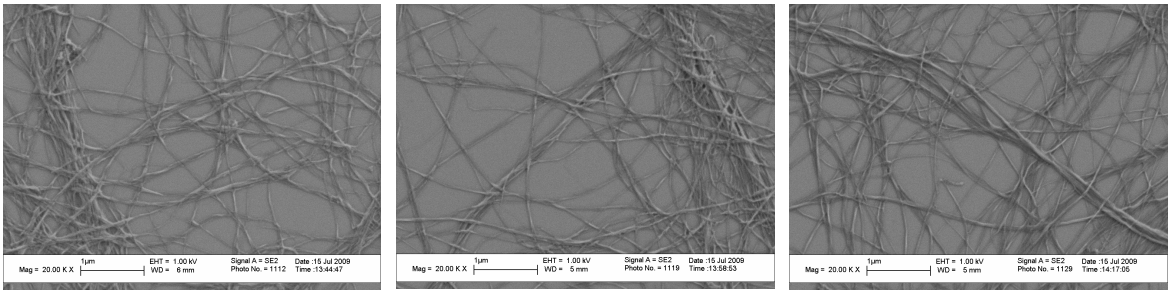

Figure 4.3.1.3: SEMs of BC fibres after 1, 2, and 4 hours of phosphorylation

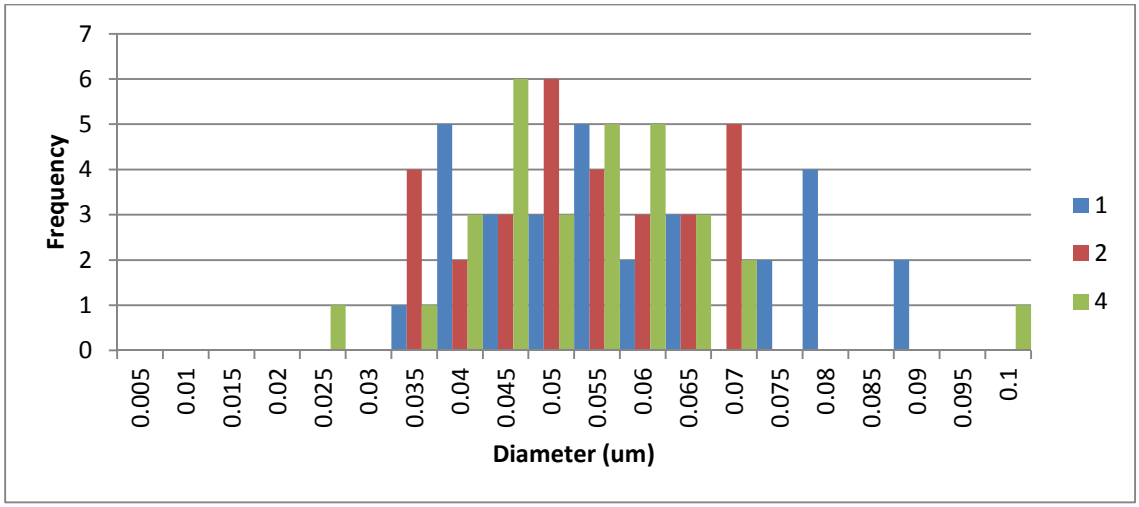

Figure 4.3.1.4: Distribution of BC fibre diameters for samples exposed to 1, 2, and 4 hours of phosphorylation.

As shown in figures 4.3.1.3 and 4.3.1.4, the samples tend not to have any statistically significant variation in fibre morphology or diameter proportional to the increasing amount of phosphorylation, in reactions up to 4 hours of reaction time. Dimensional

analysis via ImageJ confirms this, for 1, 2, and 4 hours of phosphorylation, with fibre diameters hovering around 50 nm (56.1 ± 16.3 nm, 50.3 ± 11.7 nm and 51.2 ± 13.5 nm, respectively).

4.3.1.2 FTIR Characterization

As the ultimate goal of the investigation was to use the phosphorylated BC for the formation of BC-HA composites, samples were also examined after extended reaction in SBF for adequate HA attachment. FTIRs of a 'BC-HA' sample, in comparison with the same BC after 2 hours of phosphorylation, are shown below in figure 4.3.1.5 over the wavelength 950-1200 cm^{-1}. Infrared band assignments are collected in Table 4.3.1.1. The FTIR spectrum of untreated BC is also included as a reference.

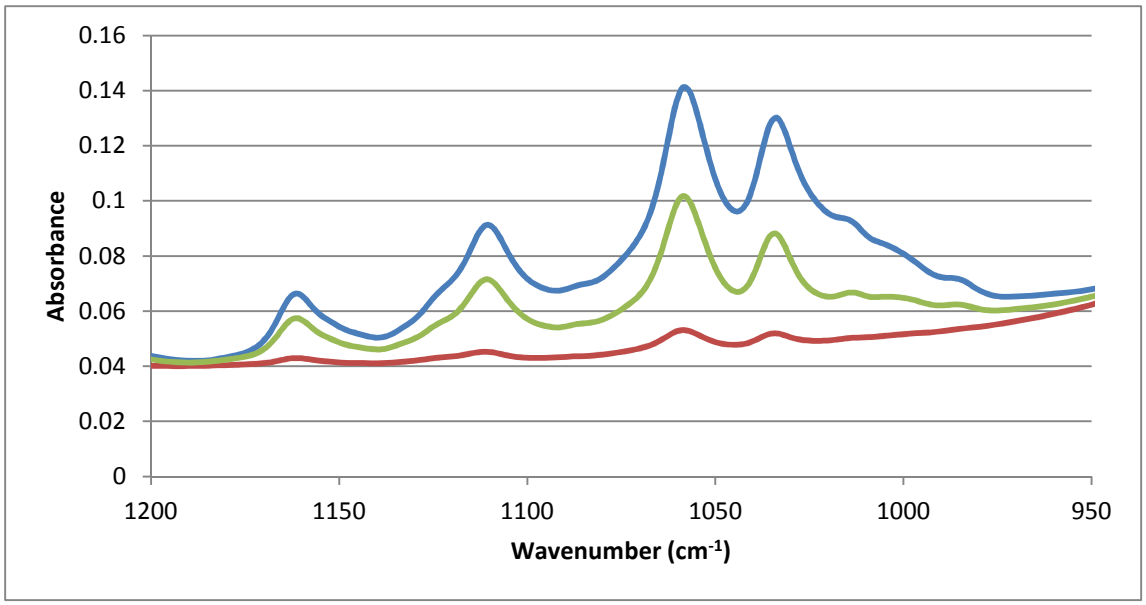

Figure 4.3.1.5: Sample expansion (950 to 1200 cm^{-1}) of an FTIR taken of a bacterial cellulose sample (red), a BC sample after 2 hours of phosphorylation (green) and the same sample after 14 days in SBF (blue). The FTIR has been limited in order to provide more detail on the significant peaks in this range.

Table 4.3.1.1: Wavelength assignment of most significant PO_4^{3-}/HA peaks (950-1200 cm^{-1})

v (cm^{-1})	Assignment
985	PO_4^{3-} in HA[6, 65]
1004	PO_4^{3-} asymmetric stretch[65]
1020	HA nonstoichiometry[65]
1030	PO_4^{3-} stretch in HA – strongest peak in all FTIRs[6, 65]
1055	PO_4^{3-} in HA[65]
1075	PO_4^{3-} in HA[65]
1112	HA nonstoichiometry/acid-phosphate containing derivatives[65]
1145	Acid-phosphate containing derivatives[65]

Note that, in figure 4.3.1.5 above, the FTIR trace for the phosphorylated BC mimics that of the BC-HA composite material, and both of these correspond with key FTIR peaks illustrated by the above table 4.3.1.1. This is indicative of a similarity in chemical composition of the two samples, and serves to encourage beliefs that, to some extent, the phosphate groups are attached to the cellulose backbone in a means that is conducive to inducing HA formation. Similar FTIR traces were produced for the 1 and 4 hour samples as well, and will be discussed further in section 4.3.2.

4.3.1.3 EDX Characterization

In order to ascertain the quantitative success of the phosphorylation, the phosphorus-to-carbon, or P/C, ratio was used. This correlates the amount of quantifiable phosphorus per sample relative to the cellulose content of other samples, and allows for comparative views of the degree of phosphorylation. To that end, for the 1, 2, and 4 hour samples, the P/C ratio was fairly comparable irrespective of the phosphorylation time. Results are summarized in figure 4.3.1.6 below.

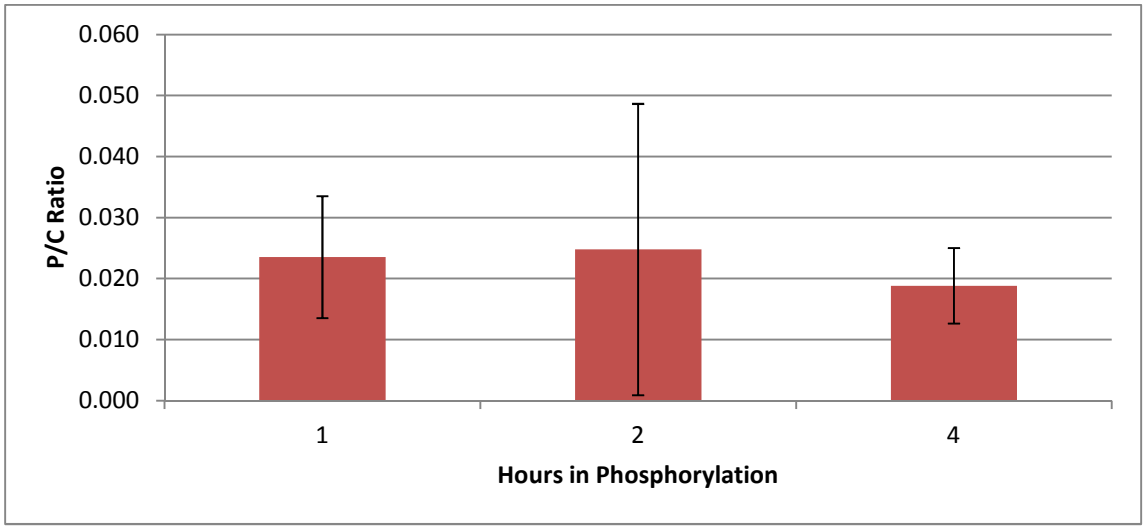

Figure 4.3.1.6: P-to-C ratio for BC samples after 1, 2, and 4 hours of phosphorylation

As proposed by Wan et al., in 2006[6], a more measurable quantification for the amount of relative phosphate added is the formula for DS_P or degree of phosphorylation,

$$DS_P = \frac{162 \times P(wt)\%}{3100 - 84 \times P(wt)\%} \quad \ldots\ldots\ldots\ldots \quad Eq.\ 1$$

This formula results in the following values for the degree of phosphate substitution from the phosphorylation reaction alone:

Table 4.3.1.2: DS_P as a function of length of phosphorylation time

	DS_P	SD (+/-)
1 hr	0.147	0.050
2 hr	0.132	0.123
4 hr	0.116	0.040

As it can be seen, the P/C ratio seems to hover around 0.025 for all samples of the phosphorylated BC, with phosphorus amounting to 1.25% of the sample, on average, by atomic weight. Large variability (particularly in the P/C ratio for the 2 hour samples), is likely due to varied population size in this particular set of experiments, as well as much smaller values for the average, both factors of which exacerbate the apparent difference. Using the formula for degree of phosphate substitution described above, this corresponds to an average DS_P of all samples of 0.133, implying that 13.3% of available –OH groups are replaced. This value is comparable to that found previously in literature[66, 67].

4.3.1.4 Titration Experiments

Titration experiments were also performed in order to observe the diprotic nature of the phosphorylated cellulose. Two millilitre samples were diluted in 50 mL of water and then titrated with 1 M NaOH in order to ascertain the extent of the pH inversions. These tests followed a predicted pattern, having multiple inflection points in an otherwise smooth curve function, and indicating that the protons attached to the phosphate were indeed

being systematically reacted, characteristic of a polybasic acid having multiple sites for H+ neutralization. The result of this phenomenon is shown below in figure 4.3.1.7.

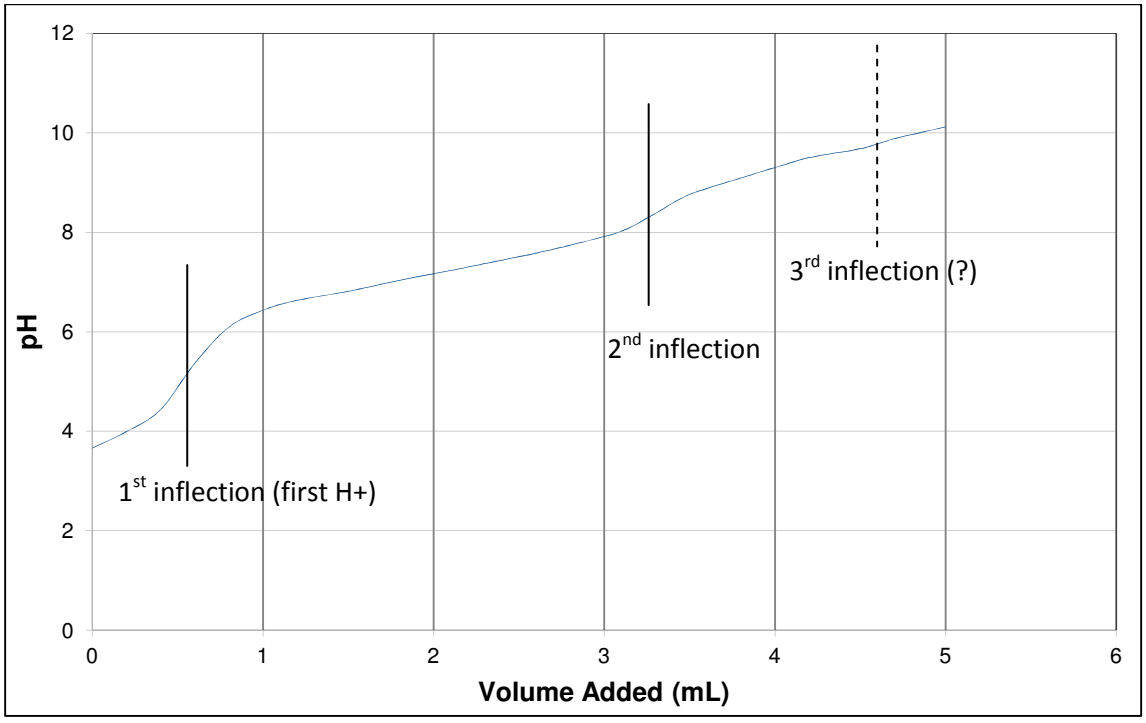

Figure 4.3.1.7: Titration curve for a two hour phosphorylated cellulose sample (titrated with concentrated 1 M NaOH). pK_a values (determined from the observed pH, halfway between equivalence points) confirm the legitimacy of the titration.

From the above graph, 0.6 mL of 1 M NaOH neutralized the first dissociative proton of the phosphate group. This implies a molarity of phosphoric acid in the sample of 0.6 mmols, or 0.3 mmols/mL of cellulose fibre sample. Taking into account the dry cellulose weight (0.013 g/mL) and the molecular weight of glucosidic monomer (142.11 g/mol), as well as the carbon content of each monomer (6 carbons per monomer unit), one can determine the maximum theoretical P/C ratio for the samples of around 0.5.

The above titration data leads to a P/C ratio that is approximately 10 times larger than that observed via EDX. This may be caused by discrepancies between the techniques (molarities are highly sensitive to cellulose bottle weights and concentrations) or otherwise by the presence of phosphate groups that could not be washed out by the post-phosphorylation purification process. The latter is the most likely occurrence, and is further justified by the appearance of a subsequent inflection point around a pH of 10, which would only be present if the phosphate existed in a PO_4^{3-} conformation (in the phosphorylated BC, phosphates would instead in PO_4^{2-} form as one oxygen atom is covalently bonded to the cellulose backbone).

4.3.2 Characterization of Phosphorylated BC After Treatment in SBF

Despite the purported necessity of the phosphorylation process in obtaining BC-HA composites, the degree to which phosphorylation acts as the *de facto* nucleation for all phosphate groups, or whether it simply just begins the process of phosphate addition, is questionable. The subsequent steps (calcium pre-treatment and SBF) both appear in literature[6-8] to be key players in producing hydroxyapatitic biocomposites, occasionally occurring *without* adequate phosphorylation beforehand, and, as the phosphate must be integrated into the HA matrix beyond that provided in phosphorylation alone, an additional source of phosphate ions must be present. As the calcium pre-treatment does not contain any phosphorus, the source of these additional phosphate groups must be exclusively from the biomimetic SBF treatment. To this end, the previous samples, at various phosphorylation times, were compared to the end goal Ca/P and P/C ratios of the final composites after treating them in SBF for 14 days.

4.3.2.1 FTIR Characterization

As demonstrated previously in figure 4.3.1.5, employing values outlined in the above table 4.3.1.1 of key FTIR peaks, it could be argued that the phosphorylation of the sample leads to the formation of further HA-conducive phosphates on the BC. However, consideration must be given to the added effects of the subsequent SBF immersion reaction, which at first glance appears to provide more significant development of the phosphate groups and, ultimately, HA, on the surface of the phosphorylated-BC.

It should be noted that the FTIR of pure cellulose has several strong, distinct peaks which overlap with the desired calcium phosphates, namely those at 1035, 1060, 1110, and 1160 cm^{-1} (various vibrations of the C-C and C-O bonds, as well as an asymmetric stretch in the C-O-C bond at 1160 cm^{-1}[68]). Hence, peaks at the 1030, 1055, 1112 cm^{-1} wavenumbers listed in Table 4.3.1.1 cannot be taken as incontrovertible evidence for the presence of PO_4^{3-} and HA. Nevertheless, remaining peaks at 985, 1004, 1020, 1075 and 1145 cm^{-1}, taken holistically, provide significant evidence of the success of the phosphorylation reaction and the potential for the final HA composite.

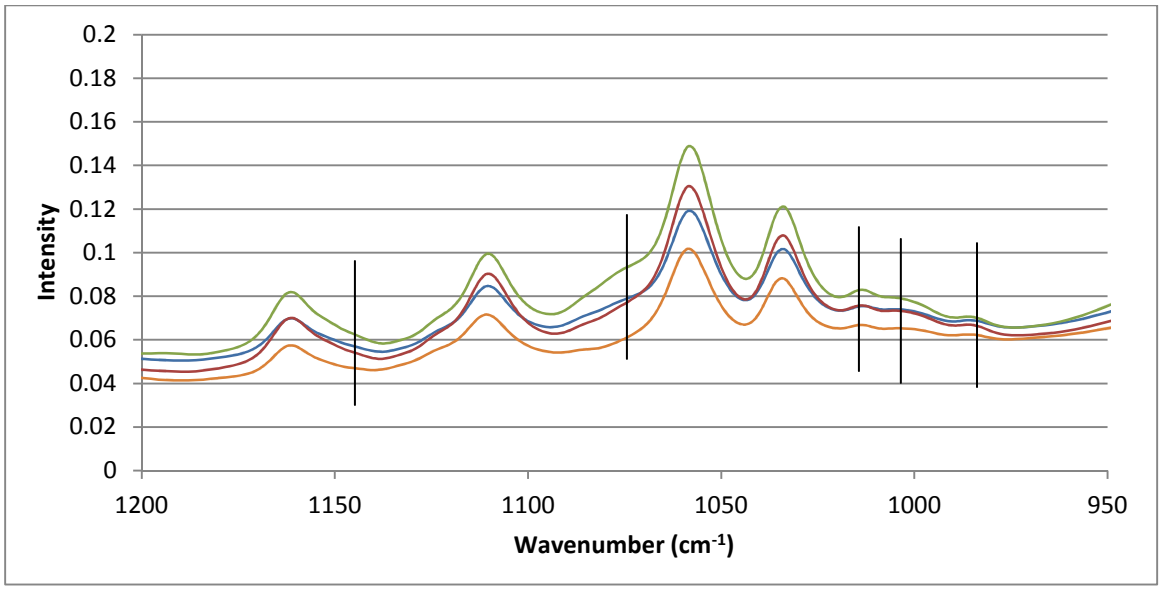

Figure 4.3.2.1: Expanded FTIR region (950-1200 cm^{-1}) for HA-BC fibre dispersions after 1 (blue), 2 (red), and 4 (green) hours of phosphorylation and subsequent treatment in SBF for 14 days. The base sample, without any SBF and after just the phosphorylation step (2 hours) is also shown (orange). Note the obfuscation of significant peaks as discussed earlier (see Figure 4.3.1.5).

Again, the characteristic region for hydroxyapatitic composite materials was determined to be between 900 and 1300 cm^{-1}, as previously described by Gadeleta and colleagues[65]. Arguably, all of the above FTIRs show the presence of characteristic peaks associated with the crystalline forms of the phosphate ion overlaid with that of cellulose, in and around 1000-1200 cm^{-1}. These peaks occur irrespective of the form of bacterial cellulose sample, or the phosphorylation time. Of note, however, is that in increasing the amount of phosphorylation, the FTIR peaks of the sample appear to be more defined and emphatic, leading to the hypothesis that the 4 hour sample of BC has a higher crystalline deposition of phosphate ions, and thereby hydroxyapatite. This is in no way quantifiable without relative intensities; however, it is nonetheless an interesting occurrence and one that warrants further investigation.

4.3.2.2 EDX Characterization

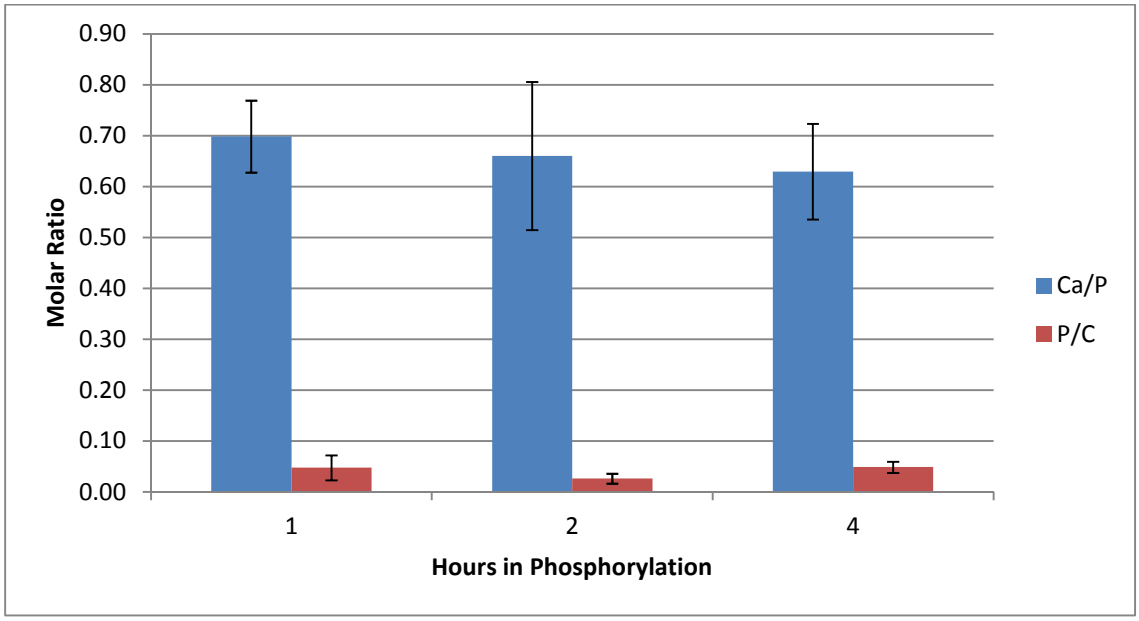

Figure 4.3.2.2: The Ca-to-P and P-to-C ratios as functions of the number of hours of phosphorylation after week long reaction in SBF

As shown in figure 4.3.2.2, phosphorylation time has no effect (not statistically significant), on the experimentally determined P/C and Ca/P ratio of the samples after reaction in SBF for any significant amount of time. This may be due to the inability to isolate the fibres from solution and, because the depleted SBF could not be removed, a consistent dilution of the SBF. Centrifugation was thought to be detrimental to the crystallite development, as several sources[47, 69-71] implied that the higher forces on the HA crystals could potentially cause them to fracture and disperse in the case of large-scale fibre coating. In hindsight, this supposition is chiefly dependent on the applied forces from the centrifugation process, which, based on the crystallite size, is hard to justify. Nevertheless, the assumption permeated through the rest of the experimentation, causing potential discrepancy in results.

The relationship between Ca-to-P ratio and phosphorylation time is shown in Figure 4.3.2.2, above. As before, it is perceived that sensitivity of the experiment to the length of reaction time is minimal. As discussed earlier, the phosphorylated BC samples, with reaction times from one to four hours, appeared physically different after removing them from the phosphorylation chamber, leading to the belief that the varied phosphorylation times generated a significant and quantifiable effect. The fibres appeared to be qualitatively more similar to a crystalline solid, becoming more tacky and brittle with increasing time in the chamber. However, these phenomena disappeared after subsequent washing and purification, with characterization results indicating little difference in terms of the Ca/P, P/C and C/O ratio among the samples. This effect is emphasized in samples after SBF treatment (Figure 4.3.2.2) as the Ca/P ratio in particular falls within the narrow range of 0.5-0.8. Although this ratio is significantly lower than the 1.67 standard expected of HA formation, relative similarities hint that it is likely a result of inadequate calcium pre-treatment (see Chapter 4.4). Comparatively, the graph below (Figure 4.3.2.3) shows this same tendency as tightly grouped series of points by the 14^{th} day; indeed, as the phosphorylation time increases, there is conversely very little corresponding increase in the observed Ca/P ratio.

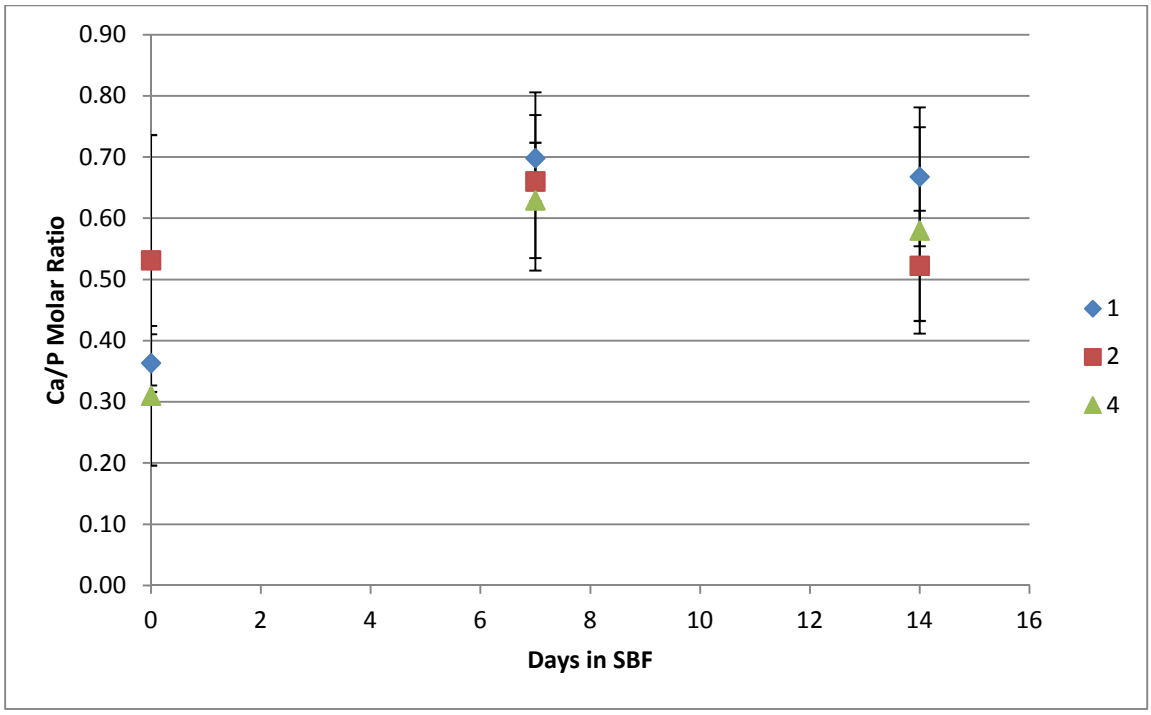

Figure 4.3.2.3: Ca-to-P molar ratio for samples undergoing 1, 2, or 4 hours of phosphorylation time and subsequent SBF reaction

In terms of the phosphorylation reaction time of the sample, at any point in the submersion of the sample in SBF, the Ca/P ratio remains relatively constant within statistical range. Ultimately, what the above graph implies is that the length of time in SBF, instead of length of phosphorylation time, has the desired positive effect on the ratio of calcium to phosphate. According to figure 4.3.2.3 above, independent of the phosphorylation time, all samples appear to have a smooth grade upwards, plateauing around the week-long marker of exposure to 1.5x SBF.

An interesting point of note here, however, is that the above effect is not exclusive to the analysis of the Ca-to-P ratio. In fact, a similar understanding can be drawn about the P-to-C ratio in all the samples as described earlier. The amount of phosphate on the samples

increases dramatically from the first to the fourteenth day in immersion in SBF, an increase much more significant than that of transitioning between one to four hours in the phosphorylation chamber. The DS_P calculation discussed earlier confirms this with yields as high as 0.285, by the 14^{th} day of submergence in simulated body fluid, although this is largely due to ionic phosphate, rather than PO_4 covalently bonded to cellulose. Nevertheless, this does confirm that the SBF contributes to a further degree of detectable phosphate than the phosphorylation reaction itself. This is consequently understandable when considering that the SBF is fine-tuned to increase not only calcium, but also phosphate, in ratios mimicking those of hydroxyapatites.

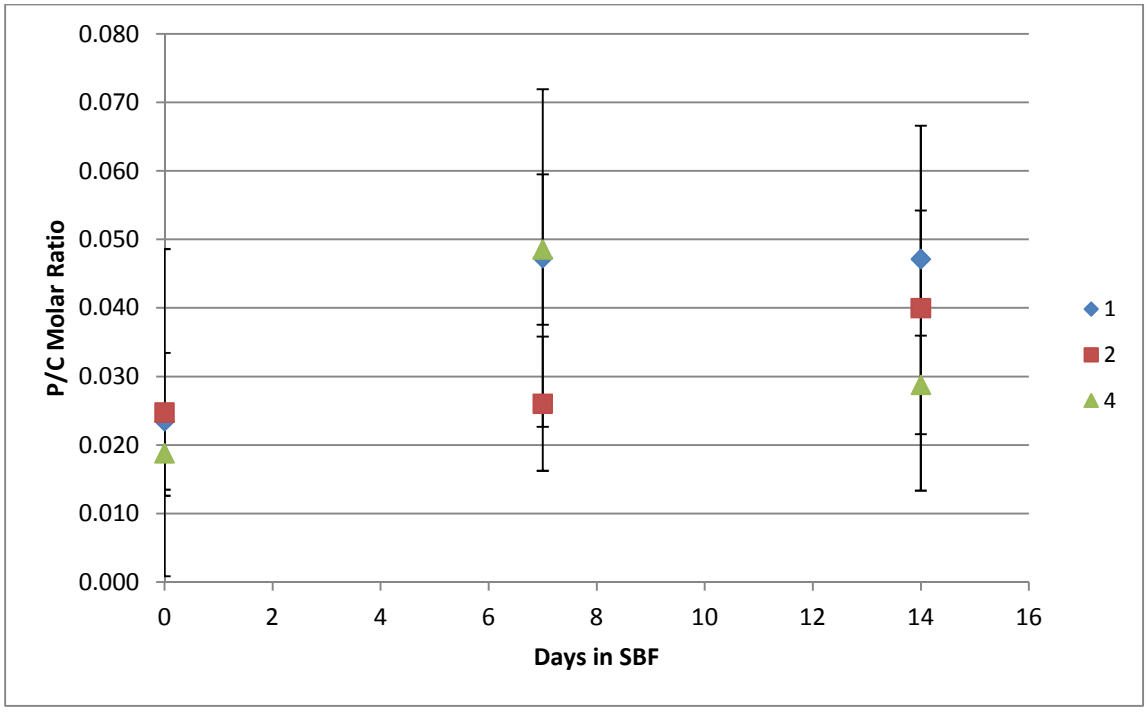

Figure 4.3.2.4: P-to-C ratio for samples undergoing 1, 2, or 4 hours of phosphorylation and subsequent SBF reaction

As seen in figure 4.3.2.4 above, samples with different phosphorylation times all appear to have comparable ratios of phosphorus-to-carbon after 14-day submergence in SBF, similar to the trend observed in the Ca-to-P ratio earlier. Unfortunately, the variability appears to be significantly higher in the above graph, effecting itself in the shown standard deviations which are severely exacerbated. This is likely due to the sensitivity of the characterization to localized concentrations of phosphate, as well as background carbon native to the EDX characterization. Nevertheless, all samples trend upwards, again reaching a plateau around day seven, and maintaining an average phosphorus content at least equivalent to about 3% of the total atomic weight of the sample, an increase from the 1.25% seen earlier.

In short, the effect of a prolonged exposure of the samples to a phosphate-rich environment is negligible on the quantity of the resultant hydroxyapatitic layer, as the SBF provides its own phosphate groups. However, this does not negate the possibility of an effect from an enhanced crystallinity. In all cases of experimentation above, the composites appeared to be largely amorphous, a trend which is often replicated in literature[72]. This is justifiable though; the hydroxyapatite found in nature is similarly amorphous, owing to the incongruence and imperfection of the natural world. That is not to say that efforts should not be made to make samples more crystalline and exact; rather, further emphasis should be placed on the creation of a compound with a higher calcium-to-phosphate ratio and a more significant coating of the fibres (higher yield) rather than extending the phosphorylation time for relatively marginal increases in potential crystallinity.

4.4 Effectiveness of Pre-treatment of BC

In determining the efficacy of the experiment, the potential effects due to the addition of a pre-treatment step were also examined. After phosphorylation, the accepted ensuing pre-treatment step is to place the sample into a calcium salt solution in the hope that the attached phosphate groups would form the initial nuclei for hydroxyapatite. The time period for this pre-treatment step is usually one to three days, in similar temperature and humidity conditions to the hydroxyapatite growth step, aiding the transition of the material from room temperature and acidic pH to the body temperature and neutral pH required by the SBF. As such, the typical and predominantly suggested compound for this initial reaction was a solution of 0.1 M $CaCl_2$, so chosen for its high solubility, relative non-reactivity, and neutral pH. This step is done in the hopes that the resultant calcium-phosphate groups would be the nucleating sites for furthering the hydroxyapatite growth, in alternating reactions with subsequent calcium and phosphates, whilst suspended in the SBF solution. Characterization was performed largely using SEMs and EDX, and final crystallite dimensions examined via ImageJ software.

4.4.1 SEM Characterization

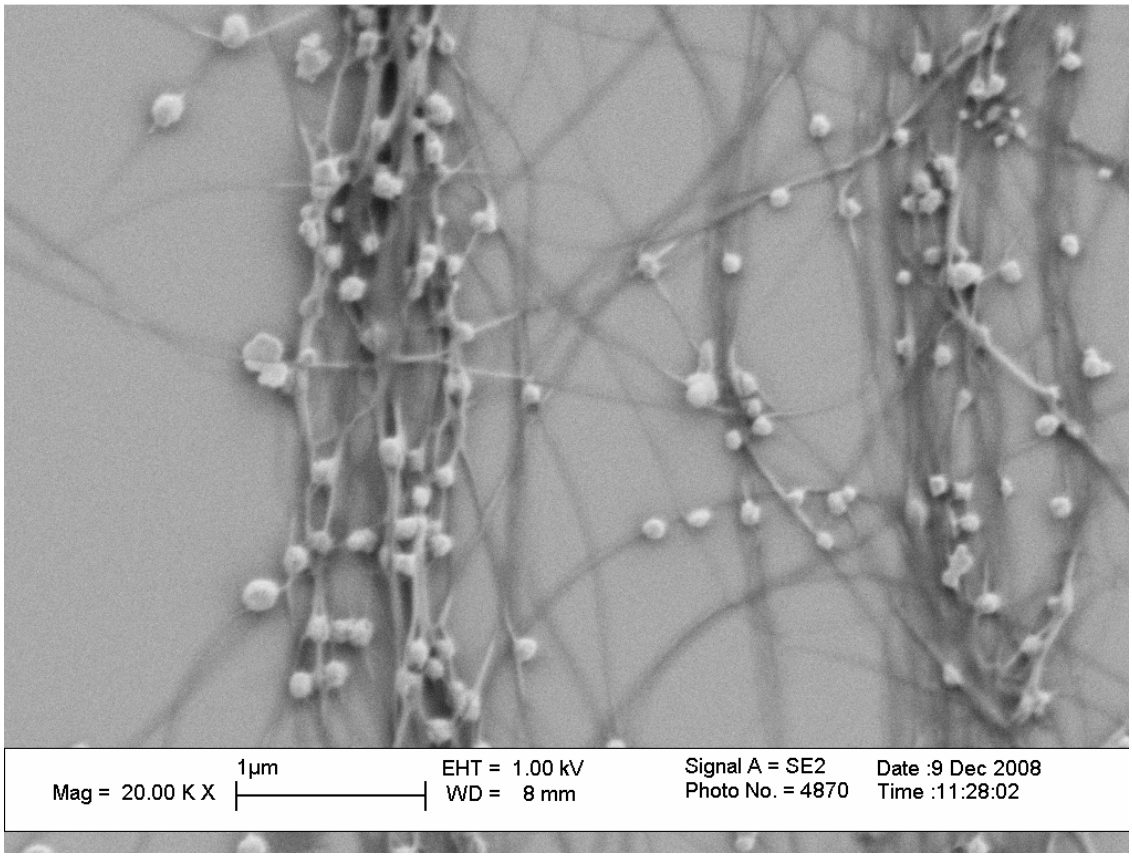

Figure 4.4.1.1: SEM of pre-treated BC fibres after 3 days in SBF

Interestingly, when the samples are phosphorylated, pre-treated, and placed in SBF, the initial growth of calcium phosphate crystallites appears to be almost spherical in nature, as seen above. This is confirmed in literature[6, 43, 73], and is believed to be sensitive to several factors; the temperature, the adequate and precise concentrations of calcium and phosphate in the sample, and the consistently maintained local pH. Unfortunately, as the samples were completely suspended in solution and centrifugation was thought to be out of the question (crystallites were predicted to shear off by the simple act of agitation[69-71]), requisite solutions could only be added to the sample, and not removed. This

includes solutions used in the pre-treatment and the SBF, and effectively negates the potential of any buffering agent. To this end, the pH of the concentrated cellulose sample began at approximately 3.6, and occasionally ended at pHs as high as 11, despite repeated attempts to adjust and compensate accordingly. It is for this reason that, although samples began with these loosely defined, tightly knit, spheres, they all ultimately evolved into the platy, rose-like crystals seen in figure 4.4.1.3.

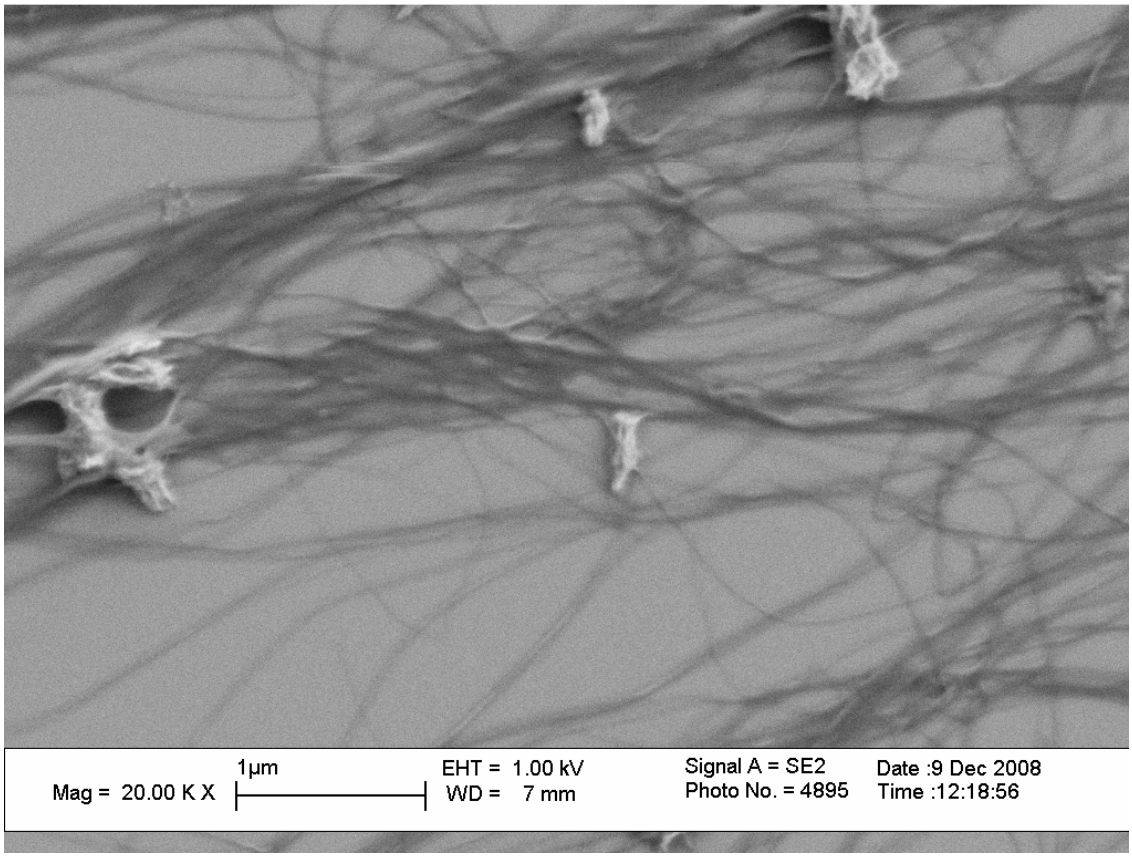

Figure 4.4.1.2: SEM of untreated BC fibres after 3 days in SBF

Comparing both the Ca-pre-treated and untreated samples of fibres (figures 4.4.1.1 and

4.4.1.2), one can see glaring differences in structure of the crystals, taken at the exact same period in development, despite otherwise identical conditions of crystal growth. In regards to the latter, when samples are untreated, the crystals, take a significantly *shorter* time to visibly nucleate and grow. Regarding these untreated samples, the SBF must first create phosphate binding sites on the phosphorylated cellulose by adding calcium ions, cascading down into raw calcium phosphate growth, before ultimately resulting in any form of a HA crystal, amorphous or otherwise. This means that there was a severely limited amount of usable sites where crystal genesis could take place, and formed crystals were likely bigger than their pre-treated counterparts, although not necessarily more crystalline or adequately stoichiometric. In maintaining reaction conditions, the crystals of either sample still ultimately formed the aforementioned plate-like agglomerates. EDX results, in conjunction with speculative FTIR and SEM data in all cases, confirm that these are all calcium phosphates, if not hydroxyapatite, albeit with a low crystallinity and atypical stoichiometry.

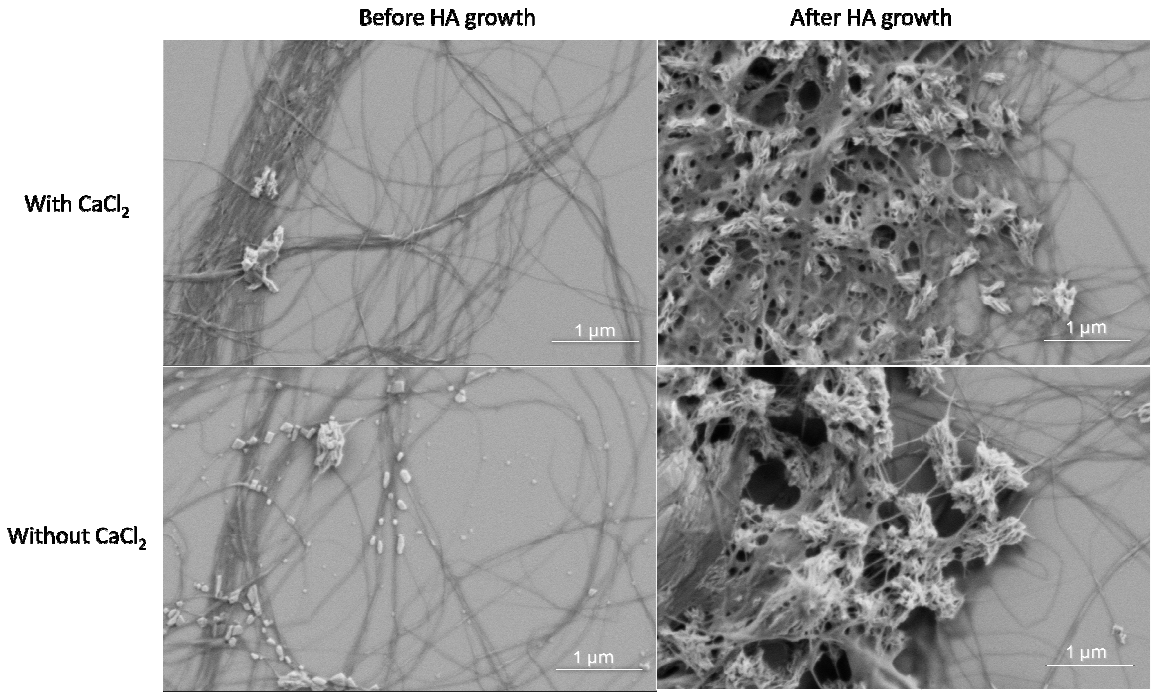

Figure 4.4.1.3: Comparison of pre-treated and non-pre-treated samples of BC (3-day immersion in $CaCl_2$) before (left) and after (right) 14-day term in SBF

The above figure 4.4.1.3 shows the effects of pre-treating a sample of bacterial cellulose with a calcium solution more drastically, by comparing SEMs from the initial complexes, left, to those after a full 14 days in SBF solution, right. When the aqueous $CaCl_2$ is initially added to the mixture, the qualitative effects are apparently negligible. Fibres do not appear to be more dispersed nor does there appear to be any additional sites of HA nucleation. Instead, the effect manifests itself after the subsequent days of exposure to the simulated body fluid. The samples that had the added benefit of a pre-treatment in a calcium solution have a much finer HA crystal deposition, leading to the belief that, with enough tuning of parameters, a cohesive and complete coating of the fibres could be established. Comparatively, with the non-pre-treated analogue, the crystals that form are

instead ‘bulked’ together, usually where fibres have netted together, and appear to be much larger (2-3 times) than their pre-treated counterparts.

4.4.2 EDX Characterization

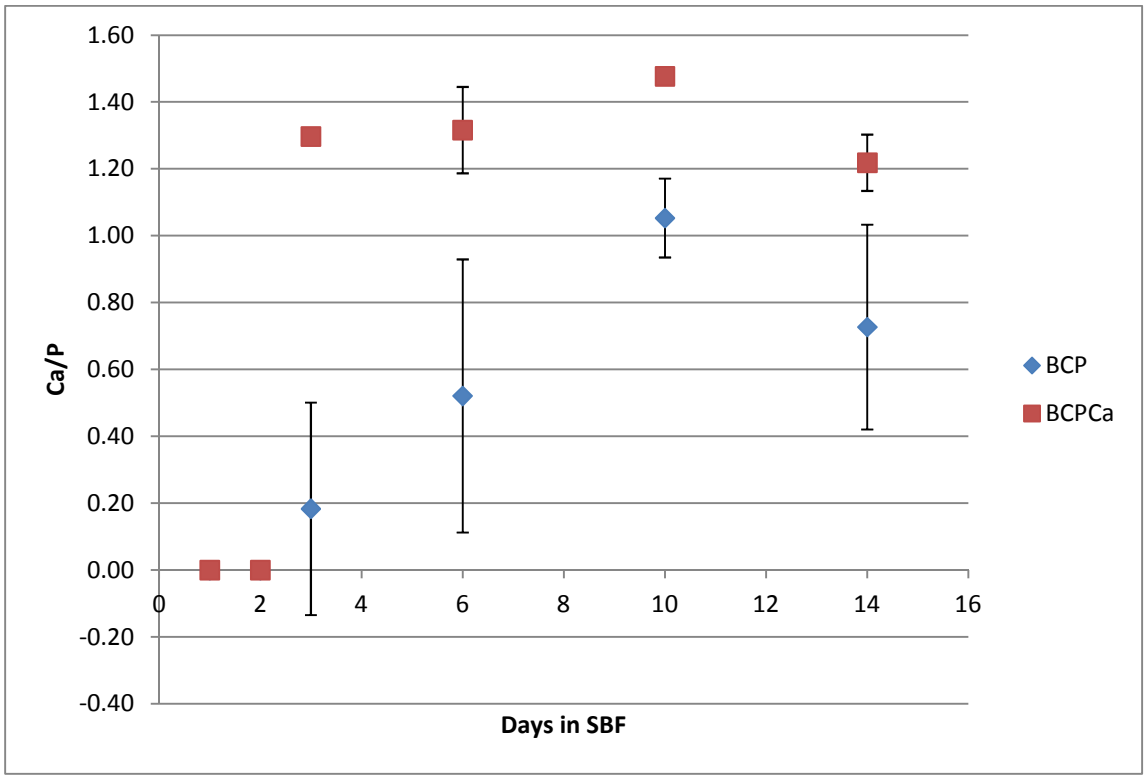

Figure 4.4.2.1: Observed Ca-to-P molar ratio of the bacterial cellulose/hydroxyapatite fibre sample over the course of 14 days. The samples were tested both with and without the Ca pre-treatment.

The graph above, figure 4.4.2.1, shows the observed Ca/P growth patterns between a non-pre-treated sample and one that has been pre-treated with calcium ions. Regarding the pre-treated samples, the Ca/P molar ratio quickly spikes by the third day in SBF. Comparatively, the untreated sample takes more than a week to achieve approximately equal amounts of calcium and phosphorus, with a high standard deviation owing to

inconsistent deposition. Even then, the Ca/P ratio never comes close to that of the pre-treated samples. With the Ca pre-treatment, samples were more likely to achieve the 1.67 molar ratio indicative of the pure HA standard, doing so in the allotted time of 14 days.

4.4.3 Crystallite Dimensional Analysis

Upon further analysis using ImageJ, it can be shown quantitatively that the diameter and length of the resultant crystallites increase with respect to SBF exposure, again, dependant on the presence of the pre-treatment step. In order to ascertain the crystallite dimensions, it was necessary to model the crystals as cylindrical solids, with their major axis running concurrently along the length of the bacterial cellulose fibre. To this end, results below show both the length (Figure 4.4.3.1) and diameter (Figure 4.4.3.2) of the resultant crystals.

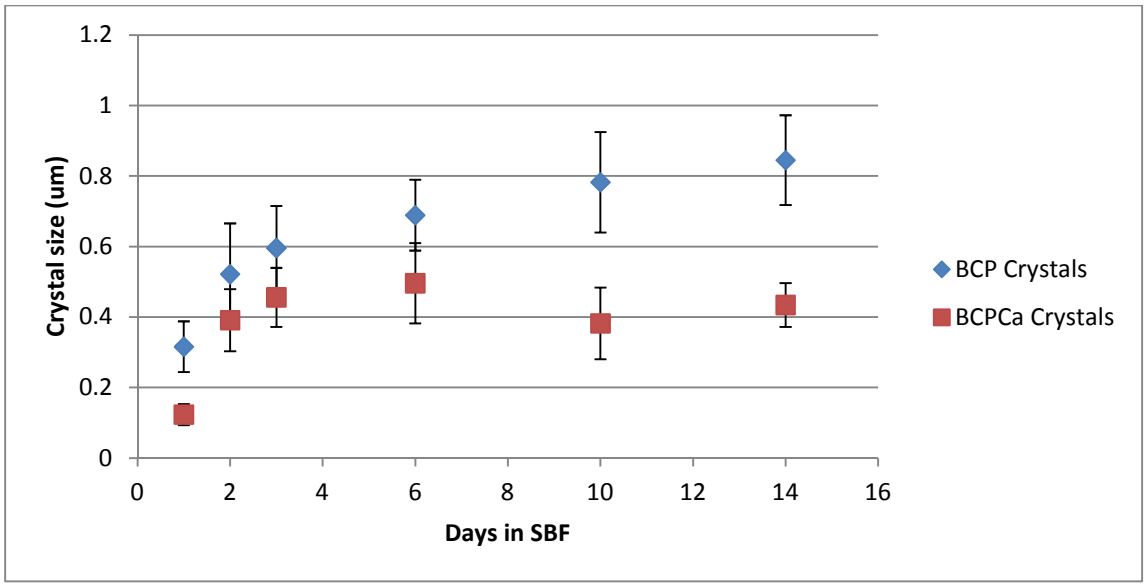

Figure 4.4.3.1: Major HA crystallite dimension (length) as a function of the length of time in SBF

Reasoning behind this trend is as follows. Whilst the non-pre-treated samples must first generate nucleation sites by the reaction of Ca^{2+} with phosphate groups, pre-treated samples already possess said sites for subsequent HA crystallization and growth. In other words, the most HA conducive sites in non-pre-treated samples occur where HA has already been nucleated, and hence, crystals tend to grow bigger instead of nucleating throughout. In the samples that have calcium pre-treatment, instead, the crystals attain a capped crystal size around 500 nm in length (note that this is the maximum dimension of the size of a crystallite, and should not be taken as the fibre diameter), and become more prevalent throughout SEMs (see figure 4.4.1.1). With regards to the latter case, this means that since the sites of phosphate addition are already seeded with larger deposits of calcium ions, there is a better chance of an orderly deposition of phosphates and calcium, forming better defined HA crystals. This also consequently explains the higher Ca/P ratio observed. In the case of the former non-pre-treated analogues, the substrate-bound phosphates must first be reacted with the sparse, ionic calcium in solution, bottlenecking the process. This then generates a thinner distribution of nucleation sites, localized ionic concentration, and, as a side effect, larger, albeit less stoichiometric, crystals.

As a corollary to this conclusion, it can also be seen that the maximum crystallite diameter is somewhat fixed, independent of the length of time in SBF, although, again, samples that have not been pre-treated tend to have a larger dimension along the fibre length than their pre-treated counterparts.

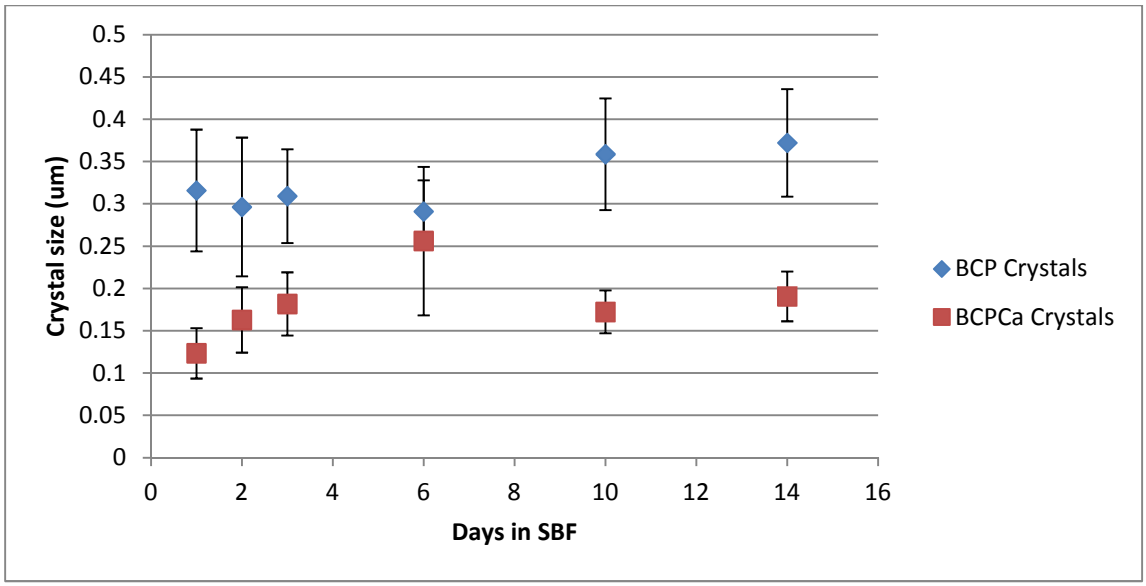

Figure 4.4.3.2: Minor HA crystallite dimension (diameter) as a function of the length of time in SBF

Samples that have not been pre-treated have an average crystal diameter of around 300 nm; those with Ca pre-treatment instead have a diameter of approximately 190 nm.

According to literature, however, even these smaller pre-treated crystallites are still 8 times bigger than expected in comparable experimental conditions. Rusu et al. in 2005[4], as well as Pang et al. in 2003[74] both found that resultant HA prepared from the same chemical precipitation methods after 14 days in aqueous solution had maximum dimensions of 53 nm at most, although this was calculated, based on the Scherrer-Debye equation and the XRD spectra. This leads to the speculation that the experimental samples above are poorly developed sites of calcium phosphate attachment. The phenomenon does, however, correlate well with the findings of Wan et al.,[7], who ultimately determined that, due to poor calcium deposition in conjunction with a low crystallinity (less than 1%) and incomplete coverage of the fibres, crystals are much

bigger than reported in the past, and concentrated in localized areas. In addition, as a likely corollary with the low crystallinity and larger crystal size, there is means to believe that the larger crystals imply an imperfect stoichiometry and inconsistencies in formation[72].

Still, the above results indicate that the use of a pre-treatment step causes the nucleation of smaller, albeit more stoichiometrically relevant, HA crystals on the fibres. In addition, in the course of exposure to the SBF solution, the crystals, irrespective of the pre-treatment, grow longitudinally, in the direction of the fibre, and not in cross-sectional diameter. This effect is made even more dramatic by the maintenance of an apparently consistent crystal diameter (depending on pre-treatment) and higher Ca/P ratio, both of which suggest that the success of a viable and tunable biomaterial derived from BC and HA hinges largely on the essential use of a legitimate Ca-ion pre-treatment solution.

4.5 Characterization of HA

In the above experimentation, it was essential to compare the samples as legitimately as possible, relative to their specific conditions, in order to ascertain any form of congruence between testing methodology. In addition, the resulting quantities of HA were so small that justification of the *bona fide* crystal could not be made without compromising the results of the independent approach. Hence, contamination of the characterization of BC-HA by artefacts from the BC, the procedure, or the equipment was commonplace. Further characterization of the HA itself was abandoned to give way to characterization of the

entire composite instead. Nevertheless, it is the assurance of subsequent characterization with respect to the HA exclusively that provides evidence to its presence in all composites, to varying degrees and purities.

Samples in all cases were found to possess an arguably congruent FTIR trace, reminiscent of that shown in literature[6, 7, 43, 58].

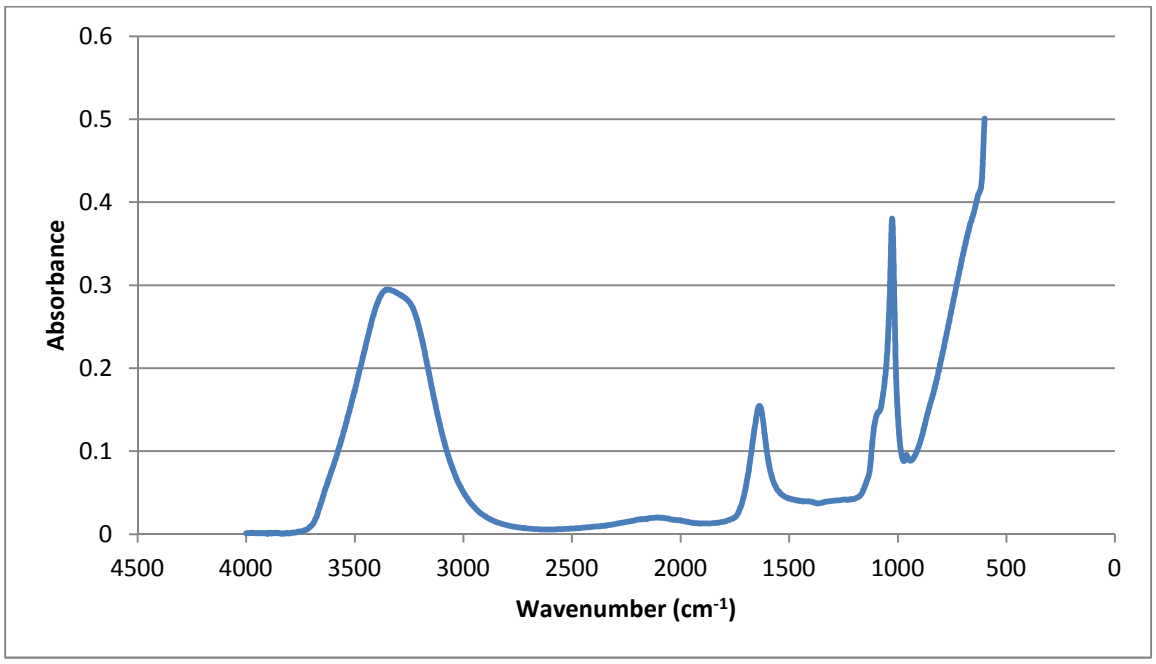

Figure 4.5.1.1: FTIR for hydroxyapatite prepared via biomimetic conditions

The above figure 4.5.1.1 is indicative of the pure hydroxyapatitic sample obtained through a biomimetic process identical to that described previously. In order to remove the contamination of the sample with the overlapping bacterial cellulose backbone, crystals were instead isolated by providing excess calcium and phosphate in the SBF

solution and allowing for only HA crystal growth. Small solutions of 0.1 M calcium hydroxide and 0.06 M orthophosphoric acid were mixed in the presence of nitrogen[43] and then allowed to further precipitate in excess SBF solution, in identical culture conditions (temperature, time, etc.) to the composite samples. The resultant mixture, which began as a clear solution, soon became precipitated an off-white solid. After 14 days of SBF submergence (removing the clear upper portion and adding a fresh batch, with agitation, every day), at a precisely maintained temperature of 36.5 °C, the samples were removed from the incubator, washed with dH_2O, and run through a vacuum flask, in order to procure the biomimetically-produced HA powder samples.

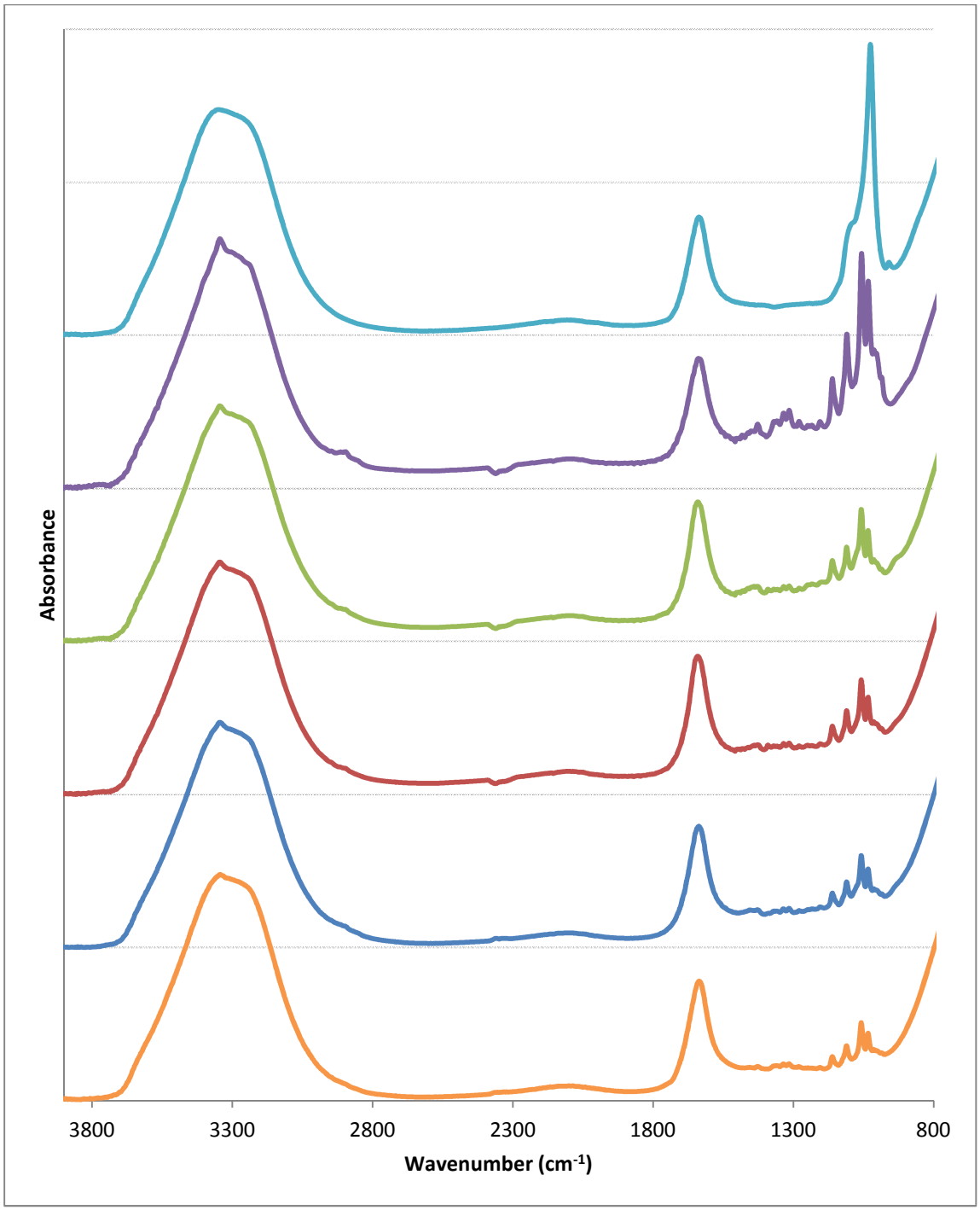

Figure 4.5.1.2: FTIRs for, from bottom to top; BC-PO_4H_2, 1 hr long phosphorylated BC-HA, 2 hr long phosphorylated BC-HA, 4 hr long phosphorylated BC-HA, 2 hr long phosphorylated HA-Biofill®, and "pure" hydroxyapatite procured via a chemical precipitation method in conjunction with SBF.

In the above figure 4.5.1.2, similar FTIR peaks are observable throughout the range of phosphorylation times (also refer to figures 4.3.1.5 and 4.3.2.1 in earlier sections; note the aforementioned overlapping of peaks). Evidence of phosphate groups, suggesting both amorphous and pure HA crystallites are seen, in all ranges of the spectrum, as indicated by literature. Peaks in the range of 1600-3600 cm^{-1} should be loosely indicative of both the cellulose substrate and the hydroxyapatite, signifying the presence of –OH groups and oxygen double bonds (present in carbonated hydroxyapatites[75] and phosphorus). This indication is somewhat overshadowed by the fact that the samples are contaminated by water and carbonates in the environment as discussed previously. However, the peaks in the range from 1500-500 cm^{-1} (also known as the 'fingerprint region') remain fairly significant, and noteworthy conclusions can be drawn from them. In this range, overlapping peaks from both cellulose and hydroxyapatite can be seen, as indicated by figure 4.5.1.3. In fact, the intensities of the peaks are comparable throughout the 1, 2 and 4 hour phosphorylations, indicating a similarity and reproducibility of the results.

For the sake of comparison, the FTIR of a 2-hour phosphorylated and SBF-treated sample of Biofill®, a commercial bacterial cellulose-based wound dressing, is also shown. This then begets an interesting anomaly. Differences in the FTIR trace between the latter wound dressing and the former BC fibres are likely attributable to Biofill®'s post-production method as well as the pre-treatment; dehydration of the sample leads to the matrix collapsing upon itself and losing its three-dimensional structure. In this way, the improved crystallinity of the substrate bacterial cellulose, in conjunction with the assumed physical deposition of the calcium phosphate crystallites on the surface of the

sample contribute to the appearance of a much more crystalline HA. This, as such, lends itself to a higher intensity on all recorded peaks in the FTIR spectrum. The added side effect of this resolve, however, leads to the understanding that the calcium and phosphate are being adsorbed onto the surface of the impermeable sample, rather than chemically bonded to the individual fibres; a belief that will be expounded upon later.

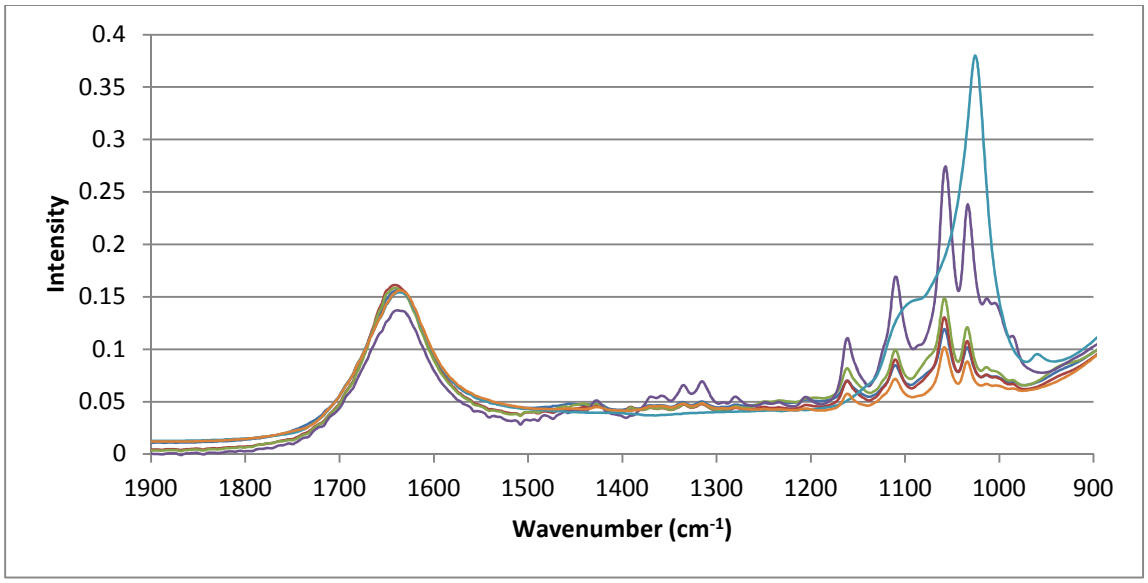

Figure 4.5.1.3: Expansion (900 – 1900 cm^{-1}) of the characteristic region of HA-BC composites shown in figure 4.5.1.2 (from bottom to top, phosphorylated cellulose, 1 hr long phosphorylated HA-BC, 2 hr long phosphorylated HA-BC, 4 hr long phosphorylated HA-BC, 2 hr long phosphorylated HA-Biofill®, pure HA.

Overlaying the resultant FTIR spectra, combining them into one graph, and focusing on a more specific wavelength range, one can note the similarities of the above graphs (figures 4.5.1.2 and 4.5.1.3) to the peaks evident in the samples of BC-HA and the phosphorylated analogues. The peaks indicated at 3000-3600 cm^{-1} and 1650 cm^{-1} are indicative of the O-

H bond in the hydroxyl group and the ν_2 bending of water, as well as the C=O stretch from carbonate groups. The former is present in the fact that all materials were suspended in solution with water, in addition to 'normally occurring' –OH groups necessitated by the stoichiometric equation. The latter indicates that the HA is partially substituted by carbonate ions (CO_3^{2-}) from the cellulose, the carbonate in SBF, and ambient carbon dioxide, as confirmed by Hong et al., 2006[75]. This is understandable as the literature has often reported similar results with similar samples, and is expounded by the fact that natural bone mimics this effect of carbonate uptake in its final composition. This may, in turn, induce better tissue response, which is a major driving force in such experimentation. The last major peak of note is the previously discussed one found at 1030 cm^{-1}, which, in conjunction with a minor peak seen at 987 cm^{-1} (and a minor overlapping shoulder around 1112 cm^{-1}) is attributable to the stretching mode of PO_4^{3-} vibration (see table 4.3.1.1).

EDX data shows promise in all samples (including the BC-HA composites), with requisite peaks of calcium and phosphate, as well as minor indications of additional components such as magnesium, chlorine and sodium found in non-stoichiometric hydroxyapatite (akin to that found in bone). Of particular note is the potential for BC-HA composites formed using reconstituted Biofill®, which possessed a Ca-to-P ratio as high as 1.76 ± 1.46.

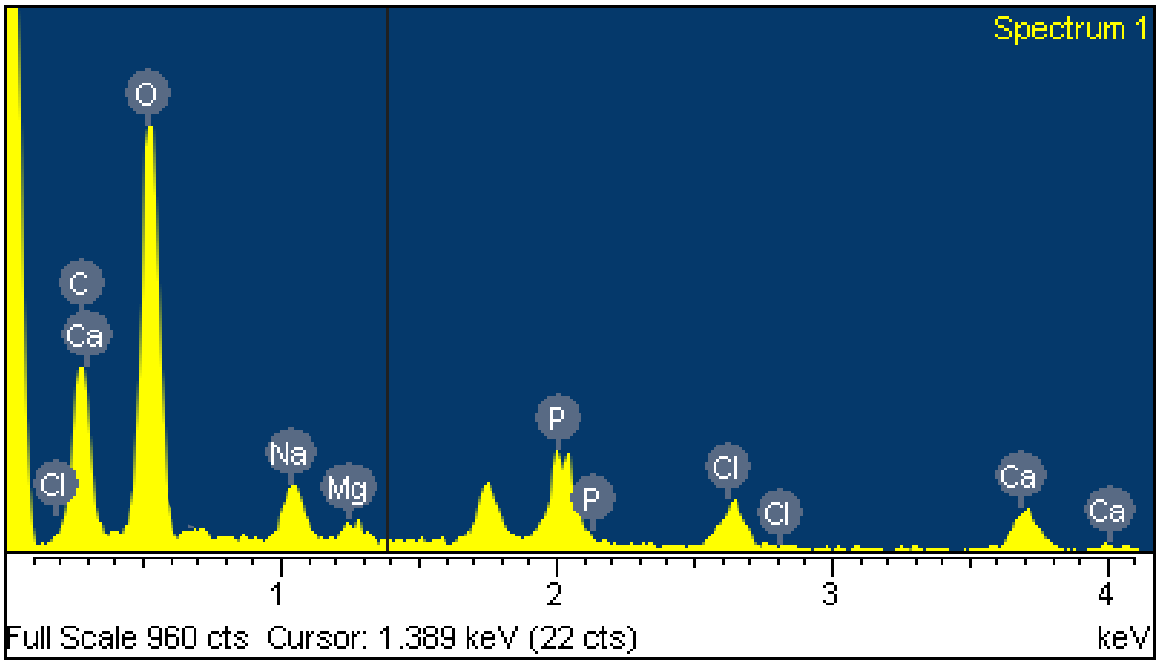

Figure 4.5.1.4: A sample EDX pattern for the BC-HA pellicle samples. Note the presence of both phosphorus and calcium in the samples, as well as a trace smattering of additional essential elements.

Calcium and phosphorous atoms were detected on the samples (Figure 4.5.1.4, above), in varying quantities, depending on the reaction conditions. This serves to indicate that a procedure of phosphorylation followed by pre-incubation in the calcium ion solution was an effective measure in the stimulation of precipitation on the samples. Ca-to-P ratios were taken to ascertain the relative success of the formulation in obtaining true hydroxyapatite; ratios should be ideally around the theoretical stoichiometric ratio of 1.67 for truly crystalline HA, and lower than that for amorphous HA, OCP or TCP. As this lower-than-expected ratio is evident in several samples discussed throughout the course of this dissertation, it is largely acceptable to claim that the samples contain adequate amounts of calcium phosphates, potentially non-stoichiometric amorphous hydroxyapatites, or other precursors (tricalcium phosphate, octacalcium phosphate, etc.).

Examining the EDX data for hydroxyapatite produced biomimetically without a cellulose backbone, the numbers appear to corroborate with the above. The Ca/P ratio is found to be 1.51 ± 0.22, which encompasses the 1.67 target. Interestingly enough, the 'pure' HA sample was found to only contain 53% hydroxyapatite on an atomic weight basis. The remainder was a mixture of sodium and chloride; a known impurity derived from the SBF formulation (typically rinsed out in successive washings). This is a notable factor which helps explain the presence of significant amounts of Na and Cl in BC-HA samples discussed previously. Remaining atomic weights are summarized in table 4.5.1.1 below.

Table 4.5.1.1: EDX results for biomimetically produced HA ($Ca_{10}(PO_4)_6OH_2$)

Element	Theoretical No. Of Atoms	Theoretical Percentage	Actual Percentage from EDX
Ca	10	23.8	20.4
P	6	14.3	13.8
O	26	61.9	65.8
H	2	--	--
Total	42	100	100

This table indicates that the actual observed percentage of each element is very close to the theoretically obtainable amount of that element in hydroxyapatite. As such, this lends credibility to the experimentation, and certainly with regards to the growth of HA crystallites and their purity.

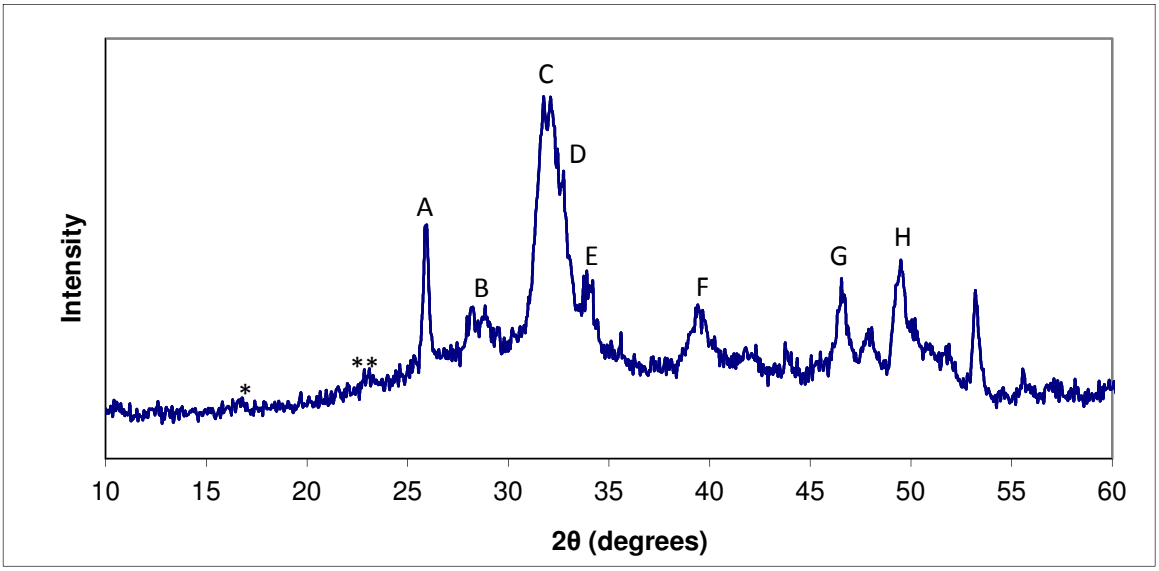

Figure 4.5.1.5: Sample XRD of the produced HA crystallites. Note the similarity of peaks to those discussed in literature, specifically with regards to Markovic et al., 2004[76], Hong et al., 2006[75] and Saeri et al., 2003[73].

The XRD spectrum of a sample of the resulting HA is shown above in figure 4.5.1.5. In the case of the aforementioned paper by Wan et al.[7], the purity of the sample was characterized by the presence of several distinct peaks on the trace, indicated by letters A through F. Each of these peaks corresponds to a significant diffraction of a plane of the HA crystallites. The corresponding plane is found in table 4.5.1.2 below; in brief, however, the strong peaks of 25.8°, 31.8-32.1°, 32.9°, and 34.1° should be noted as they are identical to those found by Markovic and colleagues. In addition, the broader swelling of the graph underlying the peaks in question is significant as well; known as the 'halo' effect, it is grounds to believe in an impurity of the crystal and is a general indicator of low crystallinity[73]. In this specific case, the broader nature of the peaks, as well as the overlapping of the noise evident in the graph, calls into question both the purity of the sample as well as the innate deviations in the characterization technique and equipment.

Table 4.5.1.2: Assignment of peaks from XRD shown in figure 4.5.1.5 and corresponding diffraction planes (adapted from Saeri et al.[73] and Markovic[76])

Peak	2θ (degrees)	Diffraction Plane
A	25.8	002
B	27-29	210
C	31.8-32.1	211 and 112 (overlap)
D	32.9	300
E	34.1	202
F	39.8	310
G	46.7	222
H	49.5	213

Of particular note, the hypothetical location of two significant peaks are indicated by * and ** on the above figure 4.5.1.5. These would be the expected locations of extremely weak peaks courtesy of the bacterial cellulosic substructure in an adequately produced composite structure. The weaknesses of these peaks are expected; Wan et al.[7], noted a highly diminished nature of these peaks in their XRD traces of BC-HA after 14 days of growth in SBF, attributing it to the advanced thickness and crystallinity of the hydroxyapatite crystals on the fibres, which obscure that of the BC. Similarly, the peak around 54° is indicative of the above contamination from the sodium chloride salt.

It is the culmination of all these experimental characterizations that lead to the acceptance of the legitimacy of the procedure in its production of potential hydroxyapatite deposition, although the fine tuning of the parameters leaves a lot to be imagined. No

amount of characterization will lend credibility to a procedure that does not coat the fibres entirely or that cannot be controlled by virtue of an inability to wash, centrifuge, and otherwise handle the biomaterial. The variability and incongruence of the methodology of experimentation itself, and not the samples tested, should be called into question, as there were significant roadblocks to the desired adherence to a generally accepted procedure.

4.6 Variations in Choice of Pre-treatment Media, and Cellulose Morphology in HA Growth

In examining samples that had been pre-treated with calcium ions and left in SBF solution, it became necessary to discern a mechanism of calcium attachment to the existing phosphate. To this end, several attempts were made to more accurately characterize the means by which replicable and more succinct results could be obtained by varying factors such as the formation of the bacterial cellulose microstructure and the effect of a varied pre-treatment media on the indefinite long term production of HA composites. Hong et al.[75] proposed a means by which existing quantities of calcium would be ascribed to the adsorption and physical entrapment of molecules via the three-dimensional network structure of samples, such as BC, in conjunction with the ionic interaction of negatively charged phosphates. These salt deposits would then be systematically converted into calcium ions, which could then be used in forming calcium phosphates. As such, experiments with Biofill®, a bacterial cellulose wound dressing that is largely dehydrated, were used to observe the effects of the physical deposition and how

it relates to the formation of apatite crystals. Similarly, in several studies[5, 8, 58, 77], the use of a calcium hydroxide media for pre-treatment was undertaken. To account for this, and to look at a more holistic approach, various pellicles of bacterial cellulose were prepared and treated with both types of pre-treatment media - the remaining conditions being identical - and characterized via EDX and SEM to examine differences in production.

4.6.1 HA-Biofill® Composites

Compared to the samples of individually suspended fibres, the samples of Biofill® appear to have a film of hydroxyapatitic crystals seeded at certain areas of the sample as evidenced below in figure 4.6.1.1.

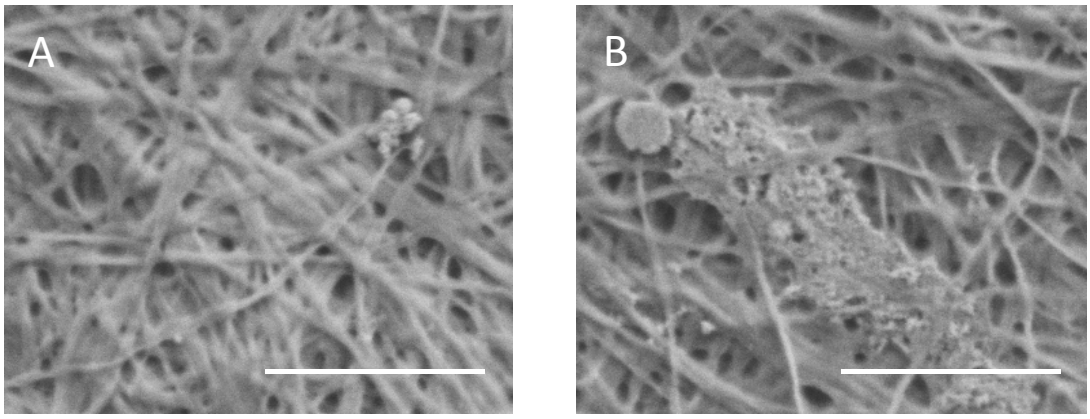

Figure 4.6.1.1: SEMs of the HA-Biofill® composites. The samples of Biofill® that were immersed into SBF were found to have variable nucleation sites of hydroxyapatite, with areas seemingly barren of HA (A) and areas of significant crystallite growth (B) (scale = 1 µm).

In the above SEMs, the small crystallites of HA appear to aggregate and sit on the surface of the samples, rather than permeating through them. Whilst this is likely due to the

nature of the Biofill® - specifically, the fact that the drying process effectively closes off the trans-material pores - the layering and deposition of pure crystallites gives credence to the conclusions drawn from previous results that the Biofill® is more crystalline than that of the isolated fibre networks. However, this effect also calls into question the extent of the presence of HA in the interstitial width of the never-dried bacterial cellulose pellicle.

FTIRs of the resultant Biofill®-HA composites are shown in previous sections (see section 4.4). Although the spectra show the presence of phosphate groups attributable to HA, when incorporating the subsequent EDX results it becomes apparent that they also possess variable amounts of calcium ions, in addition to the requisite phosphorus. This is likely owing to the ability of Biofill® to physically entrap large amounts of calcium, and is confirmed with the wide variation of quantifiable calcium phosphates in the EDX results. In these samples, a Ca/P ratio of about 1.76±1.46 is observed; as the phosphate is consistently 4%, on average, of the atomic weight, this implies that the amount of calcium varies uncontrollably, even within the samples themselves.

4.6.2 Calcium Hydroxide Versus Calcium Chloride

In the course of comparing the competing pre-treatment methodologies, the use of calcium hydroxide versus calcium chloride was also explored. Kokubo first took a notable stand on this approach in the original published work[8], which proposed such a biomimetic synthesis via simulated body fluid. The reasoning at the time was that, due to the very specific composition of the media and the scaffold, and the high sensitivity of the procedure to factors such as pH, temperature and availability of precipitation sites, the

samples would not be adequately coated in hydroxyapatite should there be a harsh environment, or if adequate calcium ions could not be provided due to poor solubility.

As bacterial cellulose was not in mind when the SBF solution was initially considered, and in cases where the scaffolds themselves were highly sensitive to pH or lacking a certain degree of permeability, this posed legitimate problems with HA growth. This was most notably the case in samples lacking a phosphorylation step (instead opting to replace functional groups with reactive sulphates, silicate gel, etc.[7, 8, 78]) or in samples that were solid/impermeable in and of themselves (such as titanium). Upon the discovery of the benefits of phosphorylation however, the prevailing trend soon became to employ a calcium salt, with a marginally basic residue group, to neutralize any acidic functionalized groups of a phosphorylated analogue; SBF has been shown to nucleate HA even in samples lacking any adequate pre-treatment. The most common choice with this regard was then calcium chloride, $CaCl_2$, with its high degree of solubility and relatively low reactivity; it has, as a result, been used infallibly up until this point.

To this end, an alternative calcium salt was experimented with to provide some substance to the above rationale. The return to the use of calcium hydroxide, $Ca(OH)_2$, as a legitimate replacement for the pre-treatment media was entertained by Kokubo et al., in subsequent formulations of the SBF media, and has since been employed in all papers from this group relating to simulated body fluid synthesis. Mucalo[5, 58] and colleagues show a similar reliance, confirming that the supersaturated solutions of calcium hydroxide would be a legitimate means of pre-treating their fibres (cotton, at the time), with FTIR assuring the presence of calcium phosphate derivatives such as $CaHPO_4$ H_2O; a known predecessor to octacalcium phosphate and, ultimately, hydroxyapatite.

Arguably, the major problem with this form of calcium pre-treatment is the inability to acquire high enough molarity in solution, as the solubility of the compound is much lower than that of other calcium ion-containing solutions. Similarly, there seemed to be a lack of confidence in the calcium hydroxide, perhaps as a predicted weakening of certain materials in extended pre-treatment times, as the higher alkalinity of $Ca(OH)_2$ could be detrimental to the scaffold. As this is not the case with bacterial cellulose fibres – the fibres themselves are purified in concentrated sodium hydroxide – there is little reason to become concerned in this particular case. To that end, due to the higher degree of alkalinity (pK_b = 2.4[79]), the reactivity of a relatively stronger base with a strong acid (phosphoric acid in the cellulose) and the lack of introduction of additional cursory ions (OH^- ions are used in the production of hydroxyapatite as well, as opposed to the chloride ion, Cl^-, which is not directly used in HA synthesis, but was found in excess in several fibre samples), $Ca(OH)_2$ is a potentially adequate pre-treatment media replacement.

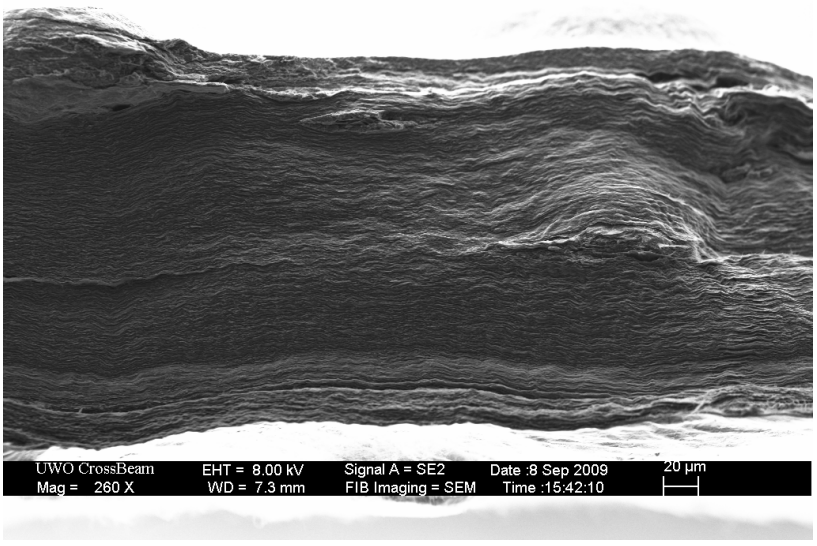

Figure 4.6.2.1: Cross section of a BC pellicle pre-treated with calcium chloride

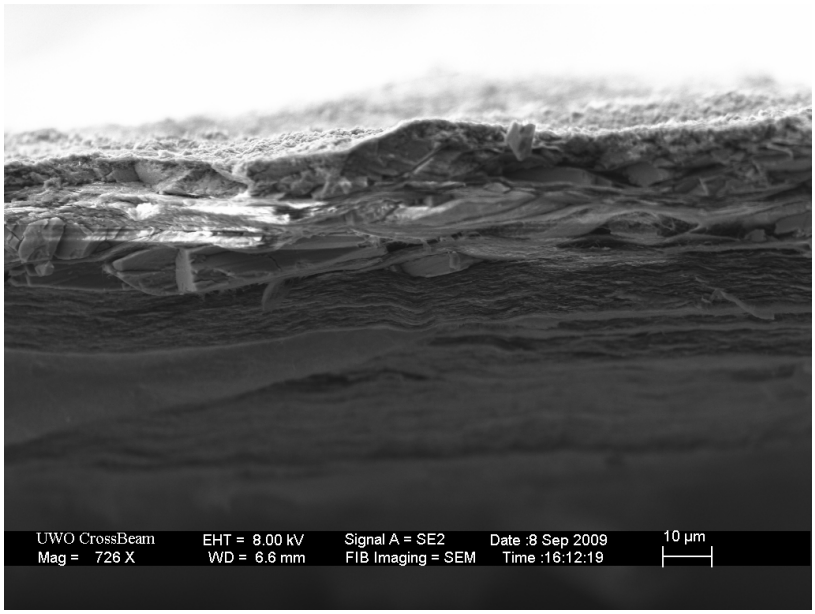

Figure 4.6.2.2: Cross section of a BC pellicle pre-treated with calcium hydroxide

To that end, two 10 mm thick, 25 mm in diameter BC-HA pellicles were produced, using the procedure for static BC growth discussed previously. Samples were phosphorylated and treated with 1.5x SBF as before, differing only in the pre-treatment media composition. Observable, qualitative, results of the superiority of calcium hydroxide pre-treatment are evident in the above SEMs. In the case of the latter image, the hydroxyapatite can be seen distinctly as the rough, platy surface of the sample; a factor which is not as evident in the $CaCl_2$ analogue. This is akin to the findings of many groups in literature - Al-Qasas[43] being a prime example - all of whom report similar forms of the calcium phosphate, which, depending on the length of time of immersion, can range from spherical crystallites to the 'rose-shaped' crystals discussed earlier. In addition, the calcium to phosphate ratio is much higher in the $Ca(OH)_2$ pre-treatment, at least on the surface of the samples, if not within the pellicle sample.

4.6.3 Effect of Pre-treatment Methodologies Internally Within the Pellicle

In the figures 4.6.3.1 and 4.6.3.2 below, the calcium-to-phosphate molar ratios are shown as functions of the depth into the pellicle sample for two samples pre-treated in either calcium chloride or calcium hydroxide. In both cases, all the samples were found to have an average phosphorus content of 4% of the atomic mass of the sample, similar to individual fibre samples produced previously. In addition, although phosphorus-to-carbon ratios varied locally, this atomic percentage of phosphorus was relatively maintained throughout the thickness.

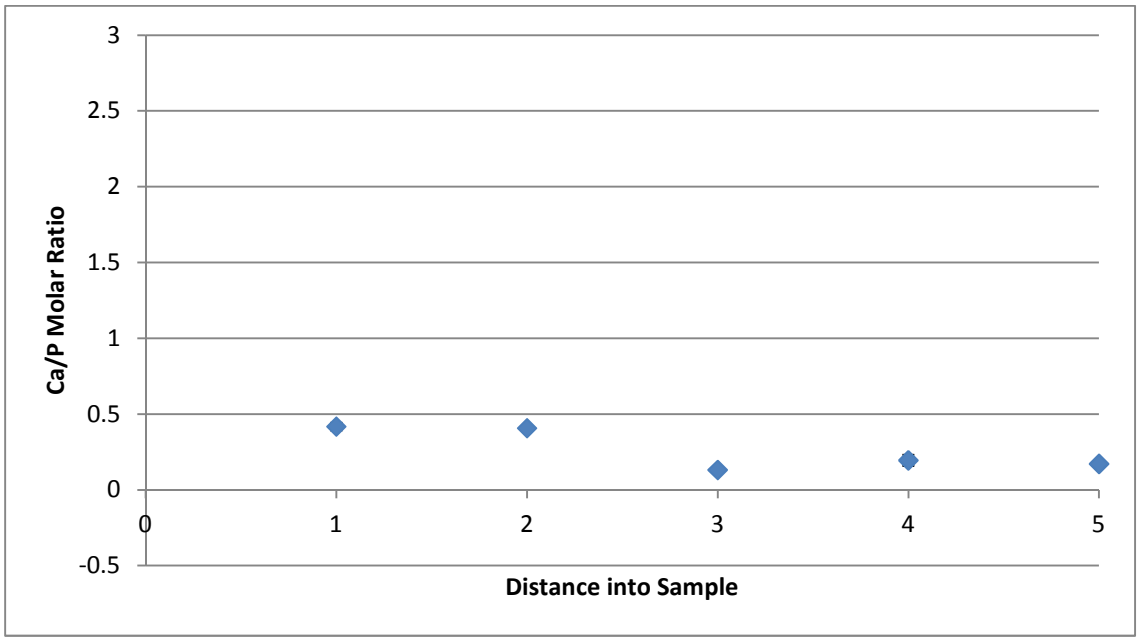

Figure 4.6.3.1: Molar ratio (Calcium to Phosphorus) of the pellicle immersed in $CaCl_2$ pre-treatment as a function of the interstitial thickness (each unit of distance is approximately 10% of the thickness; standard deviations smaller than the markers)

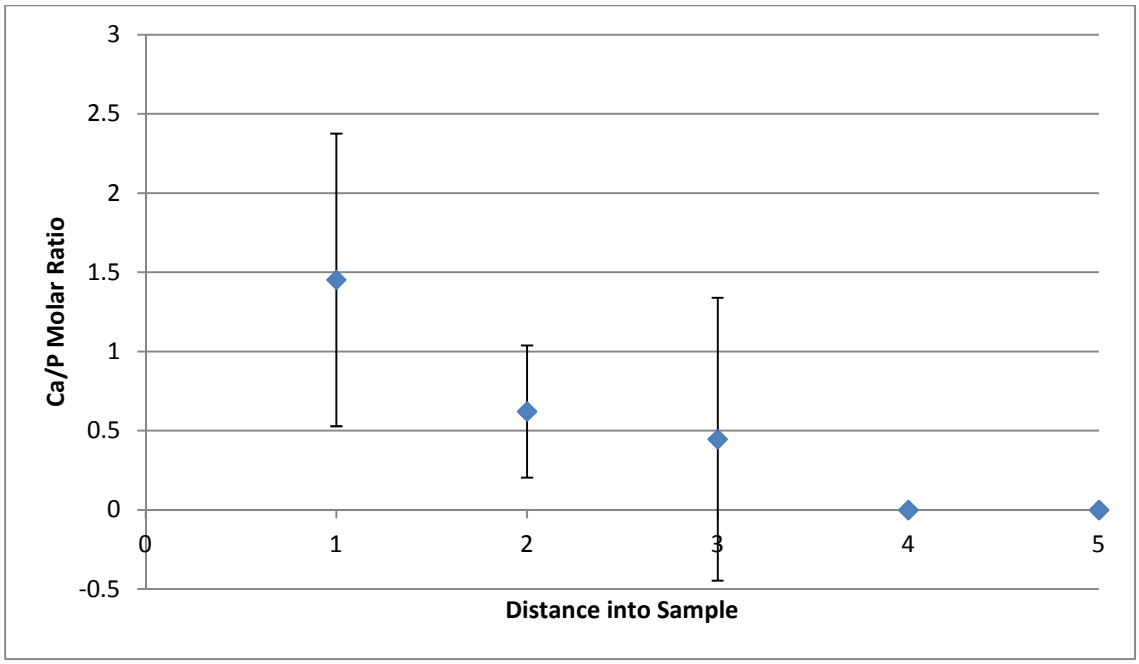

Figure 4.6.3.2: Molar ratio (Calcium to Phosphorus) of the pellicle immersed in $Ca(OH)_2$ pre-treatment as a function of the interstitial thickness (each unit of distance is approximately 10% of the thickness of the sample)

The above graphs show a dependency of the calcium content on the thickness of the sample. They indicate that the sample is affected by its tendency to be physically deposited, rather than chemically reacted, as trends in the calcium to phosphate ratio decrease with increasing depth into the sample. This trend may largely be caused by the pH issues stated above, the physical entrapment of calcium molecules, or systematic errors inherent to the equipment. However, based on the provided data and researched theory, it seems more likely to be indicative of poor permeability. Similarly, the SEM images (see figures 4.6.2.1 and 4.6.2.2) appear to show an agglomeration of crystallites clearly on the surface of the samples, with a declining amount of apparent crystals towards the center. In both samples, there is next to no evidence of crystals as soon as one gets to approximately 43.7 μm into the dry sample. This corresponds to 0.2 cm of the

wet pellicle, or 20.3% of the dry sample thickness.

Interestingly enough, however, the phosphorus concentration does not seem to follow a similar decreasing trend as one moves through the sample. Instead, phosphorus tends to be fairly constant, as emphasized in figure 4.6.3.3 below.

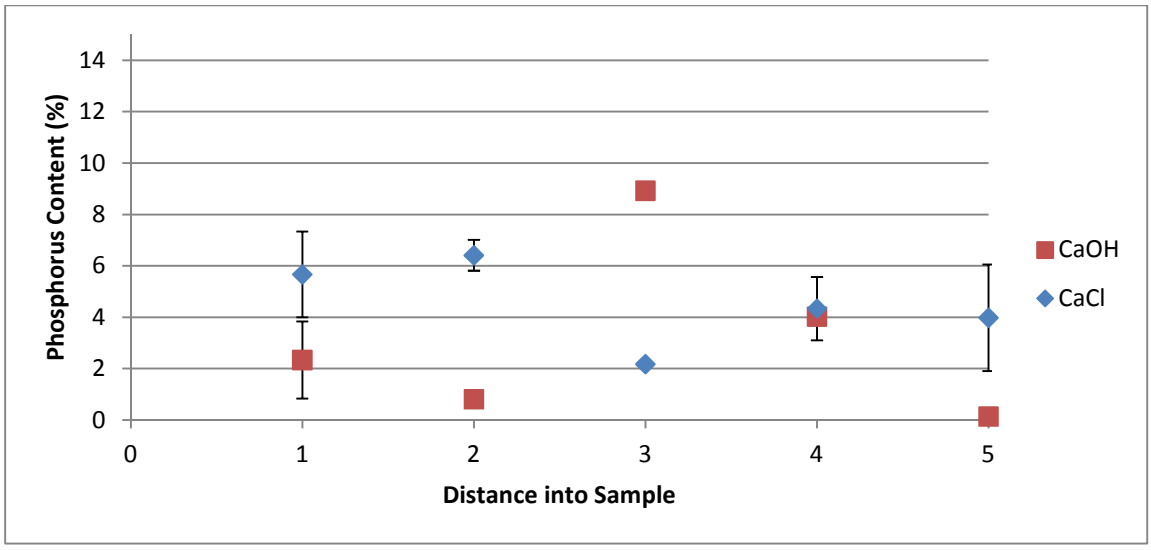

Figure 4.6.3.3: Phosphorus content as a function of distance into the sample

In short, the trend indicates that the sample may adsorb larger hydroxyapatite crystals, or compounds with higher calcium contents, onto the immediate surface or within the first couple of micrometers. This is in direct opposition to the original belief that the sample would nucleate significant crystallites within the bacterial cellulose matrix itself, and ultimately supports the findings of Hong et al., in 2005[75]. In addition, this is further confirmation of the discrepancies in results above; if the samples are not being adequately phosphorylated in the form of the individual fibres, or if sites of calcium ion

deposition are not being fully utilized throughout the thickness, then the HA crystals will not form on the entire length of the fibre. Instead, the trend is towards a direct crystal deposition on certain inconsistent sites upon the surface, which is then likely to be washed out in purification or even preparation of samples for characterization. This belief also corroborates with the inability to centrifuge the fibres; agitation of this nature could induce shear forces that would loosen and otherwise pare away the crystals. Nevertheless, this does seem to indicate that it is necessary to provide the samples with some minimum amount of agitation to at least expose the potential sites of hydroxyapatite attachment to the SBF and/or permit the permeation of calcium deposits.

The above graphs also appear to confirm that the pre-treatment of the samples with $Ca(OH)_2$ benefits the generation of any form of calcium phosphate to a larger extent than the $CaCl_2$. In fact, the surface of some of the calcium hydroxide pre-treated samples were observed to have a Ca/P ratio much higher than that of HA and closer to that of 'raw' SBF. This 'higher-than-theoretical' ratio indicates the abundance of calcium ions present and again corroborates with Wan and Hong in that the molecules of calcium salt are being entrapped. Note that this value is theoretically likely to decrease as a function of the length of subsequent submersion in SBF; as the concentration gradient gets smaller, the depositions similarly decrease. In addition, the weaker alkalinity of the $CaCl_2$ has less of an effect on the artefacts left over from the strongly acidic phosphorylation process. This phenomenon is confirmed in literature through Mucalo in 1995[58] and Granja in 2001[59], and is likely attributable to less primary adsorption of Ca ions in the initial pre-treatment with the $–PO_4$ groups and the –OH groups on the cellulosic backbone, as well as the aforementioned ionic entrapment.

Due to the understanding that the $Ca(OH)_2$ formulation of the media is more of a suspension, and is significantly more reactive to existent acidic functional groups, it is no wonder that the samples that were pre-treated with calcium hydroxide possess a much higher, yet substantially more variable, Ca/P ratio. Not only are the calcium ions in solution reacting with the phosphate groups and becoming physically deposited, but the remnant hydroxides are neutralizing any existing protons from the solution. This is evidenced by the large increase in the pH of the samples (pH of $Ca(OH)_2$ samples hovered around 11; that of the $CaCl_2$ samples was closer to 9). As the fibre dispersion samples during titration started at a pH of approximately 3.6, it is apparent that this is in fact an acid-base neutralization reaction occurring during the pre-treatment. In addition, it is the belief of the experimenter that, as the pre-treatment media is washed out before exposure to the SBF (most effectively in the case of the pellicles), this is ultimately a more efficient means of reaction; with care and specific exposure times, the variability of the pre-treatment media becomes tunable. This advantage potentially becomes moot with fibre dispersions though, as, in the absence of a method of isolating the fibres nor any significant means of the fibres entrapping calcium, one must be cautious about centrifuging after generating any calcium phosphates, lest the nucleation sites be washed away. Similarly, as one must aspire to a neutral pH whilst immersed in the SBF formulation, and as the centrifuged fibres will ultimately contain some residual alkaline solution, this may result in some numerical ambiguity and require further fine tuning of parameters.

Based on this knowledge, it appears that the experimentation could be assuaged into a more concrete procedure should the choice of pre-treatment media and the use of

pellicles be fine-tuned. Granted, one method seems to preclude the other when individual fibres are desired; if one is pre-treating pellicles, the fibres cannot be isolated afterwards without blending the sample and breaking up the nucleation sites formed in the scaffold. Nevertheless, the use of calcium hydroxide to initially provide sites for HA attachment is still a legitimate substitute to the traditional calcium chloride-based solution.

In short, the addition of calcium hydroxide over calcium chloride as a legitimate pre-treatment step for producing bacterial cellulose-hydroxyapatite composites is well founded. The setbacks that the new media would generate could be easily tempered by careful monitoring of the pH in the procedure, and a general understanding of the acidic nature of the phosphorylation experiments. In addition, the potential of a physical entrapment of calcium into a matrix as a precursor to further calcium ion diffusion throughout the sample should not be ignored. There is evidence to the necessity of this step, both in literature, and with regards to SEM and EDX data shown above, and this thought leaves a lot to consider for individualized fibre composites that lack any three-dimensional benefit. Nevertheless, the advantages found from this technique are significant in that they can ultimately affect the stages of composite production, and the accepted understanding of the mechanisms of calcium phosphate crystal attachment.

Chapter Five

5.0 Conclusions and Future Work

Hydroxyapatite, and, in turn, Guided Bone Regeneration, as a veritable means of growth and proliferation of human bone cells, has been at the forefront of medical research and biomaterial experimentation for several years. Texts as far back as the early 1970s have indicated that, in mandibular implantation defects in canines, the addition of hydroxyapatitic coatings and semi-permeable membranes promotes the osteointegration of foreign materials into the natural tissue with minimal scarring and increased new bone formation[41]. Nevertheless, the use of polysaccharide *fibrous* composites has greatly been ignored as the biological necessity of three-dimensional fibres capitulates to the simplicity, accessibility and familiarity of a porous, albeit, largely macromolecular (100+ μm pore diameter), HA powder analogue. Despite the prevalence of successful experimentation on chitin[3], cotton[5, 58], reconstituted cellulose[49], starch[48] and collagen[47]-based scaffolds, and despite the allure of the biocompatibility, strength and fine fibre diameter of bacterial cellulose, fibre-based HA scaffolds have been left at the wayside of an already hindered prospective opportunity.

That said, individualized fibres of bacterial cellulose-hydroxyapatite composites for application in the field of GBR have been explored in the course of this investigation, using Kokubo's Simulated Body Fluid to attach HA to the BC backbone. To this end, factors such as the development of the bacterial cellulose substrate, the variability and success of the phosphorylation/pre-treatment of the material and the legitimacy of the

resultant hydroxyapatite crystals have been tested. Recommendations for the use of alterative types of pre-treatment media, and alternate morphologies of the bacterial cellulose have been divulged, with the intent of familiarizing the reader with the intricacies of the experimentation process and the sensitivity of the product to a multitude of tunable parameters.

Originally, the drive of the experimentation was to develop the composites by elaborating upon the procedure for the cellulose production itself. To this end, the carbon source of the growth medium was questioned, with maple syrup potentially replacing the traditional fructose in the media. Whilst maintaining carbohydrate content in both formulations, the effects of the change in sugar were characterized. In experimentation, however, it was found that the consequently higher variability in maple syrup sugar concentration between batches lead to a similar variability in the beneficial effects. As such, the use of maple syrup fell out of favour for the rest of the experimentation. Nevertheless, the different formulations of growth media were explored and the structure and functionality of the bacterial cellulose was found to be comparable.

Once bacterial cellulose samples were obtained, it became necessary to perform some initial chemical treatment before hydroxyapatite adherence. The initial treatment involved a phosphorylation of the cellulose to replace some of the hydroxide groups on the backbone with that of phosphates. The reaction placed large, negatively-charged, functional groups within the BC resulting in the fibres ‘debundling’ and becoming finer. Ultimately, this advanced higher surface area-to-volume ratios, and an improved biocompatibility. Length of phosphorylation time was similarly considered, yet was found to have a minimal proportional effect on the amount of phosphate attached or fibre

diameter. Phosphate substitution of the hydroxides was found to be around 13% of all available functional groups - comparable to that found in literature. To this end, the phosphorylated cellulose was found to be conducive to the attachment of hydroxyapatitic coatings, and independent of the phosphorylation time.

Pre-treatment was performed using calcium chloride solutions, to react with the phosphates now on the cellulose. SBF was used to promote endgame HA precipitation and realize the effect of pre-treatment. All samples, again, independent of phosphorylation time or pre-treatment, were found to nucleate comparable HA growth after 14 days of immersion. An interesting outcome was the discovery that samples undergoing pre-treatment initially nucleated *less* visible crystal growth than their counterparts. Samples without any pre-treatment were found to grow larger crystals quicker, although they were relegated to localized sites where fibres converged. The prevalence of finer crystals in pre-treated samples was much more extensive, however, and initially appeared as spheroids before eventually evolving into crystals with sharp petals, or 'squama', covering the surface. The calcium chloride pre-treatment also provided more stoichiometric HA growth; samples that had the pre-treatment step were found to more accurately emulate the expected 1.67 Ca-to-P molar ratio for hydroxyapatite. In all cases, via FTIR and EDX characterization, the growth of calcium phosphates, if not pure hydroxyapatite, was seen on all samples of nanometre-scaled BC.

The purity of the resultant hydroxyapatite was also tested independently. This was done by isolating smaller crystals of amorphous calcium phosphates in aqueous solution, and growing them in excess SBF in order to obtain biomimetically-produced analogues. The ratio of calcium to phosphate of these samples was found to be 1.51 ± 0.22, which is

within the predicted value of 1.67 stipulated by the stoichiometry. FTIR and EDX showed the similarity of the compound to calcium-deficient, carbonate-containing samples seen in literature. X-ray Diffraction (XRD) experiments confirmed this quite effectively, showing evidence of several peaks singularly identical to HA standards, and an overall background indicating amorphous regions reminiscent of bone.

In experimenting on the individualized fibre samples of BC-HA composites, it became apparent that the prevalent successes in the field depended on the use of pellicles or pre-existing, reconstituted forms of fibres for calcium phosphate attachment. To this end, sample pellicles were made in accordance with others in literature, and treated with the same pre-treatment procedure and SBF described above. Cross-sectional slices of the pellicle showed a Ca/P ratio that decreased proportional to the depth, despite a relatively constant amount of phosphorus. This implies that samples are more likely to have a better quality and concentration of HA growth if they have a three-dimensional structure in which molecular calcium can become entrapped, gradually broken down and subsequently dispersed. This is similarly confirmed in literature by groups who observed a directional growth of legitimate calcium phosphate nucleation sites, dependant on the exposure to calcium deposits created in the pre-treatment step[75].

In addition to the significance of diffusion in hydroxyapatite growth, the applicability of varied pre-treatment media was also tested. In this case, the traditional $CaCl_2$ pre-treatment solution was compared to a novel calcium hydroxide solution instead. Samples, after pre-treatment and 14-day submergence in SBF, were tested via EDX in order to ascertain differences. The $Ca(OH)_2$ solution was found to perform better than that of the calcium chloride analogue, owing to an increased reactivity, calcium suspensions caused

by lower solubility, and the acid-base neutralization of the acidic phosphate group. This resulted in a higher superficial Ca/P ratio (more closely approximating native HA), and a more significant discrepancy in said ratio between the respective depths into a pellicle sample, justifying the belief that similar formulations could perform better in individualized fibre dispersions.

This study has provided greater insight into the techniques and methodology of depositing apatite-like crystals on cellulotic biomaterial samples. Founded in this understanding comes a significant drive to identify and isolate the successful techniques of coating single fibres of cellulose in HA for tissue regeneration purposes. Factors such as the potential of $Ca(OH)_2$ suspensions, advancing permeability of the BC substrate using agitation or extended pre-treatment times, and the enhanced growth of bacterial cellulose using varied growth media should not be ignored. Unfortunately, the current experimentation provides indications that a successful technique to produce hollow HA fibres is unobtainable with current methodology. Future developments in the field could produce the desired bone fibres, which, given time and research, could be extended to a growth factor-seeded composite material, with unlimited applicability and variation in morphology, along with a high degree of biocompatibility and minimal fear of donor site rejection. The field should nevertheless lean towards innovation in the individual fibres' growth and modification, rather than the continued research in the pre-moulded forms, as this would ultimately promote the desired mouldability, porosity, and requisite cell growth for a legitimate tissue engineering construct in Guided Bone Regeneration therapy.

References

1. Joseph, G., *Studies of bacterial cellulose production in agitated culture*, 2001, Faculty of Graduate Studies, University of Western Ontario, University of Western Ontario (Faculty of Engineering Science, Dept. of Chemical and Biochemical Engineering), 2001.: London, Ont. p. xv, 115 leaves.

2. Millon, L.E., G. Guhados, and W. Wan, *Anisotropic polyvinyl alcohol-Bacterial cellulose nanocomposite for biomedical applications.* J Biomed Mater Res B Appl Biomater, 2008. **86B**(2): p. 444-52.

3. Yokogawa, Y., et al., *Growth of calcium phosphate on phosphorylated chitin fibres.* Journal of Materials Science: Materials in Medicine, 1997. **8**(7): p. 407-412.

4. Rusu, V.M., et al., *Size-controlled hydroxyapatite nanoparticles as self-organized organic-in organic composite materials.* Biomaterials, 2005. **26**(26): p. 5414-5426.

5. Mucalo, M.R., et al., *Growth of Calcium-Phosphate on Surface-Modified Cotton.* Journal of Materials Science-Materials in Medicine, 1995. **6**(10): p. 597-605.

6. Wan, Y.Z., et al., *Synthesis and characterization of hydroxyapatite-bacterial cellulose nanocomposites.* Composites Science and Technology, 2006. **66**(11-12): p. 1825-1832.

7. Wan, Y.Z., et al., *Biomimetic synthesis of hydroxyapatite/bacterial cellulose nanocomposites for biomedical applications.* Materials Science & Engineering C-Biomimetic and Supramolecular Systems, 2007. **27**(4): p. 855-864.

8. Kokubo, T., et al., *Solutions Able to Reproduce Invivo Surface-Structure Changes in Bioactive Glass-Ceramic a-W3.* Journal of Biomedical Materials Research, 1990. **24**(6): p. 721-734.

9. Garg, A., *Bone biology, harvesting, and grafting for dental implants: rationale and clinical applicatinos*2004, Carol Stream, IL: Quintessence Publishing Co., Inc.

10. Ogiso, B., et al., *Fibroblasts inhibit mineralised bone nodule formation by rat bone marrow stromal cells in vitro.* Journal of Cellular Physiology, 1991. **146**(3): p. 442-450.

11. Kahnberg, K.E., E. Nystrom, and L. Bartholdsson, *Combined use of bone grafts and branemark fixtures in the treatment of severly resorbed maxillae.* Int J Oral Maxillofac Implants, 1989. **4**(4): p. 297.

12. Dubuc, F., *The accessibility of the bone induction principle in surface - decalcified bone implants.* Clinical Orthopaedics and Related Research, 1967. **55**: p. 217-223.

13. Mulliken, J.B., et al., *Use of Demineralized Allogeneic Bone Implants for the Correction of Maxillocraniofacial Deformities.* Annals of Surgery, 1981. **194**(3): p. 366-372.

14. Jarcho, M., *Retrospective analysis of hydroxyapatite development for oral implant applications.* Dental clinics of North America, 1992. **36**(1): p. 19-26.

15. Kaban, L.B., J.B. Mulliken, and J. Glowacki, *Treatment of Jaw Defects with Demineralized Bone Implants.* Journal of Oral and Maxillofacial Surgery, 1982. **40**(10): p. 623-626.

16. Munting, E., et al., *Effect of Sterilization on Osteoinduction - Comparison of 5 Methods in Demineralized Rat Bone.* Acta Orthopaedica Scandinavica, 1988. **59**(1): p. 34-38.

17. Dahlin, C., et al., *Restoration of Mandibular Nonunion Bone Defects - an Experimental-Study in Rats Using an Osteopromotive Membrane Method.* International Journal of Oral and Maxillofacial Surgery, 1994. **23**(4): p. 237-242.

18. Miguez, P.A., et al., *Collagen Cross-linking and Ultimate Tensile Strength in Dentin.* Journal of Dental Research, 2004. **83**(10): p. 807-810.

19. Rho, J.Y., T.Y. Tsui, and G.M. Pharr, *Elastic properties of human cortical and trabecular lamellar bone measured by nanoindentation.* Biomaterials, 1997. **18**(20): p. 1325-1330.

20. Viguet-Carrin, S., P. Garnero, and P. Delmas, *The role of collagen in bone strength.* Osteoporosis International, 2006. **17**(3): p. 319-336.

21. Canalis, E., T. Mccarthy, and M. Centrella, *Growth-Factors and the Regulation of Bone Remodeling.* Journal of Clinical Investigation, 1988. **81**(2): p. 277-281.

22. Hamrick, M.W., P.L. McNeil, and S.L. Patterson, *Role of muscle-derived growth factors in bone formation.* Journal of Musculoskeletal & Neuronal Interactions, 2010. **10**(1): p. 64-70.

23. Miller, S.C., *The Bone Lining Cell - a Distinct Phenotype.* Calcified Tissue International, 1987. **41**(1): p. 1-5.

24. Nijweide, P.J., E.H. Burger, and J.H.M. Feyen, *Cells of Bone - Proliferation, Differentiation, and Hormonal-Regulation.* Physiological Reviews, 1986. **66**(4): p. 855-886.

25. Buser, D., C. Dahlin, and R. Schenk, *Guided bone regeneration in implant dentistry*1994, Hong Kong: Quintessence Publishing Corp.

26. Mattout, P. and C. Mattout, *Conditions for Success in Guided Bone Regeneration: Retrospective Study on 376 Implant Sites.* Journal of Periodontology, 2000. **71**(12): p. 1904-1909.

27. Campbell, J.B., et al., *Application of Monomolecular Filter Tubes in Bridging Gaps in Peripheral Nerves and for Prevention of Neuroma Formation - a Preliminary Report.* Journal of Neurosurgery, 1956. **13**(6): p. 635-637.

28. Hurley, L.A., et al., *The Role of Soft Tissues in Osteogenesis - an Experimental Study of Canine Spine Fusions.* Journal of Bone and Joint Surgery-American Volume, 1959. **41**(7): p. 1243.

29. Brånemark, P.-I., et al., *Intra-Osseous Anchorage of Dental Prostheses:I. Experimental Studies*. Journal of Plastic and Reconstructive Surgery and Hand Surgery, 1969. **3**(2): p. 81 - 100.

30. Adell, R., et al., *Intra-osseous anchorage of dental prostheses: II Review of clinical approaches.* Scand J Plast Reconstr Surg, 1970. **4**(1): p. 19-34.

31. Page, R.C. and H.E. Schroeder, *Pathogenesis of Inflammatory Periodontal-Disease - Summary of Current Work.* Laboratory Investigation, 1976. **34**(3): p. 235-249.

32. Dahlin, C., et al., *Generation of new bone around titanium implants using a membrane technique: an experimental study in rabbits.* Int J Oral Maxillofac Implants, 1989. **4**(1): p. 19-25.

33. Junger, F. *Guided bone regeneration (GBR)*. 2008 [cited 2010 August 19, 2010]; Available from: http://www.med-college.biz/de/wiki/print.php?id=99&lan=2

34. O'Sullivan, A., *Cellulose: the structure slowly unravels.* Cellulose, 1997. **4**: p. 173-207.

35. Guhados, G., W.K. Wan, and J.L. Hutter, *Measurement of the elastic modulus of single bacterial cellulose fibers using atomic force microscopy.* Langmuir, 2005. **21**(14): p. 6642-6646.

36. Yano, H., et al., *Optically transparent composites reinforced with networks of bacterial nanofibers.* Advanced Materials, 2005. **17**(2): p. 153-+.

37. Hsieh, Y.C., et al., *An estimation of the Young's modulus of bacterial cellulose filaments.* Cellulose, 2008. **15**(4): p. 507-513.

38. Hubbe, M.A., O.J.L. Rojas, L.A., and M. Sain, *Cellulosic Nanocomposites: A Review. Bioresources.* Bioresources, 2008. **3**(3): p. 929-980.

39. Surma-Slusarska, B., S. Presler, and D. Danielewicz, *Characteristics of Bacterial Cellulose Obtained from Acetobacter Xylinum Culture for Application in Papermaking.* Fibres & Textiles in Eastern Europe, 2008. **16**(4): p. 108-111.

40. Czaja, W.K., et al., *The Future Prospects of Microbial Cellulose in Biomedical Applications.* Biomacromolecules, 2006. **8**(1): p. 1-12.

41. Aoki, H., *Science and medical applications of hydroxyapatite*1991, Tokyo: Takayama Press System Center, Co., Inc.

42. Chow, L.C. and E.D. Eanes, *Octacalcium phosphate*. Monographs in oral science2001, Basel ; New York: Karger. 167 p.

43. Al-Qasas, N.S., *Production and characterization of hydroxyapatite for biomedical applications*, 2004, Faculty of Graduate Studies, University of Western Ontario,

University of Western Ontario (Dept. of Chemical and Biochemical Engineering): London, Ont. p. xvi, 197 leaves.

44. Cho, J.S., et al., *Synthesis of nano-sized biphasic calcium phosphate ceramics with spherical shape by flame spray pyrolysis.* J Mater Sci Mater Med, 2010. **21**(4): p. 1143-9.

45. Brown, W.E., *Octacalcium Phosphate and Hydroxyapatite.* Nature, 1962. **196**(4859): p. 1048-&.

46. Brown, W.E., et al., *Crystallographic and Chemical Relations between Octacalcium Phosphate and Hydroxyapatite.* Nature, 1962. **196**(4859): p. 1050-&.

47. Lickorish, D., et al., *Collagen-hydroxyapatite composite prepared by biomimetic process.* Journal of Biomedical Materials Research Part A, 2004. **68A**(1): p. 19-27.

48. Oliveira, A.L., P.B. Malafaya, and R.L. Reis, *Sodium silicate gel as a precursor for the in vitro nucleation and growth of a bone-like apatite coating in compact and porous polymeric structures.* Biomaterials, 2003. **24**(15): p. 2575-2584.

49. Fricain, J.C., et al., *Cellulose phosphates as biomaterials. In vivo biocompatibility studies.* Biomaterials, 2002. **23**(4): p. 971-980.

50. Svensson, A., et al., *Bacterial cellulose as a potential scaffold for tissue engineering of cartilage.* Biomaterials, 2005. **26**(4): p. 419-431.

51. Chen, Y.M., et al., *In Vitro Cytotoxicity Study of the Nano-Hydroxyapatite/Bacterial Cellulose Nanocomposites.* Materials Research, Pts 1 and 2, 2009. **610-613**: p. 1011-1016 1430.

52. Zeng, X., D.P. Small, and W.K. Wan, *Statistical optimization of culture conditions for bacterial cellulose production by Acetobacter xylinum BPR 2001 from maple syrup.* Carbohydrate Polymers, 2011. **85**(3): p. 506-513.

53. Okiyama, A., et al., *Bacterial cellulose I. Two-stage fermentation process for cellulose production by Acetobacter aceti.* Food Hydrocolloids, 1992. **6**(5): p. 471-477.

54. Okiyama, A., M. Motoki, and S. Yamanaka, *Bacterial cellulose II. Processing of the gelatinous cellulose for food materials.* Food Hydrocolloids, 1992. **6**(5): p. 479-487.

55. Kokubo, T. and H. Takadama, *How useful is SBF in predicting in vivo bone bioactivity?* Biomaterials, 2006. **27**(15): p. 2907-2915.

56. Kokubo, T., *Bioactive glass ceramics: properties and applications.* Biomaterials, 1991. **12**(2): p. 155-63.

57. Ohtsuki, C. *How to prepare the simulated body fluid (SBF) and its related solutions, proposed by Kokubo and his colleagues*. 2001 [cited 2010 August 16]; Available from: http://mswebs.naist.jp/LABs/tanihara/ohtsuki/SBF/index.html.

58. Mucalo, M.R., et al., *Further studies of calcium phosphate growth on phosphorylated cotton fibres.* Journal of Materials Science: Materials in Medicine, 1995. **6**(11): p. 658-669.

59. Granja, P.L., et al., *Cellulose phosphates as biomaterials. In vitro biocompatibility studies.* Reactive & Functional Polymers, 2006. **66**(7): p. 728-739.

60. Yezza, A., et al., *Production of poly-beta-hydroxybutyrate (PHB) by Alcaligenes latus from maple sap.* Appl Microbiol Biotechnol, 2007. **77**(2): p. 269-74.

61. Ross, P., R. Mayer, and M. Benziman, *Cellulose biosynthesis and function in bacteria.* Microbiol Rev, 1991. **55**(1): p. 35-58.

62. Suflet, D.M., G.C. Chitanu, and V.I. Popa, *Phosphorylation of polysaccharides: New results on synthesis and characterisation of phosphorylated cellulose.* Reactive & Functional Polymers, 2006. **66**(11): p. 1240-1249.

63. Monfort, F., *The Log-Normal Distribution of the Diameter of Wool Fibers in Top Slivers as Studied by R. Henon and J. Ott.* Textile Research Journal, 1960. **30**(8): p. 556-567.

64. Elazzouzi-Hafraoui, S., et al., *The shape and size distribution of crystalline nanoparticles prepared by acid hydrolysis of native cellulose.* Biomacromolecules, 2008. **9**(1): p. 57-65.

65. Gadeleta, S.J., et al., *Fourier transform infrared spectroscopy of the solution-mediated conversion of amorphous calcium phosphate to hydroxyapatite: New correlations between X-ray diffraction and infrared data.* Calcified Tissue International, 1996. **58**(1): p. 9-16.

66. Granja, P.L., et al., *Cellulose phosphates as biomaterials. I. Synthesis and characterization of highly phosphorylated cellulose gels.* Journal of Applied Polymer Science, 2001. **82**(13): p. 3341-3353.

67. Gospodinova, N., et al., *Efficient solvent-free microwave phosphorylation of microcrystalline cellulose.* Green Chemistry, 2002. **4**(3): p. 220-222.

68. Kacurakova, M., et al., *Molecular interactions in bacterial cellulose composites studied by 1D FT-IR and dynamic 2D FT-IR spectroscopy.* Carbohydr Res, 2002. **337**(12): p. 1145-53.

69. Hutmacher, D.W., *Scaffolds in tissue engineering bone and cartilage.* Biomaterials, 2000. **21**(24): p. 2529-2543.

70. Muller, F.A., et al., *Accelerated biomimetic deposition of bonelike apatite on fibrous cellulose templates.* Bioceramics 17, 2005. **17**: p. 183-186.

71. Grande, C.J., et al., *Nanocomposites of bacterial cellulose/hydroxyapatite for biomedical applications.* Acta Biomaterialia, 2009. **5**(5): p. 1605-1615.

72. Misra, M., *Adsorption on and surface chemistry of hydroxyapatite*1984, New York: Plenum Publishing Corp.

73. Saeri, M.R., et al., *The wet precipitation process of hydroxyapatite.* Materials Letters, 2003. **57**(24-25): p. 4064-4069.

74. Pang, Y.X. and X. Bao, *Influence of temperature, ripening time and calcination on the morphology and crystallinity of hydroxyapatite nanoparticles.* Journal of the European Ceramic Society, 2003. **23**(10): p. 1697-1704.

75. Hong, L., et al., *Hydroxyapatite/bacterial cellulose composites synthesized via a biomimetic route.* Materials Letters, 2006. **60**(13-14): p. 1710-1713.

76. Markovic, M., B.O. Fowler, and M.S. Tung, *Preparation and comprehensive characterization of a calcium hydroxyapatite reference material.* Journal of Research of the National Institute of Standards and Technology, 2004. **109**(6): p. 553-568.

77. Abe, Y., T. Kokubo, and T. Yamamuro, *Apatite Coating on Ceramics, Metals and Polymers Utilizing a Biological Process.* Journal of Materials Science-Materials in Medicine, 1990. **1**(4): p. 233-238.

78. Rhee, S.H. and J. Tanaka, *Hydroxyapatite formation on cellulose cloth induced by citric acid.* Journal of Materials Science-Materials in Medicine, 2000. **11**(7): p. 449-452.

79. Perry, R.H. and D.W. Green, *Perry's Chemical Engineer's Handbook*2008, New York: McGraw-Hill.

Curriculum Vitæ

Name:	Jordan A. DeMello
Post-Secondary Education and Degrees:	The University of Western Ontario London, Ontario, Canada 2003-2007 B. E. Sc. The University of Western Ontario London, Ontario, Canada 2007-2012 M. E. Sc.
Honours and Awards:	Queen Elizabeth II Aiming for the Top Scholarship 2003-2004, 2004-2005, 2005-2006, 2006-2007 Natural Science and Research Council Industrial Undergraduate Research Award 2005-2006, 2006-2007 Western Graduate Research Scholarship 2007-2008, 2008-2009
Related Work Experience:	Undergraduate Teaching Assistant – Chemical/Biochemical Plant Design The University of Western Ontario 2007-2008, 2008-2009 Graduate Teaching Assistant – Environmental Engineering and Sustainability The University of Western Ontario 2009-2010
Publications and Conferences:	The Canadian Society of Chemical Engineers Biotechnology Conference – Poster Presentation University of Waterloo Waterloo, Ontario, Canada 2009